

A FRAMEWORK FOR IMPROVING OF HEAVY TRUCK CAB CRASHWORTHINESS UNDER ROLLOVER CONDITIONS

Garrett Mattos

Keith Friedman

John Hutchinson

Khanh Bui

Friedman Research Corporation

USA

Paper Number 19-0336

ABSTRACT

In 2012 the US Congress directed the Federal Motor Carrier Safety Administration (FMCSA) to improve commercial motor vehicle safety through the MAP-21 Act. NHTSA reported to the US Congress in 2015 that heavy truck rollover crashworthiness should be improved. To that end NHTSA sent a letter to the president of SAE asking if improvements in test methods could be suggested that would result in improvement of rollover performance. In this study we review the performance of heavy truck cab structures that meet the requirements of J2422 and suggest a framework for improving rollover crashworthiness for heavy trucks.

INTRODUCTION

Historically, there has been significant work to support the advancement of heavy truck occupant crash protection. However, in many areas of heavy truck crashworthiness the results of these efforts have not been translated into adequate safety standards and/or test procedures. In many cases this can be attributed to the lack of coordination and planning between government, industry, and research stakeholders. This paper will outline a suggested framework for improving evidence-based heavy truck cab safety standards based on the lessons learned from previous efforts. Specific focus will be on the structural integrity of heavy truck cabs in response to rollover conditions.

The foundation for all vehicle safety improvements often lies in crash data. Heavy truck crash data have been collected in the U.S. at a large scale since 1966 [1]. This data has consistently shown that single-vehicle rollover crashes are a significant threat to the safety of heavy truck occupants. The use of a combination of crash data, biomechanical metrics, structural analysis, and highway parameters to develop a comprehensive strategy to minimize vehicle accident death and injury has been the backbone of safety improvements for many decades [2]. Further, coordinated efforts that include all relevant stakeholders such as government, industry, and research communities are generally provide the most beneficial and efficient outcomes. This has been a clear desire of the heavy truck industry for many years as exemplified by the recommendations provided to the National Vehicle Safety Advisory Council by the Motor Truck Manufacturers Division [3]. Coordinated efforts among stakeholders provides an opportunity for the benefit and evaluation of safety standards in conjunction with determining feasibility and the cost-benefit outcome of any proposed rules.

A three-phase cooperative research program managed by the Society of Automotive Engineers (SAE) in the 1990s followed this general framework to develop a set of recommended practices for evaluating truck crashworthiness. Cab-to-ground impact forces ranging from 150 kN to 250 kN and energy absorbed (cab only) of approximately 100,000 Nm were calculated with similar values reported for baseline and reinforced models [4]. A primary goal of the recommended practice for evaluating cab strength was to use two testing phases to reproduce both the lateral and vertical loading scenarios that were observed in 180 deg rollovers as these were lacking in the ECE Regulation 29 and a Swedish standard at the time. The ECE R29 test calls for quasi-static vertical load to be applied to the roof of the cab via a large platen with a peak force requirement of 98 kN. The Swedish standard required a maximum 147 kN vertical load followed by pendulum impacts to the A-pillar and rear cab wall. Both of these standards require a level of survival space to be maintained after loading. In the SAE recommended procedure the two test phases consisted of a dynamic impact (via sled or pendulum) to a cab rolled at 20° followed by a quasi-static roof test similar to the ECE R29 protocol. The energy value selected for the dynamic impact was not based on the amount of

energy absorbed by the cab during the rollover reconstructions, but instead based on minimum roll energy tests which had no foundation in relation to occupant injury. The final energy value used in the recommended practice (J2422) was 17,626 Nm. The authors notes deficiencies in the ability to calculate the energy absorbed during a rollover event were noted as problematic to determining an appropriate test energy.

Subsequent to the large SAE-CRP the International Organization of Motor Vehicle Manufacturers (OICA) put together a working group consisting of heavy truck manufacturers with the goal of harmonizing truck cab standards. In the latest large scale effort related to heavy truck crashworthiness the NHTSA concluded that further work should investigate the potential effectiveness of reducing injury and death and the cost-effectiveness of countermeasures related to increasing the integrity and robustness of cab structures with respect to rollover [5].

This paper describes a framework for developing and/or updating test procedures that can improve the rollover crashworthiness of heavy truck cabs. Many advancements in crash data collection, reconstruction, finite element analysis, manufacturing processes, material specifications and costs, and injury metrics have been made since the development of current heavy truck cab test procedures. These advancements can be leveraged to support improvements in cab design that are feasible and cost-effective.

METHODS

Crashes of heavy trucks that produced serious or fatal injuries were identified with the FRC internal crash database. This database includes fully reconstructed heavy truck crashes with detailed medical records and vehicle information. For each crash the detailed LS-DYNA finite element models of the vehicle and terrain, which had been produced previously, were used to simulate the rollover event. The deformation and internal energy of the cab as well as contact forces with the ground were calculated during each run. The orientation of the cab relative to the ground at the time of maximum initial deformation was determined for each case. The time of maximum initial deformation was defined as the first event with the greatest single increase in cab deformation, thus separating the primary roof intrusion event from subsequent loadings. Often a cab will experience the greatest magnitude of roof intrusion when and if it comes to rest on its roof, yet this does not necessarily describe the most injurious event.

A baseline cab structure, modeled in LS-DYNA and validated against the results of a SAE J2422 test, was subjected to select test conditions representative of the impact energy and orientation determined from the reconstructions. The test setup consisted of a flat faced platen on a sled constrained to move in a direction perpendicular to the platen face. The platen impacted a cab that was rigidly constrained at its mounting locations. The total mass of the sled was 5645 kg. The orientation between the cab and plate was defined using the following sequence of rotations and an example of the setup is shown in Figure 1. The cab was initially placed in an upright position with its x-z plane parallel to the face of the platen. The cab was then rotated about its roll axis a predetermined amount. Finally, the cab was rotated about the global z-axis which produced both a yaw and pitch relative to the platen face. Table 1 summarizes the test protocol. The baseline cab was subjected to each of the combinations listed in Table at a 35 kJ impact energy. The modified cab was subjected to the 60 deg roll, 30 deg yaw scenario at both 35 kJ and 80 kJ as this was determined to be the scenario that produced the greatest amount of damage in the baseline cab.

An additional drop test was conducted on the baseline cab fitted to a full tractor to investigate the effect of an unconstrained test on cab response. The cab was oriented relative to the ground at the same 60 deg roll, 30 deg yaw position as utilized in the sled impact scenarios.

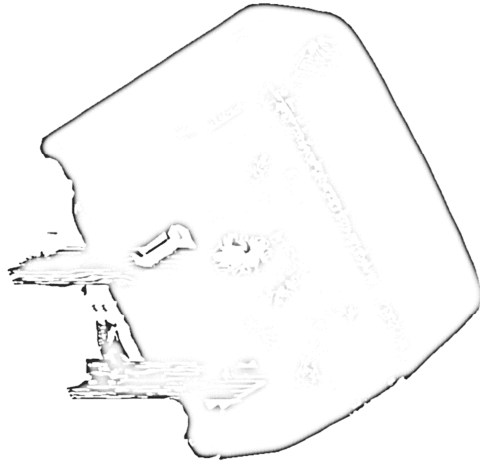


Figure 1 Baseline cab setup for 60 deg roll, 30 deg yaw platen impact (proprietary cab purposely distorted)

Table 1 Summary of simulated test protocol

Roll	Yaw				
	0	10	20	30	40
20	B35	B35	B35	B35	B35
40	B35	B35	B35	B35	B35
60	B35	B35	B35	B35/M35/M80	B35

B35 – Baseline cab, 35 kJ impact energy

M35 – Modified cab, 35 kJ impact energy

M80 – Modified cab, 80 kJ impact energy

The baseline FE cab was modified using manufacturing methods and materials available in the 1990s to improve crashworthiness, increase survival space, and reduce the risk of occupant injury in the reconstructed scenario. The modified cab was then evaluated against select test conditions to assess for comparison.

RESULTS

Due to the low counts of crashes investigated and the preliminary nature of this study some of the results have been normalized. It is not the intent of this work to propose any specific test procedure or energy level, but to demonstrate a methodology using data that was immediately available to the authors.

Three fully reconstructed heavy truck rollover crashes were identified for this preliminary analysis and are summarized in Table 1. The orientation at maximum initial roof deformation had a much greater range in the roll and pitch directions than in the yaw direction. Resultant roof deformation ranged from 408 mm to 793 mm. The amount of roof deformation was reduced from 793 mm to 255 mm with the use of a modified cab. The amount of energy absorbed by the cab varied from 32 to 50 kJ.

Table 2 Summary of reconstructed rollover crash response

Crash ID	Orientation of cab at maximum initial roof crush (deg)			Maximum resultant roof crush (mm)	Energy absorbed by cab (kJ)
	Roll	Pitch (+ve nose up)	Yaw		
1	131	27.8	50.8	408	43
2	180	6	40	553	50
3	116	-12	46	793	32
MOD3	112	-12	45	255	38

The vast majority of crash energy in typical heavy truck rollover crashes is dissipated through friction as the truck slides across the ground surface and only a relatively small percentage is associated with the damage related to the most harmful event (e.g. cab roof damage) [6]. This is demonstrated in Figure 2 which illustrates the total amount of energy that was dissipated through deformation (i.e. internal and eroded energy) vs the total amount of kinetic energy dissipated throughout the entire event. The total amount of energy associated with damage to the tractor, cab, and trailer was roughly 12 % of the total available energy.

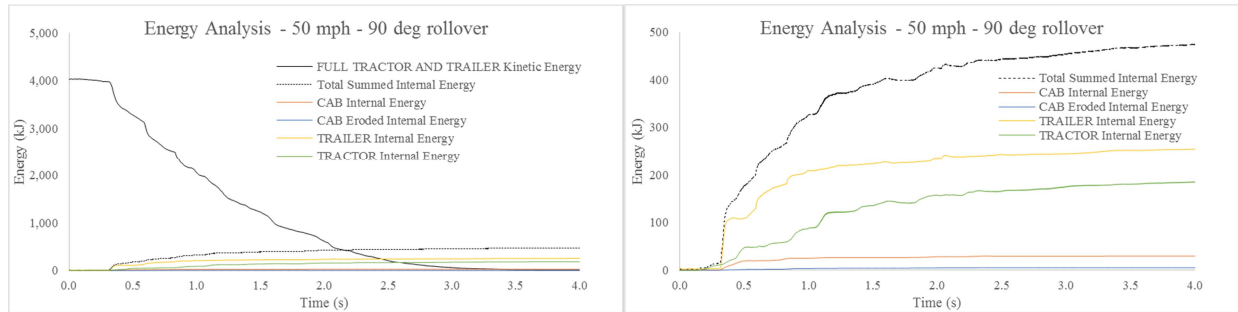


Figure 2 Energy summary for typical 90 deg heavy truck rollover

Platen motion was used to measure maximum cab deformation in the simulated sled tests. Cab deformation was highly dependent on the orientation of the platen relative to the cab as shown in Figure 3. Greater roll angles produced greater deformation. The maximum amount of deformation was achieved at a roll angle of 60 deg combined with a yaw angle of 30 deg. The lowest levels of deformation were 56% of the maximum value.

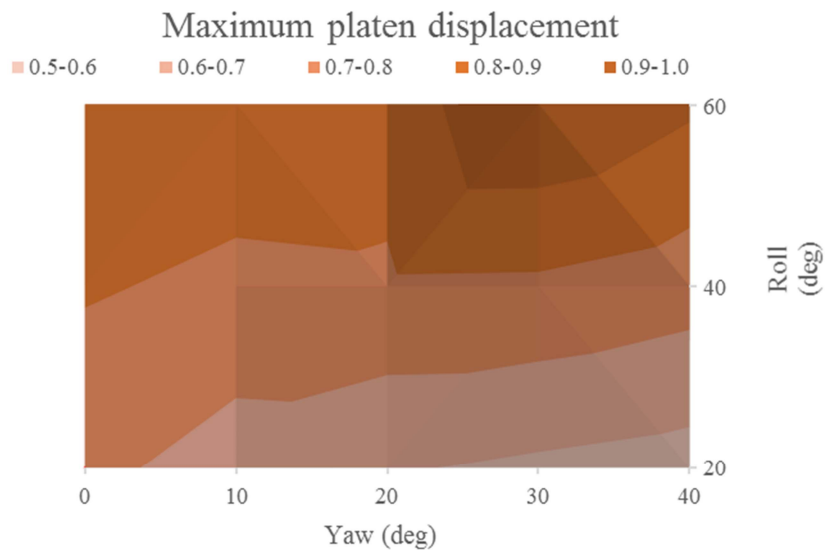


Figure 3 Contour plot of cab deformation vs orientation (data normalized to maximum value)

Platen force was inversely related to the cab deformation as described in Figure 4. The greatest platen force was measured in a 60 deg roll, 40 deg yaw orientation. Though, high force levels were also measured at 20 deg roll angles. It is expected that greater force values would be associated with lower deformations.

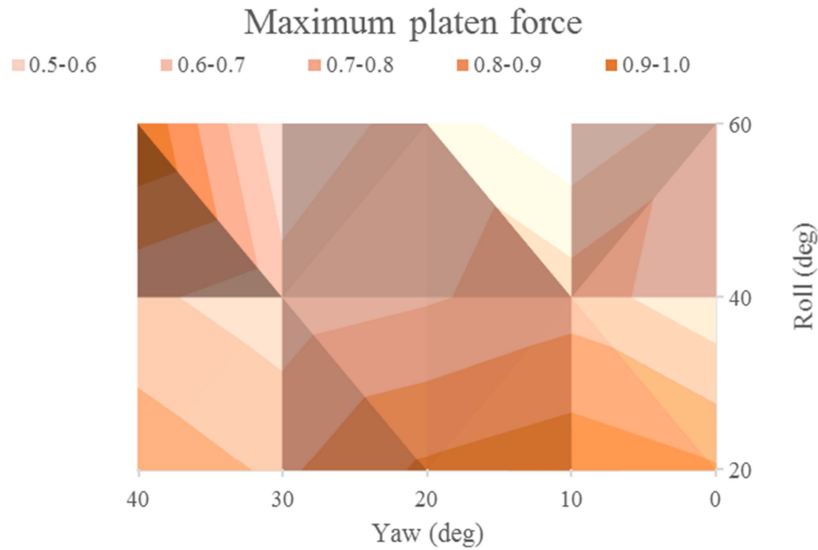


Figure 4 Contour plot of platen force vs orientation (data normalized to maximum value)

The internal energy absorbed by the cab was distributed in a similar pattern as the maximum cab deformation values. Figure 5 shows that the maximum energy was absorbed in the 60 deg roll, 30 deg yaw orientation but that the range in absorbed energy was relatively small. For all orientations the difference in the minimum and maximum internal energy was 10.9 %

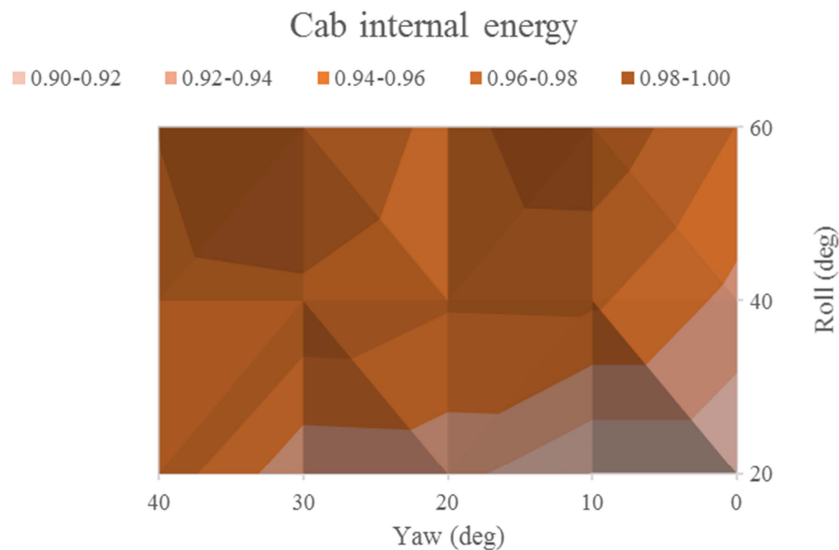


Figure 5 Contour plot of cab internal energy vs orientation (data normalized to maximum value)

The response of the modified cab to the 60 deg roll, 30 deg yaw sled impact demonstrated much less deformation yet similar amounts of internal energy. The cab experienced 60% less deformation and absorbed 4% greater energy. Under the 80 kJ sled impact (also at 60 deg roll, 30 deg yaw) the modified cab suffered 30% less deformation than the baseline did under the 35 kJ condition.

The drop test produced a maximum deformation equal to 81% of that produced in the sled scenario. The cab in the drop test absorbed 87% of the total energy absorbed in the sled test. After the initial impact with the ground in the drop test, which used a FE model of the full tractor and cab, the vehicle pitched rearward until the vehicle was horizontal. The tractor also rolled slightly toward the driver's (left) side.

DISCUSSION

The results of this effort highlight the technical and procedural issues related to developing and improving crash test protocols for heavy trucks. It has also demonstrated, on a small scale, the ability to use reconstructed crash data to develop evidence-based test protocols that could be used to evaluate heavy truck cab crashworthiness in rollovers. Perhaps most importantly, this effort also demonstrated the ability to create a generic cab that could pass a given test. Notably no pass/fail test metrics were provided in this work, yet this is would be an additional step in the process.

The proposed framework includes the creation of a database of reconstructed heavy truck rollovers that produced serious and fatal injuries under reasonable circumstances and in which the cab would have the potential to mitigate those injuries. Existing crash databases would support this effort by providing nationally representative crash data to inform the project on exposure and risk. A range of impact conditions and response metrics would be produced through these reconstructions. A matrix of potential test conditions could then be developed using some threshold (average or 90th percentile) of these values. At this point it will be important to define those injuries and/or crash scenarios that the test protocol will aim to mitigate. This can be supported by parametric finite element analysis.

It will be important that all phases of the effort are coupled with an analysis of injuries and the biomechanical response of occupants. The relationship between the structural response of the cab and the risk of injury to an occupant is the most important feature of a crash test, especially its pass/fail criteria. Finite element modeling ATDs and human body models can be used to evaluate this relationship with respect to testing methods.

Generic cabs and tractors would be created in a virtual environment to parametrically study the effects of select test conditions. The use of a generic cab has advantages. It often invites a greater level of cooperation from industry partners as they are less inclined to be involved in a project that could potentially demonstrate less-than-ideal responses from their vehicles. It can also provide a platform on which to evaluate novel techniques that would otherwise conflict with existing designs. The results above demonstrated the sensitivity of cab deformation and energy absorption to orientation of an impacting platen. Additionally, the effects of various constraint methods for both the cab and the impacting device would have to be investigated to find the right balance between test repeatability and relevance to the real world.

Two primary paths for a new test standard are envisioned. The first, traditional, path would use a limited number of physical tests to evaluate the response of a cab under a very narrow set of conditions. The second path would use a combination of physical and numerical testing to evaluate the response of a cab under a wide range of conditions. The pros and cons of each path will be investigated to determine the potential increase in performance, cost, and desired outcome from a test plan. The advantages of coupling numerical with physical testing includes the ability to conduct full-scale rollovers under a wide variety of conditions in an efficient and cost-effective manner. Numerical testing also assists manufacturers to demonstrate due diligence. Such methods of allowing for some level of certification by analysis are already in use for aircraft seats and roadside hardware.

One key aspect of the test protocol development process will be to demonstrate the feasibility of producing a cab that can pass the test. The modified cab described above is an example of this. This cab was developed using materials and manufacturing processes that were available and in use by passenger vehicle manufacturers in the 1990s. It was demonstrated to successfully mitigate injuries in a reconstructed rollover test as well as improve the response in an example platen impact. By coupling the research of developing a test protocol with the demonstration of practical conceptual designs the chance of success of producing a more stringent test protocol, and therefore better cabs in the future, is improved. A logical next step would involve working with an industry partner to develop and test a physical concept cab that is capable of passing the required test.

Along with demonstrating the feasibility of passing the test method, it will be important to provide estimates of the cost-effectiveness of modified designs as well as appropriate lead times for potential changes in standards. This will require working closely with industry to develop designs that are within the capabilities of existing manufacturing technology. Again the use of injury and crash data will support the cost-benefit analysis and continue to provide an evidence base for all decisions.

CONCLUSIONS

It is clear that much of this framework is not entirely novel or new to crashworthiness test development, however it does apply the recent advancements in finite element analysis to test design which were demonstrated above. The current state of heavy truck cab crashworthiness calls for a review and update of existing recommended practices and crash tests standards. The improvements and advancements in data recording, finite element analysis crash data collection, reconstruction, manufacturing processes, material specifications and costs, and injury metrics should be leveraged at this time to develop a modern rollover crashworthiness test that help heavy truck cabs reach their ultimate safety potential. This research supports the recent efforts of the NHTSA and SAE in improving heavy truck cab rollover crashworthiness. It presents a framework for developing improved testing methods that should include state-of-the-art modeling techniques that are becoming increasingly relevant in the design and evaluation of vehicle safety. This work is directly relevant to the improvement of physical and virtual test methods and identification of enhanced performance measures in support of vehicle safety.

REFERENCES

- [1] Ernst & Ernst, *Truck Accident Study; Report of procedures and findings*. 1968, Automobile Manufacturers Association.
- [2] Krall, F.L. *Truck, Bus and Multipurpose Vehicle Safety in The Williamsburg Conference on Highway Safety Research; a technical conference to develop a plan of needed safety research*. 1972. Williamsburg, Virginia, USA: SAE Vehicle Research Institute.
- [3] Motor Truck Manufacturers Division, *Key Issues in Heavy Truck Safety*. 1976, National Motor Vehicle Safety Advisory Council: Motor Vehicle Safety Seminar.
- [4] Parnell, T.K., et al., *Heavy truck 180 deg dynamic rollover and static roof crush simulation; Phase II-SAE Heavy Truck Crashworthiness*. 1996, SAE International.
- [5] Woodrooffe, J. and D. Blower, *Heavy truck crashworthiness: injury mechanisms and countermeasures to improve occupant safety*. 2015, National Highway Traffic Safety Administration: Washington DC.
- [6] Failure Analysis Associates, *Heavy Truck Crashworthiness, Phase I, Task B, Accident Reconstruction*. 1992: SAE International.

COMPARISON OF HIGHER SEVERITY SIDE IMPACT TESTS OF IIHS-GOOD-RATED VEHICLES STRUCK BY LTVs AND A MODIFIED IIHS BARRIER WITH THE CURRENT IIHS SIDE TEST AND REAL-WORLD CRASHES

Becky C. Mueller

Raul A. Arbelaez

Matthew L. Brumbelow

Joseph M. Nolan

Insurance Institute for Highway Safety (IIHS)

United States of America

Paper Number 19-0193

ABSTRACT

Since 2003, the Insurance Institute for Highway Safety (IIHS) has rated side impact crashworthiness based on tests involving a 1,500 kg moving deformable barrier (MDB) with the geometry of pickups and SUVs (LTVs) striking the side occupant compartment of a stationary vehicle with driver and rear passenger SID-IIIs dummies. Previous examinations of real-world side crashes revealed that one quarter of 2016 side crash fatalities were in good-rated vehicles, suggesting that more improvements in side crashworthiness may be necessary. Research focused on injured occupants suggests that a higher severity test in a similar configuration may be the most effective at driving continued crashworthiness improvements relevant in real-world crashes. This study investigates how well the IIHS MDB impact and injury patterns replicate those observed in modern striking LTVs in a higher severity laboratory test.

Four recently designed good-rated vehicles were impacted by an MDB, a pickup, and an SUV at 50 km/h and 60 km/h. Two vehicles, the Toyota Camry and Volkswagen Atlas, were chosen because they had very low structural intrusion measures at the B-pillar in the current (or established) IIHS test, with 22 and 32 cm of survival space for the driver, respectively. Two vehicles, the Honda Accord and Infiniti QX50, were chosen because their survival space measures were on the borderline of a good/acceptable rating, with 14 cm and 15 cm of survival space, respectively.

Data collection included external and internal measurements along the side structures of the vehicles. All other measures and test setup were conducted according to the current IIHS side test protocol. Observations from the crash tests were compared with real-world higher severity crashes involving good-rated vehicles with configurations like the IIHS test to understand the potential real-world benefit of a new crash test configuration.

The MDB produced vehicle kinematics, deformation, and injury patterns that were not representative of striking LTVs. LTVs loaded the struck vehicles with force concentrations at the striking vehicle's front longitudinal structures while MDBs loaded vehicles more uniformly, both vertically and laterally. Dummy injury patterns were consistent with the deformation patterns; elevated pelvis/femur injury risk was present when struck by the LTVs and elevated head and chest injury risk was present when struck by the MDB.

The four good-rated vehicles exhibited a range of performance when struck by the LTVs, suggesting that a different test configuration, speed, or crash partner may highlight those differences in performance among the current good-rated vehicles. Additionally, MDB tests at 60 km/h revealed dimensional limitations of the barrier that must be addressed prior to further higher speed barrier research.

The current research suggests that increases in severity – mass or speed – of the current MDB would not necessarily encourage vehicle countermeasures that would confer benefit to occupants in real-world side impacts. To encourage relevant real-world design changes, the MDB must be redesigned to replicate the damage and injury patterns of current LTVs in a field-representative impact condition. This test configuration could potentially address an additional 10% of real-world, injury-causing side crashes.

BACKGROUND

The Insurance Institute for Highway Safety (IIHS) began its side crashworthiness evaluation program in June 2003 [1]. SID-IIIs dummies are placed in the driver and left rear seating positions of the subject vehicle, and a perpendicular moving deformable barrier (MDB) strikes the left side of the vehicle at 50 km/h [2].

The IIHS MDB was designed to represent the front end of a midsize SUV or large pickup truck, but with a mass (1,500 kg) closer to a small SUV or midsize car. The test evaluation criteria include assessments of dummy injury measures, head protection (which was especially important when few vehicles had standard head-protecting side airbags), and structural intrusion of the occupant compartment as assessed by driver survival space. Vehicles are assigned an overall rating based on a combination of assessment criteria in one of four categories ranging from best to worst protection: good, acceptable, marginal, or poor.

The IIHS side crash test was more challenging to vehicle structures than other regulatory and consumer information tests that were being conducted in 2003. The MDB was heavier, had a higher ride height (compared with the NHTSA and Euro NCAP MDBs), and had a chamfered front end. The combination resulted in B-pillar loading and intrusion that was more severe and matched real vehicle-to-vehicle crash deformation better than other MDBs in use at the time [3]. Although the IIHS test was considered very severe for its time, an early comparison of the IIHS side test with real-world vehicle-to-vehicle side crashes indicated that 70% of serious injury (MAIS 3+) crashes and 90% of fatal side crashes exhibited more intrusion than the average IIHS crash test configuration [4] (Figure 1).

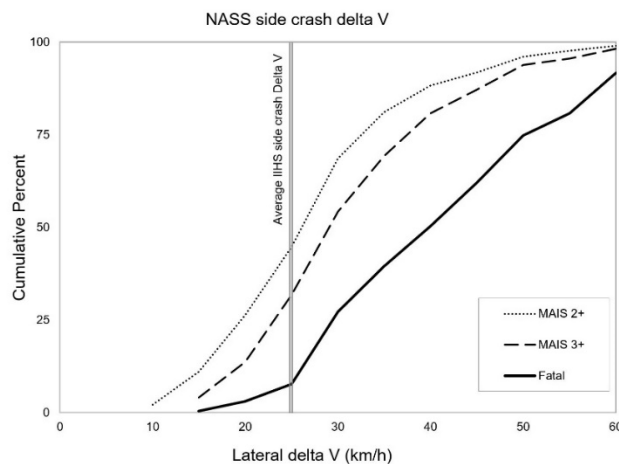


Figure 1. Delta V of side crashes causing injury and fatalities (from “Delta Vs for IIHS side impact crash tests and their relationship to real-world crash severity” by R.A. Arbelaez, B.C. Baker, and J.M. Nolan [2005])

The IIHS side crash test configuration also encouraged the installation of head-protecting side airbags, shown to reduce death risk in near-side crashes [5], which prior to 2003, were not available on most vehicle models or only available as an optional safety feature. The IIHS test encouraged fitment of these airbags because in vehicles without head-protecting side airbags, the front of the MDB often struck the dummy’s head, a result of the smaller statured SID-IIIs dummy combined with the higher front end of the MDB. To improve ratings, vehicle manufacturers strengthened vehicle side structures and fit head-protecting side airbags, initially as optional equipment and eventually as a standard safety feature by 2009. Since 2014, over 95% of new vehicles rated by IIHS earned a good side crash rating. In 2016, 40% of registered vehicles had a good rating, and this proportion of good-rated vehicles will continue to increase as older vehicles are retired from the fleet. Driver fatality rates in 1–3 year old vehicles have dropped from 22 per million registered vehicles in 2005 to 7 per million in 2017 [6] and declines may be largely attributable to improvements in vehicle crashworthiness [7, 8] (Figure 2). Despite the improvements made in side crash protection and the continued increase of good-rated vehicles in the fleet, side crash fatalities have increased slightly in recent years, leaving open the possibility that modifications to the existing side impact test could further real-world crashworthiness improvements.



Figure 2. Trends in side crash fatalities in the United States from 2000–2016 (data retrieved from NHTSA’s Fatality Analysis Reporting System [FARS])

Using methods analogous to the Teoh and Lund study [9], a 2019 analysis by Teoh and Arbelaez was conducted with the latest years of available crash data (2000–2016) but focused on the effects of crash test measures rather than component ratings [10]. Table 1 shows that reductions in crash measures are strongly associated with reductions in real-world death risk, indicating that the level of each measure matters, not just achieving a certain ratings threshold. B-pillar intrusion (survival space) showed the most promise in terms of both risk reduction and room for improvement among rated vehicles on the road. Results demonstrate that one way to improve vehicle performance in side crashes is to change the minimum criteria for good component ratings, even without changing the fundamentals of the crash test.

Table 1. Percent changes in real-world left-side impact death risk associated with the IIHS side crash test

Test measure	Reduction in measure	Reduction in death risk
B-pillar intrusion	10 cm	25%
HIC-15	100	8%
Maximum shoulder deflection	10 mm	10%
Average rib deflection	10 mm	12%
Maximum rib deflection	10 mm	12%
Maximum rib deflection rate	1 m/s	9%
Maximum rib V*C	0.5 m/s	14%
Acetabulum force	1 kN	7%
Iliac force	1 kN	9%
Combined pelvic force	1 kN	8%

Note. All values are statistically significant at the 0.01 level.

Evaluation crash tests should be based on real-world crash conditions to best develop effective countermeasures against real-world injuries. A 2015 IIHS study focused on crashes that produced serious or fatal injuries to occupants in vehicles with good ratings [11]. Queries of the National Automotive Sampling System Crashworthiness Data System (NASS-CDS) and Crash Injury Research and Engineering Network (CIREN) identified 109 occupants in crashes from 2005–2012. Differences between the real-world crashes and the IIHS test were categorized through in-depth analysis of each case. Table 2 shows the potential for various changes to the IIHS test configuration to affect the injury outcome for the study population. No single change to the current test configuration would have been relevant to more than approximately 25% of the occupants. When considering combinations of two changes, a more severe test combined with a forward-shifted impact point (relative to the existing IIHS configuration), assessment of far-side occupant injuries, or modified injury criteria had the greatest potential relevance. Upon further examination of the far-side occupant cases, configurations included a large number of unbelted and out-of-

position occupants and a variety of alignments and crash severities, which would be difficult to capture in a single test configuration.

Another IIHS study [12] explored whether the occurrence of real-world injury in a crash with an impact location forward of the current IIHS test can be identified in the laboratory, how injury risk in such a configuration compares with the current IIHS test, and whether current vehicle designs already offer improvements over the vehicles in the real-world cases (median model year was 2007). The laboratory tests were successful in replicating the damage and injury patterns seen in the real-world case. It also determined that the risk factors observed in this configuration were mitigated in the newer generation of the vehicle with more recent crashworthiness improvements. This test series further concluded that a higher severity crashworthiness evaluation would be more likely to encourage improvements in the current fleet than one with a forward-shifted impact point.

Table 2.
Potential relevance of test changes to real-world cases

Change or combination of changes	Case occupants affect (%)
Adjust injury criteria	9
Include a far-side occupant	9
Increase severity	17
Shift the impact location forward	28
Increase severity and adjust injury criteria	26
Increase severity and include a far-side occupant	37
Increase severity and forward impact location	62

OBJECTIVE

Currently, IIHS is exploring potential modifications to the side impact crash test to address real-world injuries occurring in vehicles with good performance in the existing test. Previous examinations of real-world side crashes with injured occupants suggest that a higher severity test in a similar configuration may be the most effective at achieving this aim. This study investigates how well the IIHS MDB impact and injury patterns represent those observed in modern pickup and SUV striking vehicles in a laboratory test.

METHODS

Laboratory crash tests

Four recently designed IIHS-good-rated vehicles were impacted by various crash partners at 50 km/h and 60 km/h (Table 3). Two vehicles, the Toyota Camry and Volkswagen Atlas, were chosen because they had very low structural intrusion (greater survival space) measures at the B-pillar in the ratings test, 22 and 32 cm respectively. Two vehicles, the Honda Accord and Infiniti QX50, were chosen because their structural intrusion measures were on the borderline of a good/acceptable rating, 14 cm and 15 cm, respectively.

Striking vehicles were chosen from popular modern vehicles with a focus on pickups and SUVs (LTVs), which the MDB was originally designed to best represent. In addition, one midsize car partner was chosen to understand how cars compare with the MDB. The MDB mass was increased to 1,900 kg, the registration-weighted mass of midsize SUVs in the U.S. market (Figure 3). Registration-weighted mass was calculated based on curb mass from the vehicle information databases maintained by the Highway Data Loss Institute [13] and vehicle registration data from IHS Automotive. The test speed for the striking vehicles was either 50 km/h or 60 km/h. All data were compared with results from the baseline IIHS side test in the 50 km/h, 1,500 kg MDB configuration. Data for comparison included high speed video analysis, dummy sensor measures, and pre- and postcrash static measurements on the vehicle.

Table 3. Test Matrix

	Striking Vehicle					
	60 km/h				50 km/h	
	F-150	Pilot	Camry	MDB	MDB	F-150
	2,200 kg	1,900 kg	1,500 kg	1,900 kg	1,500 kg	2,200 kg
Camry	X	X	X	X	X	X
Accord				X	X	X
Atlas	X	X		X	X	
QX50				X	X	

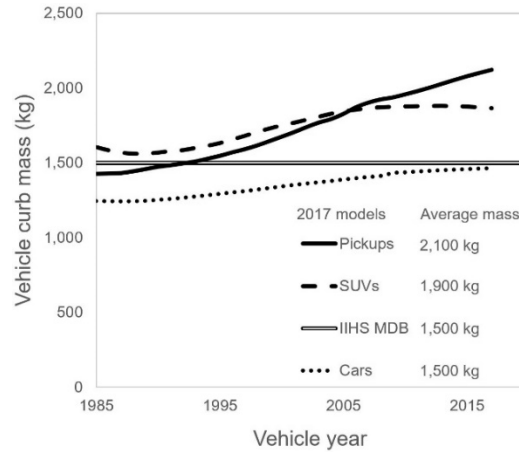


Figure 3. Vehicle curb mass over time based on weighted vehicle registrations (data provided by the Highway Loss Data Institute)

Vehicle tests were setup following the IIHS side impact crash test protocol [2] with the following modifications:

- For striking vehicle partners, a Hybrid III midsize male dummy was installed in the driver and pre- and postcrash measurements of the bumper bar were taken.
- For tests with the MDB, pre- and postcrash measurements of the honeycomb profile were taken at the bumper, mid-barrier height, and top of the barrier.

Adding the extra 400 kg on the MDB resulted in a new center of gravity location and moments of inertia, as shown in Table 4. Striking vehicles were positioned so that the vehicle’s centerline aligned with the calculated impact reference distance (IRD) from the front axle to MDB centerline in the test protocol (Table 5).

Table 4. MDB Characteristics

Characteristics	1,500 kg MDB	1,900 kg MDB
CGx rearward of front axle (mm)	990	1,056
CGy from vehicle centerline (mm)	0	0
CGz (mm)	566	530
Ix (kg-m ²)	542	572
Iy (kg-m ²)	2,471	2,560
Iz (kg-m ²)	2,757	2,870

Table 5. Impact reference distance (IRD) from front axle to striking vehicle centerline

Vehicle	IRD (mm)
Camry	1610
Accord	1614
Atlas	1648
QX50	1597

For the struck vehicle, setup followed the IIHS side impact test protocol and UMTRI ATD Positioning Procedure [14] with the addition of pre- and postcrash measurements taken along the side of the vehicle to compare deformation patterns (Figure 4).



Figure 4. Measurement locations for external crush

In addition, pre-and postcrash measurements were taken vertically along the driver-door trim at locations matching the UMTRI ATD Positioning Procedure H-point positions of the Hybrid III 5th female and Hybrid III 50th male dummies [14] to compare localized loading for different-sized occupants (Figure 5).

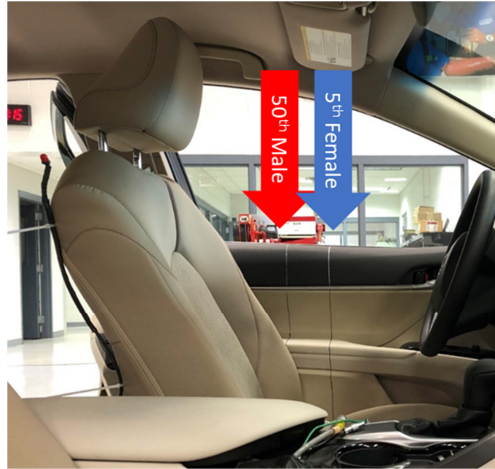


Figure 5. Door trim vertical measurements of crush at the location of dummy H-points

Real-world higher severity crashes

NASS and CIREN cases from Brumbelow et al. [11] categorized as higher severity crashes with similar impact locations as the IIHS side impact test were further examined to relate real-world crash observations to this study's laboratory tests. A list of cases is shown in Appendix C.

RESULTS

Laboratory crash tests

High-speed video footage indicated different vehicle dynamics between vehicle partners and the MDB. The struck vehicles rolled away from the MDB (positive roll, as defined by SAE [15]), while struck vehicles rolled toward (negative roll) all three of the striking vehicle partners. This pattern was observed in all four struck-vehicle models in this study. An example of these kinematic differences is shown in Figure 6 with the Toyota Camry.



Figure 6. Vehicle dynamics comparison between Toyota Camry struck by the MDB (left) and Ford F-150 (right) at 60 km/h during maximum roll

Vehicle deformation patterns were compared using measurements along the outside and inside door and B-pillar structures of struck vehicles. Appendix A has a summary of structural measurements for the striking and struck vehicles. Striking LTVs created a distinct “M” shape in the sides of struck vehicles when compared in a plan view (Figure 7). Whether the striking vehicle was a pickup, an SUV, or a car, they all produced the characteristic ‘M’ shape deformation pattern to varying degrees. The test configuration aligns the stiffer frame rails with the middle of the struck vehicle doors and the comparatively less stiff bumper center with the B-pillar.

In contrast, the uniform shape and stiffness of the MDB center section created relatively evenly shaped loading into the sides of the struck vehicles (Figure 7). For the MDB impacts, the maximum crush measured at the mid-door height varied by only 6 cm from the crush measured at the B-pillar, compared with a 12- to 19-cm differential in the LTV impacts. Vertically, the MDB resulted in only 2 to 5 cm less crush at the beltline than mid-door, while the LTV and car partners produced 9 to 17 cm less crush. The greater crush at mid-door height aligns with the striking vehicle's frame rails. These trends in vertical deformation patterns are shown in Figure 8.

Survival space measured relative to the driver seat centerline, near the theoretical H-point positions of a 50th male and 5th female dummy was less than at the B-pillar in all tests, with the lowest survival space measures recorded at the 5th female location, the furthest from the B-pillar (Figure 9). The largest differences were seen with LTV partner vehicles, with 7 to 19 cm more intrusion at the 5th female location than measured at the B-pillar. For the four vehicles in this study, the B-pillar is located, on average, 41 cm rearward of the 5th female driver dummy's H-point line. The difference between the measurement and occupant location becomes even more pronounced in two-door vehicles, where the B-pillar was an average of 57 cm rearward of the vehicle occupant being evaluated in a sample of two-door vehicles tested at IIHS. While repeatability of measuring door-trim deformation is suspect, consideration should be made for new test rating criteria to capture the magnitude of intrusion directly at the occupant location to better relate to real-world injuries.

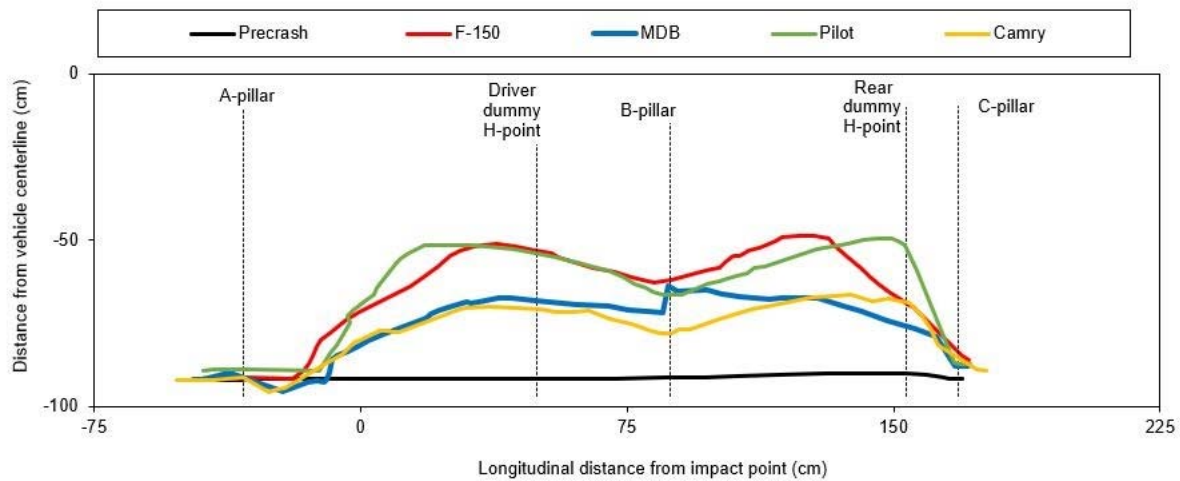


Figure 7. Comparison of external crush along the struck vehicle doors for the Toyota Camry struck by different vehicle partners at 60 km/h

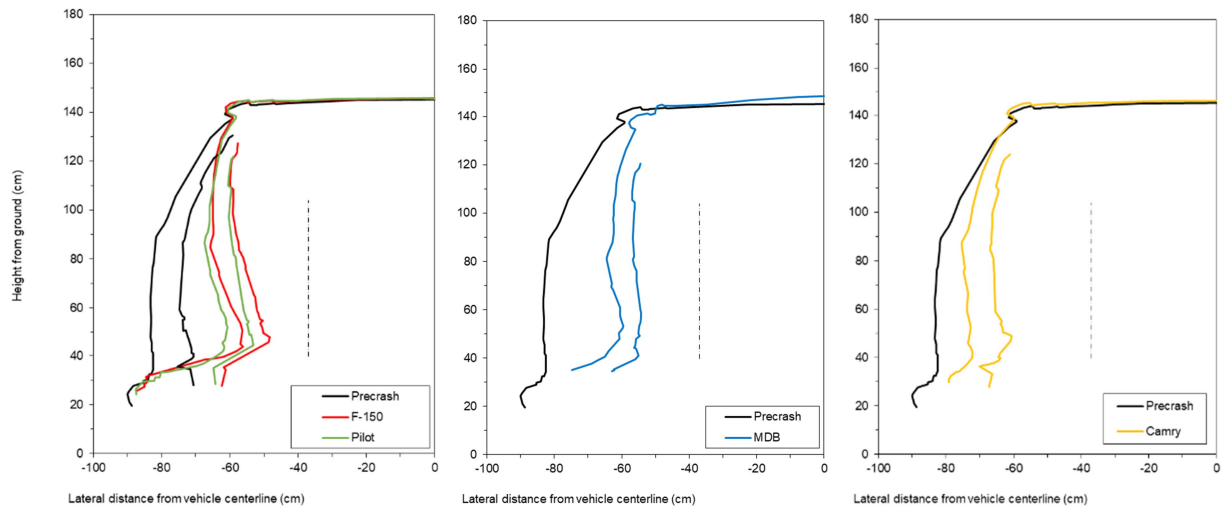


Figure 8. Comparison of B-pillar vertical deformation in Toyota Camry tests

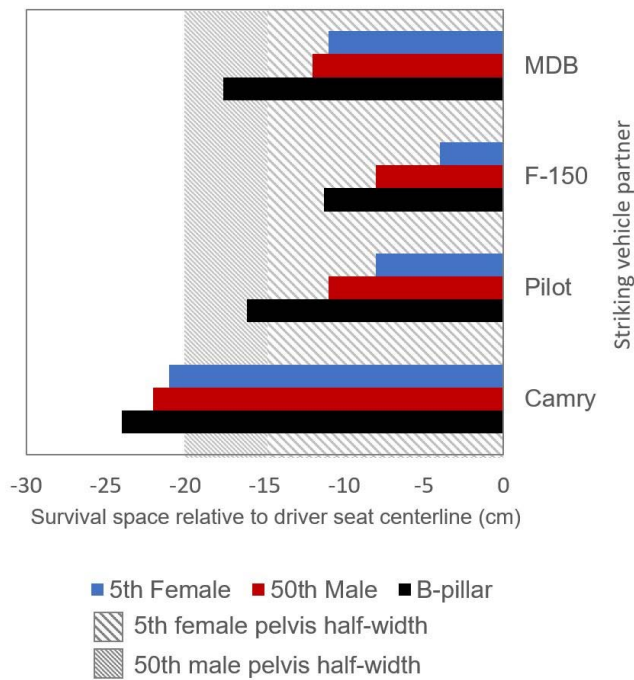


Figure 9. Comparison of occupant survival space measurements for 60 km/h striking vehicles against the Toyota Camry

The effects of crash energy on performance for the Toyota Camry when struck by the F-150 and MDB are shown in Figure 10. The 10 km/h increase in speed for the F-150 test pair represents a 44% increase in energy and resulted in a 50% increase in intrusion on the Camry. In comparison, increasing the MDB mass and speed represented an 82% increase in energy yet resulted in only a 20% increase in intrusion. These specific comparisons highlight the observations that the MDB distributes loading over a broader area of the side structure than the striking LTV.

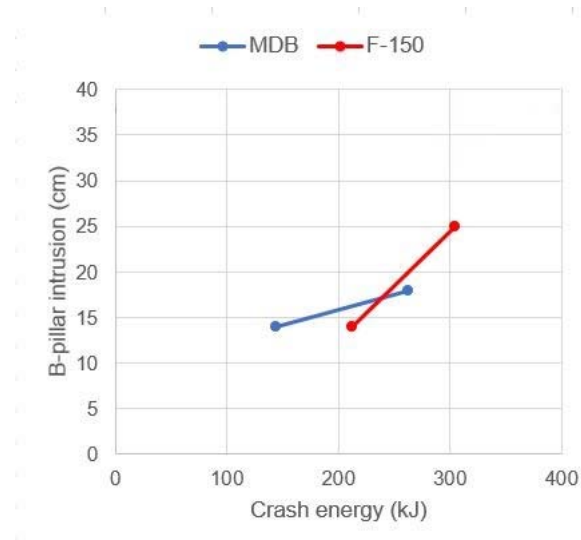


Figure 10. Crash energy and vehicle structural performance for Toyota Camrys struck at 50 km/h and 60 km/h

Peak injury measures from the driver and rear passenger SID-II's dummies are summarized in Appendix B. General injury patterns in the Toyota Camry tests are illustrated in Figure 11. Striking vehicle partners caused vertically lower structural intrusions and dummies recorded elevated pelvic and femur injury measures, while dummies in the MDB partner tests had elevated head and chest measures.

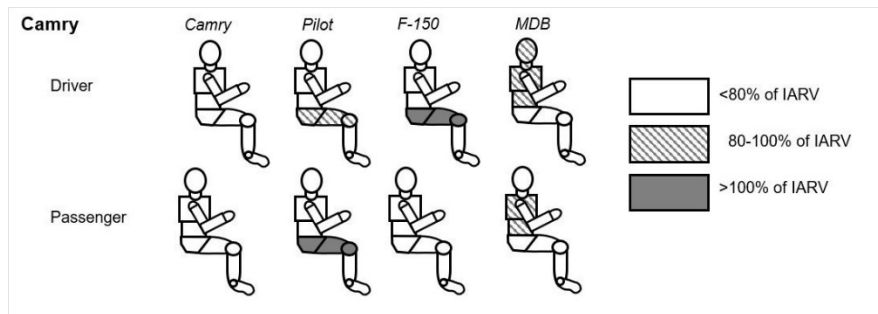


Figure 11. Injury patterns in Toyota Camry tests conducted at 60 km/h

Real-world higher severity crashes

Laboratory test results of impact and injury patterns were compared with observations from field data. NASS and CIREN cases from Brumbelow's 2015 study (Appendix C) that may benefit from vehicle countermeasures designed for a 60 km/h test were identified. Pockets of localized deformation observed in the laboratory tests with striking LTVs were also observed to varying degrees in more than half of the field cases. Maximum crush in real-world crashes was typically higher than measured in this series of laboratory tests (Figure 12). This suggests either that the real-world crashes involve speeds higher than 60 km/h or that the vehicles in this sample, which were older than those in the test series, had weaker side structures. The latter possibility is suggested by the field-study vehicles having lower structural ratings in the standard IIHS evaluations than vehicles chosen for laboratory tests. Dummies in the laboratory LTV-striking vehicle tests had pelvic injury measures suggesting a high risk of injury, consistent with the occurrence of pelvic injury seen in the majority of the field cases. However, the laboratory LTV tests did not reveal high chest injury risk, which was sustained in more than half of the field cases. Laboratory LTV tests did not predict high risks of head injury, consistent with the low frequency of head injuries observed in the field. For the two field occupants with head injuries, it is suspected that curtain airbags were not fully effective in preventing head contact with the striking pickups, resulting in contact through the airbag.

Laboratory MDB-striking-vehicle tests showed mixed trends when compared with field data. Relatively uniform loading across the struck vehicle's side was seen in about half of the field cases, but vertically, intrusion patterns were more consistent with LTV laboratory tests, with maximum crush concentrated at mid-door height and significantly less at higher locations. Dummies in the MDB tests did not reveal high pelvic injury risk, despite the large frequency seen in field cases. Conversely, the MDB tests typically predicted high risks of head injury, but the field cases typically did not. Dummies in the MDB tests were consistent with field observations for chest injury risks.

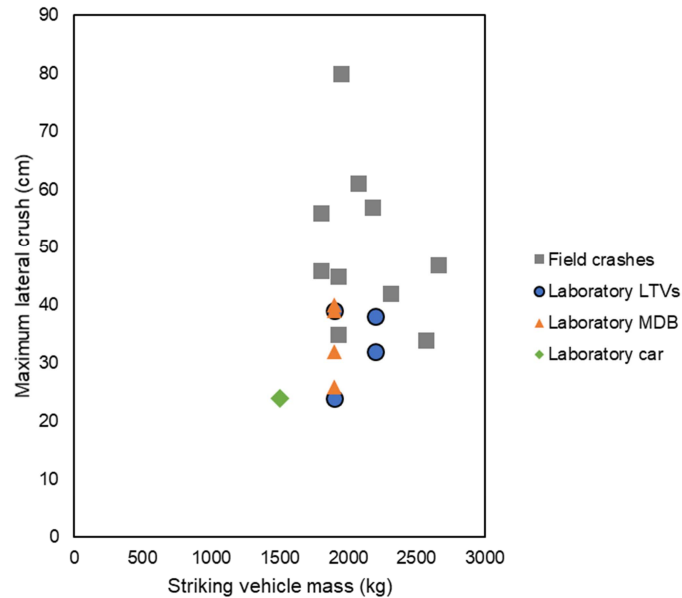


Figure 12. Vehicle maximum crush for seriously injured real-world occupants in side crashes with a striking LTV that may benefit from a higher severity ratings test compared with laboratory tests conducted at 60 km/h

DISCUSSION

In the 1990s, field evidence was clear that occupant injury risk in side-struck vehicles was significantly higher when the striking vehicle was a pickup or an SUV. IIHS developed its side barrier to mimic this elevated risk and encourage automakers to improve occupant protection. The structural changes, plus the fitment of side head-protecting airbags that resulted, have been very effective at reducing side impact fatalities.

The efforts in the current study suggest that the simplistic barrier design conceived in the late 1990s is no longer replicating the deformation and injury patterns of current striking LTVs. Design requirements in regulatory and consumer information tests in the 1990s did not necessitate structural improvements of vehicle sides to perform well, but current testing requirements require consideration for stronger vehicle structures. Consequently, the lack of fidelity of the IIHS MDB to real LTV front structures was not as apparent as the present tests show. Current side designs now tend to fend off the MDB by carrying large loads through the B-pillar, door sill, and roof rail. However, the fronts of modern vehicles are stiffer at the frame rail locations while sections outside and in the middle are softer, contrasting with the MDB's uniform stiffness. Thus, the strongest parts of vehicles' sides do not align with the stiffer portions of the striking vehicles' fronts, so less load can be carried by the B-pillar, door sill, and roof rail than is apparently the case when struck by the IIHS MDB. Additionally, the MDB is loading A-pillars and lower rear door frames of the struck vehicles, which is not seen with LTV striking vehicle comparisons (Figure 13).

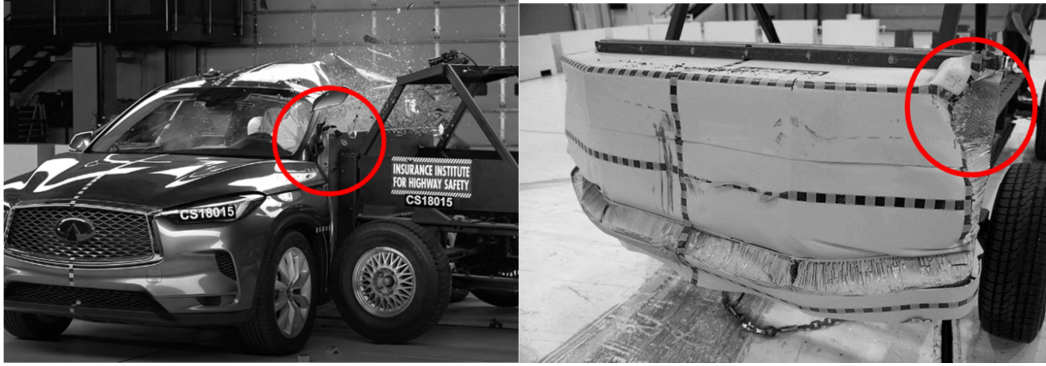


Figure 13. Barrier crush in the 60 km/h Infinity QX50 test highlights significant loading at the barrier’s edges that do not occur in laboratory LTV tests

Vehicles in this study had a range of performance in higher severity tests. The two vehicles with the strongest B-pillar structures (Camry and Atlas) performed appreciably better than their borderline good B-pillar structure comparison vehicles (Accord and QX50) in comparative tests with real striking vehicles. Differences were more dramatic in the 60 km/h MDB configuration, where the Camry had an additional 9 cm of survival space compared with the Accord and also, the Atlas had 17 cm more survival space compared with the QX50. The higher levels of intrusion in the Accord and QX50 tests corresponded to much higher risks calculated for head and chest injuries compared with the Camry and Atlas. The 50 km/h F-150 tests, with a crash severity closer to the IIHS ratings test, did not differentiate vehicle structural performance between the Camry and the Accord, but indicated that these vehicles provide different levels of pelvic protection for occupants, with pelvic injury risks up to 115% of the good-acceptable boundary for the Camry and 165% for the Accord. In comparison, for the IIHS ratings tests, neither vehicle indicated deficiencies for pelvic protection, where dummies in both vehicles measured pelvic injury below 70% of the good-acceptable boundary. A different test configuration, speed, or crash partner may capture that modern vehicles with good IIHS side impact ratings have a range of occupant protection in higher severity side crashes.

A future IIHS side crash test must be able to replicate real-world damage and injuries to encourage effective crashworthiness improvements beyond those developed for the current evaluation. IIHS is investigating barrier modifications that will better replicate common LTV crash partners in terms of mass and front-end structure. Damage patterns and injuries from real-world crashes correspond to results from 60 km/h tests with LTV partners better than tests with the current MDB. The localized pockets of door deformation observed in all LTV partner tests were seen to varying extents in about half of the real-world cases with LTV partners. Cases with more uniform loading typically had torn B-pillars, suggesting weaker B-pillar structure (many of the real-world vehicles had acceptable-rated B-pillar structure) or that these crashes had significantly more energy than the laboratory tests. Serious pelvic injuries occurred in 70% of the real-world cases (Figure 14), and LTV laboratory tests indicated risks to this body region while MDB tests did not. In contrast, the incidence of real-world chest injuries was better reflected by MDB test results. However, this may indicate that the current injury criteria can be further improved, as Teoh and Arbelaez [10] showed a 10-mm reduction in peak deflection related to a 12% increase in survivability. Additionally, rating criteria should include considerations for an elderly risk curve to provide benefit for chest-injured occupants over 60 years old. Low head injury risks from the LTV tests better agreed with the low number of real-world observations of head injury than the higher head injury risks observed in the MDB tests. A higher speed test with the current MDB could encourage countermeasures targeting body regions where the fewest amount of injuries are occurring while potentially ignoring areas of greater concern. An MDB that better replicates modern LTVs is needed to appropriately address real-world injuries. A higher speed test with a redesigned MDB could potentially address an additional 10% of real-world injury-causing side crashes. Vehicle design changes made in response to such a test would need to be evaluated for their potential to reduce protection in the more common lower severity crashes where much improvement already has been achieved.

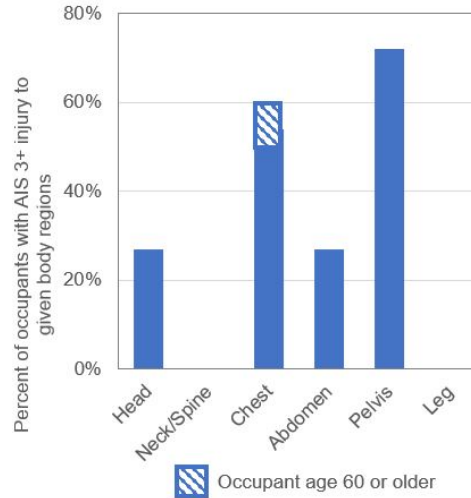


Figure 14. Injured body regions for seriously injured real-world occupants in side crashes with striking LTV partners that may benefit from a higher severity ratings test

CONCLUSIONS

The current IIHS side impact test, developed in 1999–2002, has encouraged side crashworthiness improvements that have significantly reduced driver fatality rates in side impact crashes. Findings from this research suggest that further improvements could be encouraged. Options such as a higher severity crash test show promise. To achieve this, the IIHS MDB needs modifications to better replicate the deformation and injury patterns caused by LTVs.

REFERENCES

- [1] Insurance Institute for Highway Safety. (2003, June 28) First side impact tests: How 12 small SUVs fared. Status Report, 38(7). Retrieved from <https://www.iihs.org/iihs/sr/statusreport/article/38/7/1>
- [2] Institute for Highway Safety. (2017) *Side impact crashworthiness evaluation: Crash Test Protocol (Version X)*, Arlington, VA
- [3] Arbelaez, R.A., Dakin, G.J., Nolan, J.M., Dalmotas, D.J., and Tylko, S. (2002) IIHS side impact barrier: Development and crash test experience. *Proceedings of the 2002 Vehicle Safety Conference* (May 2002). Institution of Mechanical Engineers, London, England.
- [4] Arbelaez, R.A., Baker, B.C., & Nolan, J.M. (2005) Delta Vs for IIHS side impact crash tests and their relationship to real-world crash severity. *Proceedings of the 19th International Technical Conference on the Enhanced Safety of Vehicles (ESV)*, Paper Number 05-0049. National Highway Traffic Safety Administration, Washington DC.
- [5] McCartt, A.T., & Kyrychenko, S.Y. (2007). Efficacy of side airbags in reducing driver deaths in driver-side car and SUV collisions. *Traffic Injury Prevention*, 8(2), 162–170.
- [6] Insurance Institute for Highway Safety. (2018). Fatality Facts: Passenger Vehicle Occupants [Web page]. Arlington, VA. Retrieved from <https://www.iihs.org/iihs/topics/t/general-statistics/fatalityfacts/passenger-vehicles>
- [7] Farmer C.M., & Lund, A.K. (2006). Trends over time in the risk of driver death: what if vehicle designs had not improved? *Traffic Injury Prevention*, 7(4), 335–342.
- [8] Farmer, C.M., & Lund, A.K. (2015). The effects of vehicle redesign on the risk of driver death. *Traffic Injury Prevention*, 16(7), 684–690.
- [9] Teoh, E.R., & Lund, A.K. (2011). IIHS side crash test ratings and occupant death risk in real-world crashes. *Traffic Injury Prevention*, 12(5), 500–507.
- [10] Teoh, E.R., & Arbelaez, R.A. (2019). *Association between data collected in IIHS side crash tests and real-world driver death risk, and opportunities to improve the current test*. Arlington, VA: Insurance Institute for Highway Safety.
- [11] Brumbelow, M.L, Mueller, B.C., & Arbelaez, R.A. (2015) Occurrence of serious injury in real-world side impacts of vehicles with good side-impact protection ratings. *Traffic Injury Prevention*, 16, S125–S132.
- [12] Brumbelow, M.L, Mueller, B., Arbelaez, R.A., and Kuehn, M. (2017) Investigating potential changes to the IIHS side impact crashworthiness evaluation program. *Proceedings of the 25th International Technical Conference on the Enhanced Safety of Vehicles (ESV)*, Paper Number 17-0083. National Highway Traffic Safety Administration, Washington DC.
- [13] Highway Loss Data Institute. (2018) Vehicle information database. Arlington, VA.
- [14] Insurance Institute for Highway Safety. (2004). *Guidelines for using the UMTRI ATD positioning procedure for ATD and seat positioning (Version V)*. Arlington, VA.
- [15] Society of Automotive Engineers. (1994, December). *Surface vehicle information report: Sign convention for vehicle crash testing* (SAE Standard J1733). Warrendale, PA. Retrieved from <https://law.resource.org/pub/us/cfr/ibr/005/sae.j1733.1994.html>

APPENDIX A: VEHICLE DEFORMATION

Table A1. Measurements of external crush along the struck vehicle side profile (cm)

	Lower door			Mid-door				Upper door			
	Driver H-point	B-pillar	Passenger H-point	Driver H-point	B-pillar	Passenger H-point	Max	Driver H-point	B-pillar	Passenger H-point	Max
F150	23	21	15	31	16	20	34	14	20	13	20
Pilot	13	12	16	23	12	20	31	7	6	16	14
MDB	12	16	17	33	28	17	33	27	25	15	30
F150	2	2	1	39	30	20	43	17	15	18	27
Pilot	2	2	1	37	25	38	42	25	13	27	33
MDB	0	2	4	24	28	14	28	21	17	15	23
Camry	9	9	4	22	14	21	25	3	7	9	13
50km/h F150	18	7	12	31	20	20	38	11	10	16	25
MDB	5	9	9	39	36	31	39	37	29	23	37
50 km/h F150	18	6	28	35	19	24	37	20	8	20	27
MDB	14	12	9	39	35	31	41	38	38	28	38

Table A2. Struck vehicle survival space comparison at interior locations relative to the driver seat centerline aligned longitudinally with the theoretical 5th female H-point, 50th male H-point, and centerline of the B-pillar structure as used for rating vehicles (cm)

		5th Female	50th Male	B-pillar
Camry	50 km/h MDB			-22
	F-150	-4	-8	-11
	Pilot	-8	-11	-16
	MDB	-11	-12	-18
	Camry	-21	-22	-24
	50 km/h F150	-13	-23	-22
Atlas	50 km/h MDB			-32
	F-150	-7	-11	-26
	Pilot	-22	-23	-32
	MDB	-6	-9	-21
Accord	50 km/h MDB			-15
	50 km/h F150	-16	-17	-21
	MDB	-5	-7	-9
QX50	50 km/h MDB			-14
	MDB	-4	-5	-4

APPENDIX B: DUMMY INJURY MEASURES

Table B1. Peak driver dummy injury measures

	Reference	Camry						Atlas				Accord			QX50	
		60 km/h		50 km/h		50 km/h		60 km/h		50 km/h		60 km/h		50 km/h		
		F150	Pilot	MDB	Camry	MDB	F150	F150	Pilot	MDB	MDB	MDB	50 F150	MDB	MDB	MDB
Resultant acceleration (g)		70	69	82	36		56	32	21	109		110	42		88	
Resultant acceleration (3ms clip, g)		66	66	80	36		54	29	20	92		106	38		84	
HIC15	779	412	434	723	107	334	276	65	26	696	63	1291	116	316	791	159
X shear force (kN)		-0.4	-0.4	-0.6	-0.3		-0.3	-0.4	-0.2	-0.5		-0.8	-0.4		-0.4	
Y shear force (kN)		0.5	0.4	-0.4	0.3		0.3	0.5	0.3	0.6		-0.4	-0.3		0.4	
Tension (kN)	2.1	1.4	1.4	1.5	0.8	0.9	0.8	1	0.6	1.6	0.7	1.4	1	0.9	2	1.4
Compression (kN)	2.5	0.5	0.9	0.1	0.2	0.2	0.3	0.2	0.1	0.6	0.4	0.1	0.2	0.1	0.4	0.3
X moment (Nm)	±67	-58	-45	-35	-18		-38	34	-10	29		-39	-46		-27	
Z moment (Nm)	±39	-22	-25	-18	16		-21	24	15	-17		-32	-11		-23	
Lateral deflection (mm)	60	30	39	53	15	29	19	24	24	49	23	61	13	53	61	42
Lateral force (kN)		1.6	1.6	2.1	1	1.2	1.3	1.4	1.4	2	1.1	4.8	0.8	1.5	5.2	1.7
Rib 1 deflection (mm)	34	25	29	46	9	27	15	12	11	32	21	58	17	42	58	33
Rib 2 deflection (mm)	34	23	30	40	12	28	14	17	14	31	19	54	18	37	57	36
Rib 3 deflection (mm)	34	29	35	42	16	30	20	22	18	36	17	52	20	34	56	37
Rib 4 deflection (mm)	32	33	37	36	21	28	25	23	21	46	17	43	17	29	45	32
Rib 5 deflection (mm)	32	38	40	34	25	29	33	23	22	40	16	37	21	28	35	27
Maximum Rib Deflection		38	40	46	25	30	21	23	22	46	21	58	19	42	58	37
Average rib deflection (mm)		29	34	41	16	28	21	19	17	37	18	49	21	34	50	33
Rib 1 deflection rate (m/s)	8.2	1.97	1.55		0.74	2.8	1	1.48	1.18	1.85	1.82	6.27	1.28	4.12	5.98	4.86
Rib 2 deflection rate (m/s)	8.2	2.22	1.36	3.94	0.76	2.4	1.14	1.82	1.52	2.04	1.75	6.23	1.12	3.63	6.58	4.21
Rib 3 deflection rate (m/s)	8.2	2.42	1.91	3.82	1.5	2.4	1.34	2.4	2.15	2.68	1.84	5.32	1.4	3.18	6.14	3.89
Rib 4 deflection rate (m/s)	8.2	3.11	2.12	3.1	1.63	2.1	2.13	2.25	2.37	2.98	2.14	3.32	1.98	3.08	3.56	3.75
Rib 5 deflection rate (m/s)	8.2	2.82	2.42	2.93	1.66	3.6	2.47	2.25	2.52	2.39	1.89	4.33	3.63	5.03	3.2	3.65
Rib 1 VC (m/s)	1	0.27	0.28	0.85	0.02	0.33	0.08	0.08	0.07	0.33	0.17	1.6	0.12	0.59	1.16	0.61
Rib 2 VC (m/s)	1	0.22	0.27	0.78	0.04	0.33	0.07	0.17	0.11	0.31	0.17	1.68	0.1	0.56	1.35	0.6
Rib 3 VC (m/s)	1	0.37	0.33	0.82	0.09	0.34	0.12	0.3	0.18	0.48	0.16	1.51	0.17	0.54	1.41	0.54
Rib 4 VC (m/s)	1	0.55	0.41	0.61	0.16	0.28	0.28	0.27	0.27	0.72	0.11	0.67	0.11	0.32	0.69	0.28
Rib 5 VC (m/s)	1	0.58	0.44	0.58	0.19	0.31	0.42	0.22	0.29	0.48	0.1	0.46	0.13	0.31	0.42	0.25
Lateral acceleration (g)		152	52	54	66		96	29	9	74		33	148		79	
Iliac force (kN)	4	0.5	3	0.3	2	1.3	1.9	2.9	1.6	0.4	1.2	1.7	1.7	1.1	2.4	1.2
Acetabulum force (kN)	4	3.2	2.6	1.6	1.8	1.4	2.7	3	3.1	2.4	2.3	1.5	4.5	0.9	1.4	1.2
Combined Acetabulum and Ilium force (kN)	5.1	3.7	5.2	1.9	3.7	2.6	4.6	5.6	4.6	2.8	3.5	2.7	5.3	1.3	3.7	2.3
Distal femur Y force (3ms clip, kN)	±3.9	-3.6	-1.1	-0.7	-0.5	-0.4	-0.4	-1.2	-0.5	-1.1	0.5	-0.9	-0.6	0.8	-1.3	-0.6
Distal femur X moment (3ms clip, Nm)	±356	563.7	199.1	103.6	147.9	50	247.8	138.1	52.7	120.1	40	130.9	386.7	53	186.2	94
Distal femur Y moment (3ms clip, Nm)	±356	-74.4	85.5	62.3	34.9	122	52.9	-28.1	-13.4	38.8	16	71.1	53	137	51.9	32

Table B2. Peak passenger dummy injury measures

	Camry						Atlas						Accord			QX50	
	Reference	60 km/h	Pilot	MDB	Camry	50 km/h	60 km/h	Pilot	MDB	MDB	50 km/h	60 km/h	50 km/h	MDB	60 km/h	50 km/h	
Resultant acceleration (g)		46	49	66	45		47	53	49	51		66	51		72		
Resultant acceleration (3ms clip, g)		43	48	65	44		46	53	48	48		63	51		70		
HIC15	779	171	226	425	176	151	176	258	206	199	57	379	233	111	463	90	
X shear force (kN)		-0.1	0.1	0.3	0.1		-0.1	-0.3	-0.3	-0.2		0.3	0.3		-0.2		
Y shear force (kN)		-0.5	-0.4	-0.2	-0.2		-0.3	-0.2	0.3	0.3		0.4	-0.3		-0.4		
Tension (kN)	2.1	0.4	0.6	0.2	0.2	0.1	0.2	0.7	0.8	0.3	0.1	0.9	0.4	0.3	0.6	0.4	
Compression (kN)	2.5	0.5	0.3	0.5	0.5	0.5	0.5	0.3	0.4	0.5	0.5	0.2	0.6	0.5	0.9	0.6	
X moment (Nm)	±67	-23	-31	-28	-17		-14	-42	-48	-50		-48	-30		-37		
Z moment (Nm)	±39	-21	-25	-23	-17		-18	-13	16	-19		-20	-24		-20		
Lateral deflection (mm)	60	22	23	38	25	22	22	31	21	25	17	52	43	36	38	25	
Lateral force (kN)		1	0.7	1.7	1.2	0.9	0.9	1.4	1	1.5	1	1.7	0.9	0.9	2.4	1.5	
Rib 1 deflection (mm)	34	24	27	34	31	24	25	23	19	21	15	57	45	41	31	17	
Rib 2 deflection (mm)	34	23	27	38	31	26	21	20	17	18	11	49	33	30	22	14	
Rib 3 deflection (mm)	34	24	29	39	33	24	23	32	21	15		38	16	15	13	14	
Rib 4 deflection (mm)	32	22	24	38	29	20	21	48	48	42	23	25	5	17	32	33	
Rib 5 deflection (mm)	32	24	27	28	30	21	25	54	57	52	34	26	7	15	56	46	
Maximum Rib Deflection		24	29	39	33	26	23	54	57	52	34	57	45	41	56	46	
Average rib deflection (mm)		24	27	35	31	23		35	32	29	21	39	21	24	31	25	
Rib 1 deflection rate (m/s)	8.2	1.4	1.62	2.12	1.4	1.4	0.93	2.62	3.54	2.43	2.04	6.36	3.49	2.95	2.92	1.73	
Rib 2 deflection rate (m/s)	8.2	1.45	1.6	2.2	1.76	1.6	0.97	2.56	3.38	2.42	1.98	5.56	2.37	2.44	2.64	1.64	
Rib 3 deflection rate (m/s)	8.2	1.61	1.84	2.15	2.27	1.3	1.27	2.49	2.69	1.68		4.35	1.95	1.56	1.85	1.52	
Rib 4 deflection rate (m/s)	8.2	1.69	1.92	2.19	2.03	1.1	1.45	4.09	3.34	3.5	2.05	3.48	1.15	3.48	2.63	2.39	
Rib 5 deflection rate (m/s)	8.2	1.69	1.93	1.84	2.1	3.9	1.52	5.5	4.91	4.23	2.73	4.97	0.93	2.22	3.7	3.19	
Rib 1 VC (m/s)	1	0.19	0.22	0.38	0.26	0.19	0.14	0.23	0.3	0.21	0.16	2.06	0.76	0.51	0.35	0.12	
Rib 2 VC (m/s)	1	0.2	0.23	0.49	0.24	0.22	0.1	0.21	0.26	0.17	0.09	1.39	0.3	0.32	0.18	0.1	
Rib 3 VC (m/s)	1	0.22	0.29	0.45	0.3	0.18	0.14	0.35	0.32	0.08		0.78	0.14	0.12	0.06	0.1	
Rib 4 VC (m/s)	1	0.19	0.27	0.49	0.23	0.12	0.14	0.82	0.92	0.73	0.22	0.45	0.02	0.2	0.38	0.42	
Rib 5 VC (m/s)	1	0.21	0.28	0.29	0.23	0.14	0.18	1.01	0.97	0.96	0.49	0.38	0.04	0.13	0.8	0.59	
Lateral acceleration (g)		137	165	76	83		105	95	88	73		110	77		74		
Iliac force (kN)	4	1.2	1.7	0.9	1.1	0.9	0.6	0.5	0.4	1.6	0.3	0.7	0.1	0.1	0.5	0.7	
Acetabulum force (kN)	4	2.3	6.1	1.6	2.4	1	4.6	5.8	5.3	1.8	1.8	0.7	2.9	0.5	1.7	0.5	
Combined Acetabulum and Ilium force (kN)	5.1	3.4	7.8	2.4	3.5	1.7	5.1	6.1	5.6	2.9	1.9	1.3	2.9	0.6	2.1	1	
Distal femur Y force (3ms clip, kN)	±3.9	1.2	-0.5	0.4	0.8	0.2	-0.7	-0.5	-0.9	-0.4	0.6	-2.3	1.1	0.7	-1.8	-1.3	
Distal femur X moment (3ms clip, Nm)	±356	232.4	143.3	106.9	111.8	-31	168.6	187.9	85.9	105.6	29	636.5	420	28	205.9	140	
Distal femur Y moment (3ms clip, Nm)	±356	-160.3	52.8	25.8	30.9	89	-85	-39.8	43.9	-21	16	-269.5	-193.7	206	19.2	32	

APPENDIX C: NASS AND CIREN CASE LIST

Table C1.
Crashes that may benefit from a higher speed crash test

Case ID	Crash partner	AIS 3+ injured body regions
781136585	LTV	Abdomen, pelvis
2011-73-024	Heavy vehicle	Chest (elderly)
2007-81-048	Fixed object	Leg
133129	LTV	Abdomen, pelvis
352203868	Car	Chest, pelvis
338071752	LTV	Chest, pelvis
2007-48-216	LTV	Pelvis
2010-75-043	LTV	Chest, pelvis
2009-12-289	Car	Chest (elderly)
842005511	LTV	Head, chest, abdomen, pelvis
2012-73-118	LTV	Chest
2012-78-139	LTV	Chest, pelvis
852153529	LTV	Chest (elderly)
2011-09-091	LTV	Head
554160123	LTV	Head, pelvis

Table C2.
Crashes too severe to benefit from a higher speed crash test

Case ID	Crash partner	AIS 3+ injured body regions
160151944	LTV	Pelvis
2009-79-003	Fixed object	Head, spine, chest
2009-11-180	Fixed object	Head, spine chest, abdomen
2007-09-135	Fixed object	Head
2009-09-185	Fixed object	Chest, abdomen, pelvis
2011-81-080	Fixed object	Head, chest
2009-79-180	Car	Chest
2006-09-173	Car	Head, neck, chest
2009-43-041	Fixed object	Chest
2007-74-123	Fixed object	Chest
2007-11-067	Heavy vehicle	Head, chest, abdomen
2007-45-174	Fixed object	Head
2011-11-187	Heavy vehicle	Chest
2012-48-109	Heavy vehicle	Head, chest, abdomen
2012-49-052	Fixed object	Head

Occupant Injuries Related to Rollover Crashes and Ejections from Recent Crash Data

Jingshu Wu, PhD, Stephen Summers, Stephen Ridella, PhD, Ellen Lee, Thomas Kang, James Myers
National Highway Traffic Safety Administration (NHTSA), Washington, DC
Paper No. 19-0153

ABSTRACT

The goal of this paper is to determine the recent annual occupant populations and trends related to rollover injuries and fatalities, and to assess the risk factors that may have significantly contributed to occupant injuries and fatalities when rollovers and ejections occur. Fatality Analysis Reporting System (FARS) 2004-2017 data were used to obtain the recent occupant fatalities related to rollovers and ejections. National Automotive Sampling System (NASS) – Crashworthiness Data System (CDS) 2013-2015 weighted survey data were used extensively to estimate the occupant injury severities and occupant ejection details associated with rollovers. For rollover cases, the injured body regions (e.g., head, neck, shoulder and back, and chest) and injury contact sources (e.g., vehicle roof, side door, or seat back) were investigated in detail. This study paid close attention to the interaction between the vehicle roof and occupant injuries for the consideration of the requirements from Federal Motor Vehicle Safety Standards (FMVSS) 216a and 226. Finally, occupant injury risk and key risk factors were evaluated using methods of relative risk, including multiple logit model and case-control study. The data analysis using FARS showed a decrease in annual fatalities from approximately 10,500 during 2004-2006 to approximately 7,000 during 2014-2017. Approximately one thirds of all occupant fatalities of light passenger vehicles (Gross Vehicle Weight Rating, GVWR \leq 10,000 lbs.) are related to rollovers. FARS data also provided the occupant ejection status (complete or partial ejection) and ejection path associated with rollovers. The CDS data indicated that rollovers are strongly associated with the injury sources of vehicle roof, side doors, and seat back/support; rollover crashes also resulted in primarily the injured body regions of head, neck, shoulder/back, and chest. The occupant ejection paths are usually side windows and roof opening. The analytical results also revealed that light trucks /vans, with relatively higher centers of gravity, tend to have relatively higher likelihood of rollover crashes than passenger cars, but passenger cars tend to result in a higher rate of occupant serious injuries (Maximum Abbreviated Injury Scale 3+, or MAIS 3+) than light trucks/vans, if rollovers did occur. Overall this study explored the trends and annual occupant populations related to rollovers and ejections using recent traffic data. Logistic regression model was used, with considerations of multiple risks and confounding factors, to predict the occupant injury relative risks of several key risk factors simultaneously. The analytical results using both FARS and CDS indicated that higher occupant injury risks were especially associated with higher delta-V, unbelted occupant, rollover, ejection, side impact, and older occupant age. This study, utilizing the recent crashes from three main databases of FARS, NASS CDS and NASS General Estimates System (GES), may enrich the understanding of rollover and ejection related occupant injuries.

1. INTRODUCTION AND DATA

National Highway Traffic Safety Administration (NHTSA) has been working constantly to improve vehicle safety and reduce traffic injuries. The total traffic fatalities (including occupants, pedestrians and cyclists) for the past few years are 32,744 in 2014, 35,806 in 2015, and 37,461 in 2016 (approximately 37,133 in 2017 from the recent release). Approximately two-thirds of all traffic fatalities are from the occupants killed of light passenger vehicles (cars and light trucks /vans with GVWR less than 10,000 lbs.), furthermore, approximately one-thirds of those occupant fatalities of light passenger vehicles come from rollover crashes. Vehicle rollover is a very risky crash mode that causes severe injuries to occupants, especially to the head, shoulder & back, face, neck and chest from contacts between occupants and vehicle roofs and side doors, or from ejection out of vehicles.

Rollover crashes have previously been identified by NHTSA as a high safety priority, and work has been done investigating potential countermeasures ^{1, 2, 3, 4, 5}. Recently enacted FMVSS (and now fully implemented), such as FMVSS 126 (Electronic stability control systems for light vehicles), FMVSS 216a (Roof crush resistance) and FMVSS 226 (Ejection Mitigation), have sought to reduce the incidence of rollovers, improve vehicle crashworthiness during rollovers and reduce the likelihood of ejections during rollovers. Thus, it is of interest to update the previous understanding on rollovers and injury risk, with different vehicles ages and newer data.

Data sources for this study include FARS (which contains a census of all vehicle fatalities), and the two data systems of NASS, e.g., CDS and GES. The general trends of crashes of all vehicle types and injuries of all person types can be obtained from GES, on the other hand, CDS will be most extensively used throughout this study for occupant injury details associated with light passenger vehicles. CDS data have previously been used by many NHTSA researchers to investigate crash injury details and risk factors, such as weighting factor designs of survey data, vehicle damage areas (frontal crash or side impact), occupant seating position and belt use, delta-V, occupant injured body regions, the vehicle components that contacted the occupants within a crashed vehicle, and occupant injuries and time to medical treatments^{6, 8, 9, 10, 11, 12, 19}. A similar approach is used for the current research.

CDS contains several independent data files that describe vehicle crashes and occupant injury details. The data file of 'General Vehicle' (GV) provides the crash details related to the towed crashed vehicles (i.e., vehicle type, model year, vehicle weights, delta-V, crash type and rollover status). The data file of 'Occupant Assessment' (OA) provides the occupant information (e.g., occupant age, gender, belt use, drinking status, seating position, ejection and ejection area, injury scales, or MAIS). Similarly, the 'Occupant Injury' (OI) data file provides detailed injured body regions (e.g., head, face, AIS scale, and others) and injury sources of vehicle components (roof, door, B-pillar, seat back, or others). The 'Vehicle External' (VE) file provides the principal crash damage areas (e.g., frontal damage, or side damage, useful for identifying the crash directions and crash modes), and 'Accident' (ACC) data file has information about crash location, road, weather, and case number. Starting in 2009, the CDS system collected crash data only from newer vehicles of age ≤ 10 years old only. Therefore, for this research, the vehicle age was limited to within ten years for most analysis (crash year – model year ≤ 10). The primary CDS data files related to vehicle crash types and occupant injuries, e.g., 'GV', 'OA', 'VE', 'ACC', or 'OI', can all be sorted and merged together by using 'crash year, PSU, case number, vehicle number, and occupant number'. Statistical Analytical System (SAS) procedures of 'sort' and 'merge' are used to sort and link the data files of research interest together for this data flow-chart design. SAS version 9.3 was used for this study.^{16, 17}

A detailed flowchart of using CDS data, described in Figure 1, provides the overall approach to examine the research questions. For example, merged "GV+OA" data by using 'crash year, PSU, case number, and vehicle number', with auxiliary information of vehicle external (VE) damages, can answer the questions related to overall occupant fatality and injury, vehicle damage areas, rollover, and occupant seating and maximum occupant injuries (MAIS). In the final step, the correlations, between the occupant injuries and several main independent risk factors, are examined using multiple regression model.

The objectives of this study are to continue the earlier injury research efforts and better understand the injury causes related to rollovers and ejections. Some questions of special interest, step-by-step, are summarized as follows:

- How many occupants (drivers and passengers) of light vehicles died from rollover crashes? FARS data provide complete descriptions of fatalities related to rollovers and ejections.
- How many vehicles (passenger cars and light trucks/vans not more than 10,000 lbs.) are involved in rollover crashes annually? Both GES and CDS data can provide estimates of rollover incidence.
- How many occupants are injured from rollovers annually? CDS data will be used to look at detailed injury severities associated with various vehicle types and crash modes.
- What body regions are commonly injured in rollovers (e.g., an occupant may suffer injuries in several body regions)? What are the most prevalent injury sources (e.g., vehicle roof, side door, B-pillar) that contact occupants in rollovers?
- If rollover and ejection occur, what are the common ejection paths (e.g., roof opening or side windows)?
- If there is an interaction between the vehicle roof and occupant, what are the common injured occupant body regions (e.g., head, neck, spine)?
- More generally, if rollovers, either lateral or longitudinal crashes, and other risk factors are considered simultaneously, what are the relative risks from each factor (e.g., comparing the injury odds of rollover versus non-rollovers, belted vs. not-belted occupants)? This study explores this question using a multiple regression model.
- Finally, FMVSS 216a and 226 have certain impacts on vehicle rollovers /ejections, especially for vehicle models after 2011. This study explores the effect of vehicle age (≤ 2 , ≤ 4 , and ≤ 10 years old, respectively), and uses recent CDS data from the past ten years.

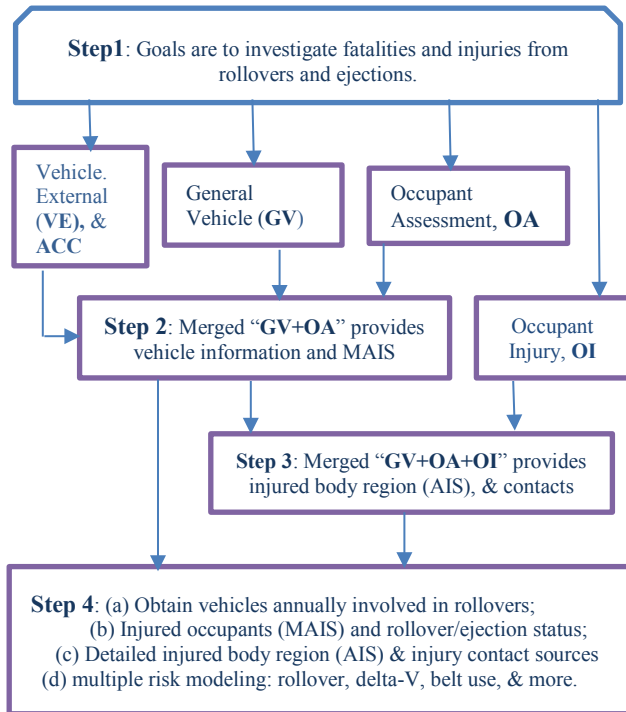


Figure 1: Data Flow-Chart for obtaining Occupant Injuries related to Rollover and ejection using CDS Data

A similar but much simpler flow-charts, using FARS or GES data files of ‘Accident’, ‘Vehicle’, and ‘Person’, can be done as Figure 1.

2. OCCUPANT FATALITIES RELATED TO ROLLOVERS AND EJECTIONS

FARS is a census of fatalities resulting from all types of crash modes. Three main data files, ‘Accident’, ‘Vehicle’, and ‘Person’, from the FARS database are used in this analysis. Several variables in FARS are of special interest, such as ‘rollover’, ‘ejection’, ‘ejection path’, and ‘injury severity’, and these key variables are used to answer various research questions.

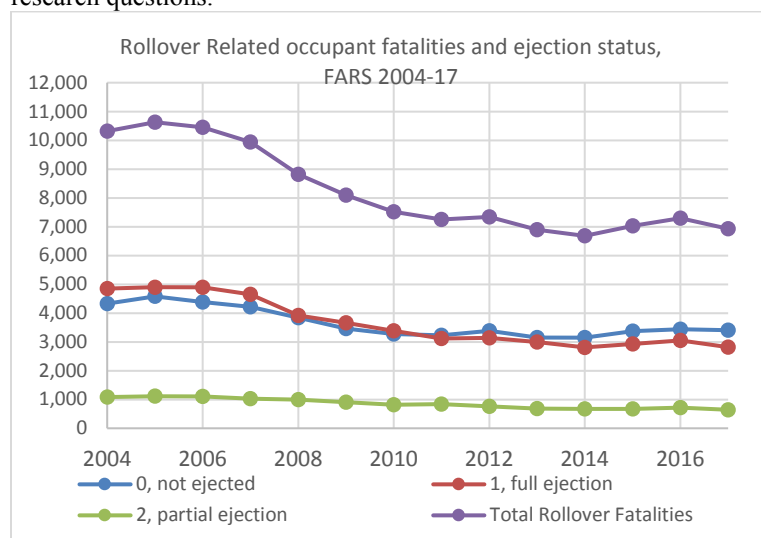


Figure 2: Rollover-crash related occupant fatalities and ejection status (FARS 2004-2017, car or light truck/van GVWR ≤10,000 lbs.)

Figure 2 provides the rollover-related fatality 14-year trends using FARS 2004-2017 for occupants of light passenger vehicles (cars and light trucks/vans GVWR <= 10,000 lbs.). The total occupant fatalities due to rollover crashes decreased from 10,627 in 2005, to a lower 6,681 in 2014, and then slightly increased to approximately 6,933 in 2017. The annual average of rollover-related occupant fatalities was 8,227 during 2004-2017. Figure 2 shows the ejection status of either ‘not ejected’, ‘partial ejection’, or ‘full ejection’ out of all rollover-related occupant fatalities, and the occupant fatalities include the occupants (driver or passenger) in the motor vehicles-in-transport only (not including the vehicles-not-in-transport).

For passenger cars and light trucks /vans, the percentage (%) of rollover-related occupant fatalities among all occupant fatalities dropped from the high peak of approximately 35% during 2008-09 to the lower values of approximately 31% in 2016 and 30% in 2017, and this percentage decreasing trend was especially obvious during 2011-2017, as shown as Figure 3. The extensive efforts for higher fitment of vehicle stability control and stronger roof designs may have helped to reduce the rollover-related fatality percentage during recent years. ^{1,3}

Vehicle rollovers often result in occupant ejections. Figure 4 shows ejection paths of light passenger vehicle occupants during rollovers. The average number of occupant fatalities during ejections out of the roof opening (sunroof, moonroof or others) is 87 during the 14 years of 2004-2017, but this number is higher, 97 and 109, in 2015 and 2016, respectively. Figure 4 also indicates that the ‘side windows’ are the most frequent ejection path, with an average of 773 fatalities during 14 years. The highest number of fatalities from side window ejection occurred in 2005 (1064), while the lowest occurred in 2016 (593) and in 2017 (576). The occupant fatalities associated with various known ejection paths (e.g., side windows, roof, etc.) are approximately 15% of rollover-related fatalities (unknown ejection paths are commonplace and FARS data contain complete fatalities but only partial injuries).

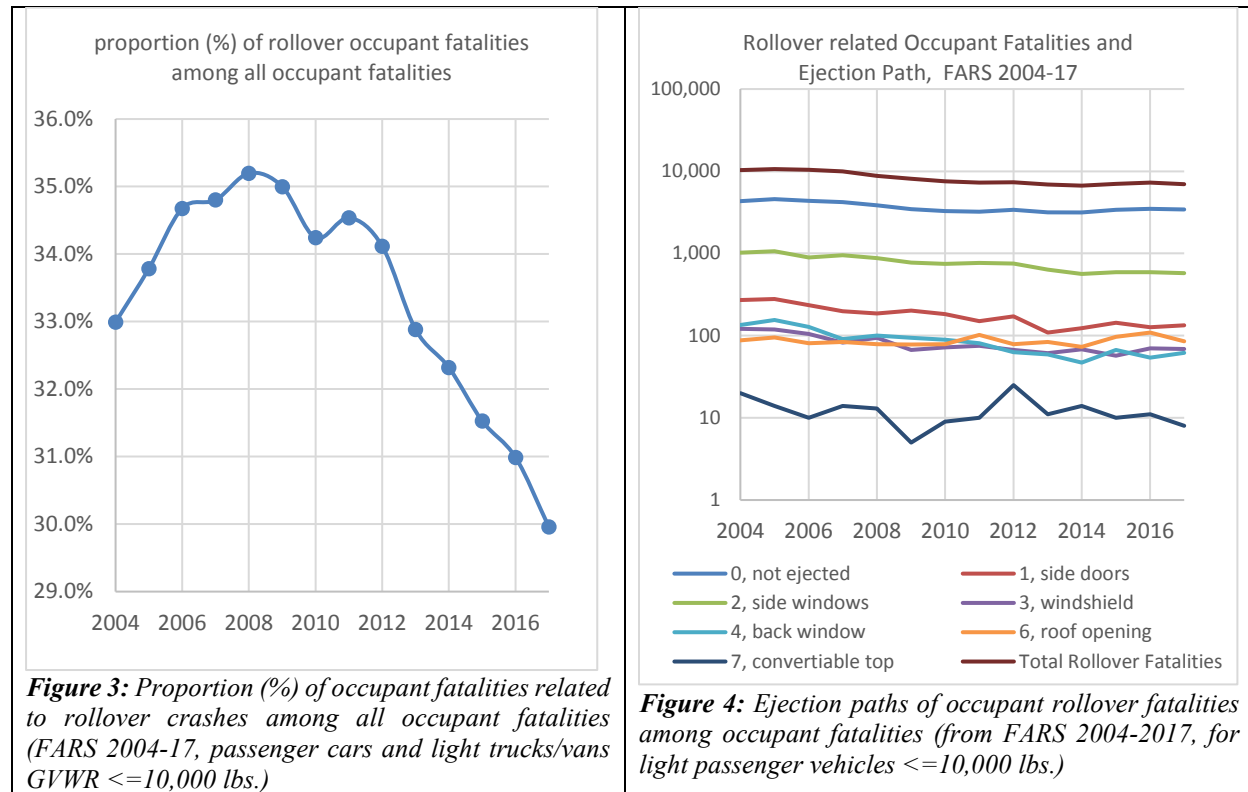


Figure 3: Proportion (%) of occupant fatalities related to rollover crashes among all occupant fatalities (FARS 2004-17, passenger cars and light trucks/vans GVWR <=10,000 lbs.)

Figure 4: Ejection paths of occupant rollover fatalities among occupant fatalities (from FARS 2004-2017, for light passenger vehicles <=10,000 lbs.)

When rollovers occur, belt or restraint use is critically important to occupant safety. Although FARS does not contain details of specific injuries, the data clearly indicate the belt effect by relative comparison of injuries of ‘unbelted’ occupants versus the ‘belted’ (Table 1). In Table 1, the unbelted group has a fatal incidence of 70,796/105,521 = 67.1%. However, in the belted group, the fatal incidence is 33,423/84,441 = 39.6%.

Table 1: Belt use status and occupant fatalities related to rollover crashes (light passenger vehicles GVWR <=10,000 lbs., FARS 2004-2017)

Belt status	Fatal Injury	Not fatal	Total Occupants
Unbelted	70,796	34,725	105,521
Belted Occupants	33,423	51,018	84,441

Hence, the relative risk (RR) of fatal injury when unbelted versus belted is $0.671/0.396=1.7$; and the fatality Odds Ratio (OR) of unbelted versus the belted is 3.1. The interpretation is that an unbelted occupant's odds of fatality are approximately 3 times compared with the belted occupant, if a rollover occurred. In this comparison, only one risk factor (belt use) is considered without considering other risk factors. Similar two-by-two table can be made for heavier vehicles with GVWR over 10,000 lbs. If multiple risk factors of belt use, occupant age, travel speed (crash severity, or delta-V), and rollover are considered simultaneously, a multiple regression approach is discussed in section 5.

3. ROLLOVER TREND FROM GES

To examine how many vehicles are involved in rollovers annually, GES 2006-15 weighted data from 36 Primary Sampling Units (PSU) can provide more general annual trends and populations of crashes of various vehicle types and injuries of all person types. The weighted annual averages of light vehicles and other vehicle types, if involved in rollover crashes during 2006-2015, are listed as Table 2.

Table 2: Weighted Annual Vehicle Types Involved in Rollover Crashes (GES 2006-15, including all model years)

Year	combination truck	Single unit truck	bus	car & light truck /van
	GVWR >10,000 lbs.			<=10,000 lbs
2006	9,769	5,645	55	251,543
2007	9,461	5,385	111	263,058
2008	7,303	4,307	67	248,543
2009	6,333	3,117	0	213,675
2010	6,344	2,916	17	189,445
2011	6,343	2,722	233	184,867
2012	8,124	4,442	229	196,236
2013	7,046	3,809	139	184,082
2014	9,047	4,030	20	199,734
2015	6,909	4,698	0	193,349
Total	76,678	41,070	871	2,124,530

The weighted averages of light passenger vehicles (GVWR <=10,000 lbs.) involved in rollovers from GES data may be used as a reference to the similar rollover results from CDS data.^{6, 7}

4. ROLLOVER AND INJURED OCCUPANTS FROM CDS

CDS data, that are survey data from 24 PSU and focused on the crashes of light passenger vehicles (GVWR not more than 10,000 lbs.), include details of occupant injuries and vehicle crash conditions. Recent CDS data (from 2013-2015 mainly) are used in this study to explore occupant injuries from rollover crashes. In CDS, occupant injuries are coded using AIS, a numerical scale system by Association for the Advancement of Automotive Medicine (AAAM) to rate

the injury severity (e.g., AIS 0=not injured, 1=minor injury, 2=moderate injury, 3=serious injury, 4=severe injury, 5=critical injury, 6=maximum injury or fatal, 7=injured but severity unknown), although a high percentage of AIS codes are missing or unknown. In CDS data, each occupant injury is assigned an AIS severity level and each injured body region has a maximum severity AIS injury level within that body region. Also, one value of overall Maximum AIS (e.g., MAIS, the maximum AIS severity from all body regions) for each occupant, hence, each occupant has one count of MAIS and may have several regional AIS results. The data flow-chart of Figure 1 is used extensively for CDS data analysis, this flow-chart analyzed the ‘top-down’ data structure in CDS and searched the vehicle crashes and occupant injury details from ‘Accident’ to ‘Vehicle’, then to ‘Occupant’, and finally ‘Injured Body Region’ or ‘Contact Source’ were searched. All listed results are from weighted data calculations (Tables 3-7 and Figures 5-15).

CDS survey data are associated with weighting factor for each crash, the general ‘weighted population mean’, \bar{y} , is defined by following formula: ^{6, 8, 13}

$$\bar{y} = \frac{\sum_{i=1}^n \omega_i y_i}{\sum_{i=1}^n \omega_i} \quad \text{Eq. (1)}$$

where ‘ y_i ’ is the value of ‘i-th’ unit or crash, and ‘ ω_i ’ is the weighting factor associated with ‘i-th’ unit or crash. The weighting factors in CDS came from the three-stage sampling designs, in which the selection of each PSU among 24 PSUs, the probability of crashes selected by police in each PSU, and the selections of various crash severities /types were considered statistically, stage-by-stage. ^{6, 8}

4.1 Cars and Light Trucks Involved in Rollovers and Occupant Injury Comparison

First, overall numbers of vehicles (passenger cars and light trucks) involved in ‘rollover’ crashes or ‘non-rollover’ crashes were obtained. ‘Rollovers’ were further categorized as “side rollovers 1-3 quarter”, “side rollover ≥ 4 quarters” (quarter refers to number of quarter turns during the rollover, each quarter is 90 degrees of revolution), and “end to end rollover /tilt”; non-rollover crashes were categorized as single vehicle plane damaged (front damage, side damage, rear damages or top/under damage), or multiple vehicle planes damaged, as described in Figure 5 and Table 3. Secondly, the number of occupants injured from passenger cars and light trucks was determined, from both rollover and non-rollover crashes (Table 4).

During the years of 2013-2015, approximately 161,000 (annual weighted average including all model years) passenger cars and light trucks were involved in rollover crashes, and rollover crashes comprised approximately 6% of all crashed vehicles of approximately 2.7 million annually, shown in Table 3. Furthermore, Table 3 shows that passenger cars experienced a smaller percentage of rollover crashes (3.7%) among all car crashes than the light trucks (10.3%).

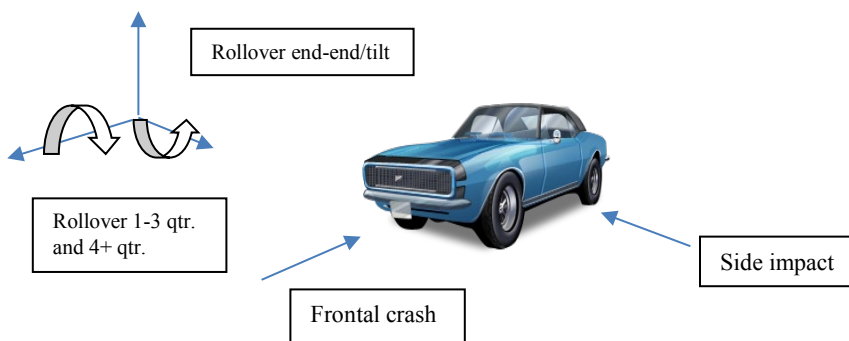


Figure 5: The rollover types of light passenger vehicles (car or light truck/van in CDS, GVWR $\leq 10,000$ lbs.)

Table 3: Annual weighted averages of passenger car and light truck/van crash types ('Rolled' and 'non-Rolled', CDS 2013-2015, GVWR <=10, 000 lbs.)

Crash Types of Passenger Cars	Crash Modes of Light Trucks/Vans
Rollovers 1-3 Quarter: 48,063 Rollovers 4+ Quarter: 19,050 Rollovers end-end: 815	Rollovers 1-3 Quarter: 53,225 Rollovers 4+ Quarter: 39,188 Rollovers end-end: 641
Total Rolled Cars: 67,928	Total Rolled Trucks: 93,054
single front damage: 229,309 single side damage: 76,927 single rear-damage: 4,796 single top/under damages: 9,904 multiple front damage: 807,459 multiple side damage: 407,182 multiple rear-damage: 194,483 multiple top/under damages: 1,948	single front damage: 103,484 single side damage: 25,215 single rear damage: 529 single top/under damage: 1,636 multiple front damage: 416,958 multiple front damage: 190,947 multiple front damage: 69,461 multiple front damage: 527
Total non-Rolled Cars: 1,732,008	Total non-rolled Trucks: 808,757

It is known that light trucks or vans, in general, have higher centers of gravity than passenger cars, and Table 3 using CDS 2013-2015 indicated that light trucks or vans tend to rollover more frequently than passenger cars.

The occupant injury rates from passenger cars and light trucks/vans were different, too, which shared the similar trends as vehicle crash data of Table 3. From a perspective of injured occupants within light passenger vehicles, Table 4 indicates that passenger car occupants (injured or not) involved in rollovers count approximately 3.4%, or 83,917 divided by (83,917+2,359,792) of all car crash occupants; while the light truck/van occupants involved in rollover crashes count approximately 10.3%, or 134,146 divided by (134,146+1,170,789). All model years of light vehicles were included in Tables 3, 4.

Table 4: Annual weighted Averages of Occupant Injuries (MAIS) of Light Passenger Vehicles (CDS 2013-15, Rollover, 'R', vs. Non-Rollover, 'N')

Car Occupant Injuries (by MAIS)							
	unknown	MAIS=0	1	2	3 -6	7	Total
R	39,137	16,295	19,557	4,438	2,813	1,676	83,917
N	1,059,612	834,998	347,400	65,381	19,987	32,414	2,359,792
Light Truck/Van Occupant Injuries (by MAIS)							
	unknown	MAIS=0	1	2	3 -6	7	Total
R	90,526	11,923	24,608	3,460	3,037	591	134,146
N	564,165	440,081	128,403	22,698	6,178	9,263	1,170,789

Passenger car occupants are more likely to be seriously injured when in a rollover crash, compared with a non-rollover. Table 4 indicates that approximately 2,813 car occupants are seriously injured (MAIS =3,4,5,6) in rollover crashes annually (weighted data of MAIS 3=1948, MAIS 4=479, MAIS 5=212, MAIS 6=174), which is 4.2% of the total number of injured car occupants in rollovers (MAIS not 0, or 67,622 annually). For non-rollover crashes, approximately 19,987 car occupants are seriously injured (MAIS = 3,4,5,6) (14,532 + 3737 + 1169 + 549), or only 2.7% of all injured car occupants (MAIS not 0, or 730,708 annually) of non-rollover cars. Hence, rollover crashes usually result in more serious injuries than other crash types for car occupants.

For light trucks/vans, seriously injured occupants (MAIS =3,4,5,6) make up of 2.5% of all injured occupants in rollovers (MAIS not 0). For non-rollovers, seriously injured occupants (MAIS = 3,4,5,6) of light trucks/vans are only 0.85% of all injured light truck occupants (MAIS not 0). Thus, in rollover crashes, light truck/van occupants (2.5%) have lower serious injury rate than car occupants (4.2%). This injury severity difference may possibly be due to smaller head room in cars compared with light truck/vans, meaning that the occupant head and /or neck may be more likely injured from contacting the roof in a car. Occupant contacts and injury sources will be examined using CDS

data in a subsequent section of this study. The difference between roof designs and roof strengths associated with car and light truck/van may also contribute to the occupant injury severities,^{2,5} and more future research may shed a light on this challenging topic.

4.2 Rollovers and Ejection Areas of Light Passenger Vehicle Occupants

Since 2009, CDS data collected the crashes from vehicle age ≤ 10 only, hence, the sample sizes could be smaller after 2008.⁸ Figure 6 provides yearly trends of occupant injuries (MAIS 2-7) including all vehicle ages and vehicle age ≤ 10 years old, respectively. This study also focuses on the crash data of recent years, 2013-2015.

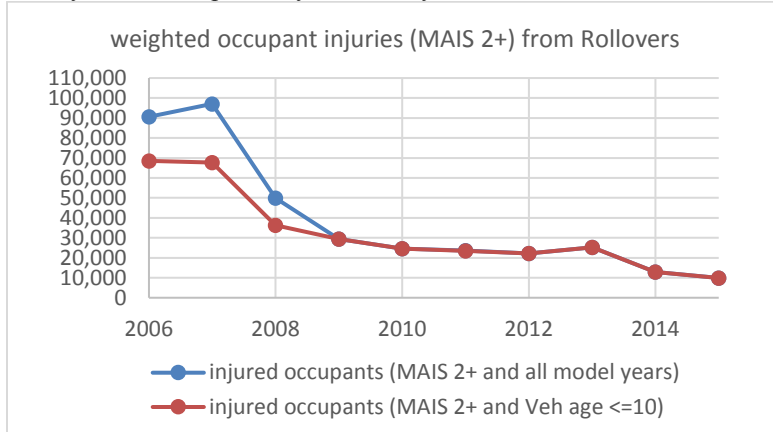


Figure 6: Weighted occupant injuries (MAIS 2+) related to rollovers (CDS 2006-2015 light passenger vehicles including all model years, and vehicle age ≤ 10 , respectively)

As discussed previously, rollovers are usually associated with occupant ejections. Figure 7 shows annual averages of ejection areas related to rollovers (CDS 2013-2015 including all vehicle model years and occupant injury levels). Occupants were more frequently ejected from the front side windows (left or right) and roof opening. In CDS 'OA' data file, there are four variables that are insightful to rollover and ejection details - 'ejection' (partial or full ejection status), 'ejection area' (windshield, left or right front, or roof, and 'ejection area' in CDS data is similar to the variable of 'ejection path' in FARS data), 'ejection medium' (non-fixed roof, fixed or non-fixed glazing, or integral structure), and 'entrapment' (entrapped or not, jammed door/fire).^{20,21} This paper will not include all related data explorations due to the paper size limit. All CDS data analysis included the occupants who were within the rolled vehicles or ejected, only Table 6 focused on the ejected occupants of rolled vehicles. Also, the CDS analytical results including AIS2+ could have much larger sample sizes than the similar results including AIS 3+ only, and the missing or unknown AIS, ejection status, and several key variables are still commonplace.

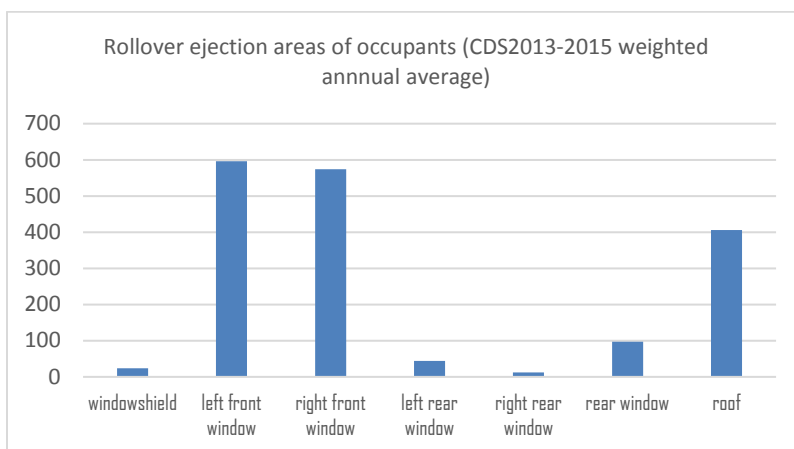


Figure 7: Annual weighted average of ejection areas related to rollovers (CDS 2013-2015 light passenger vehicles with all model years)

4.3 Injured Body Regions and Vehicle Contacts Related to Rollovers

When occupants are involved in rollover crashes, they are most frequently injured in the body regions of head, neck, and chest.^{2,3} CDS data of Occupant Injury (OI) contain very detailed descriptions of injured body regions and injury contact sources of vehicle components. Again AIS, a numerical scale system by AAAM to rate the injury severity, is used here to describe the injured body regions. ‘OI’ data file is merged together with general vehicle (GV) and occupant assessment (OA) data especially during 2013-15 (Figure 1). This study intends to explore several questions about rollover crashes and related injuries: one question may be what are the commonly injured body regions (head, face, chest or others)? What are common injury sources of vehicle components (e.g., roof, door, B-pillar) that contact the occupant in rollovers?

For rollover crashes (including vehicle age ≤ 10 years old), the main injured body regions (AIS 2+) are head, chest, shoulder and back, and neck (Figure 8).

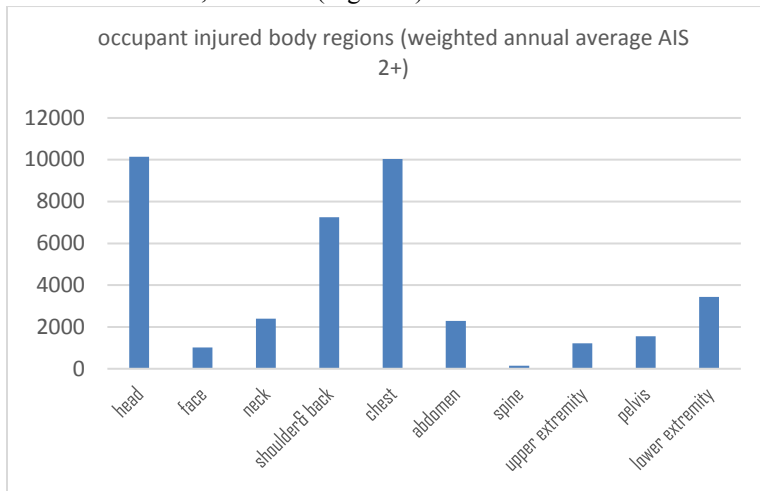


Figure 8: Annual weighted average of injured body regions (AIS 2+) due to rollovers (vehicle age ≤ 10 years, CDS 2013-2015)

When a vehicle is involved in a rollover crash, some vehicle components are more likely to contact the occupants (driver and passenger), and these vehicle components become so called ‘injury contact sources’. The main injury sources associated with AIS 2+ injuries in rollover crashes are roof, left side door/interior, instrument panel and seat back, as indicated by Figure 9.

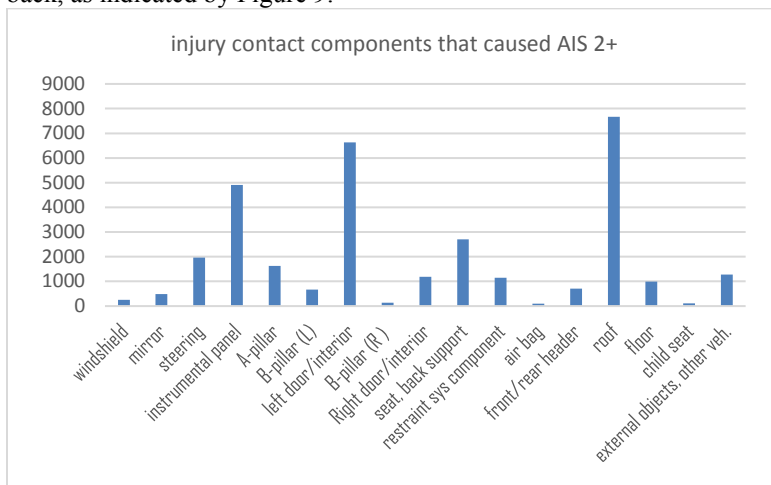


Figure 9: Annual weighted average of injury vehicle component sources that caused AIS 2+ from rollovers (vehicle age ≤ 10 years), CDS 2013-2015

4.4 Injured Body Regions by Roof Contact Only Associated with Rollover

Injuries caused by the interaction between occupants and the vehicle roof only, when rollovers occurred, are of special interest in this study. Figure 10 shows the weighted average of injured regions, especially three body regions of head, neck, and shoulder /back, due to contacting the roof during rollovers (vehicle age ≤ 10 years and AIS 2+, CDS 2013-2015). The interaction odds between the roof and head were especially high if a rollover crash did occur.

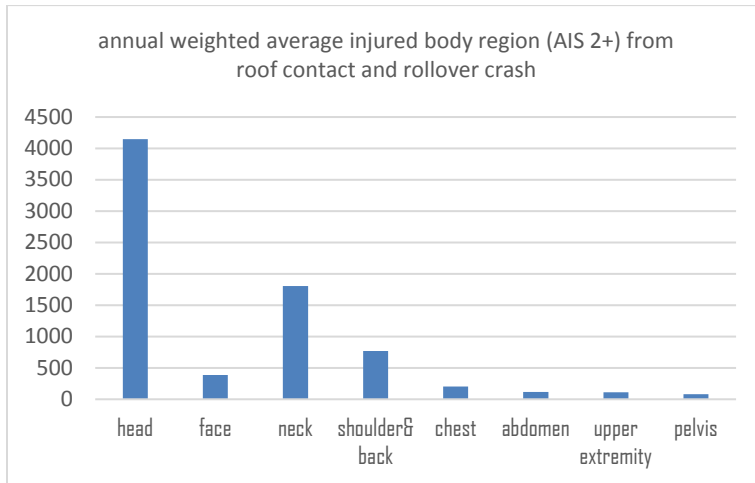


Figure 10: Annual weighted average of injured regions due to contacting roof only of rolled vehicles (vehicle age ≤ 10 years and AIS 2+, CDS 2013-2015)

If additional years are included and CDS 2006-2015 data are used, Figure 11 shows that if the roof was the injury source and rollover occurred, the main injured body regions are head, neck, shoulder/back, and face. CDS 2006-2015 data provide a yearly trend of roof caused injured body regions when the vehicles were involved in rollover, where vehicle age, determined by (crash year – model year), is limited not more than ten years old. The weighted annual averages of injured body regions were lower during 2013-2015 than the similar averages of 2006-2009. This study also explored AIS results related to rollovers /ejections with vehicle age under 3-4 years only, but the sample sizes were small especially during 2011-2015 (not listed in this study).

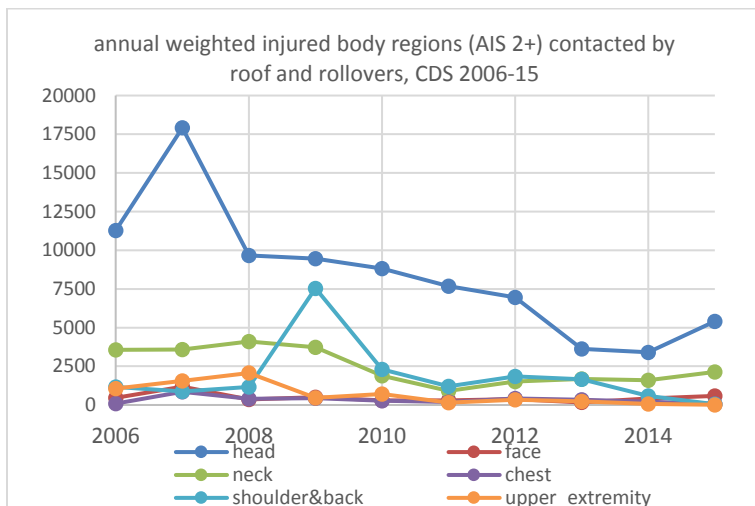


Figure 11: Annual weighted injured body regions (AIS 2+) related to rollover crashes and roof contact only (vehicle age ≤ 10 years, CDS 2006-15)

5. ANNUAL TREND OF ROLLOVER INJURIES AND MULTIPLE RISKS

This section explored the yearly trends of rollover-related occupant injuries using CDS 2006-2015. In this trend analysis, MAIS is used to describe the overall maximum severity injury sustained by an occupant during 10-year span. Then a more general correlation investigation of occupant injuries is done by a multiple regression approach, when various risk factors, including rollover, side or longitudinal impact, delta-V, occupant age and belt use, are considered, simultaneously.

5.1 Occupant Injury Yearly Trend from Rollovers

The injured occupants involved in the rollover crashes per year, using MAIS versus calendar year during ten years (CDS 2006-2015), is shown as Table 5 and Figure 12, where only vehicle ages <=10 years old are included. It can be observed that the weighted injured occupants decrease after 2009, the injured occupant number could be even smaller, if only newer vehicles of vehicle ages not older than 4, or 2 years old are included.

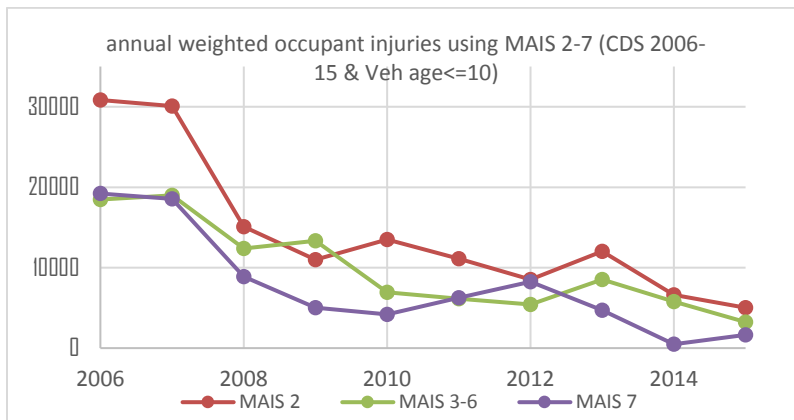


Figure 12: Annual weighted occupant injuries (MAIS) related to rollovers crashes (CDS 2006-2015 including vehicle age <=10 years only)

Table 5: Weighted annual averages of occupant MAIS from rollovers crashes (CDS 2006-15 including vehicle age <=10 years only)					Table 6: annual weighted injuries (MAIS) of both "rolled vehicle and ejected occupant" (CDS 2006-15 and vehicle age <=10 years only)				
YEAR	MAIS 1	MAIS 2	MAIS 3-6	MAIS 7	YEAR	MAIS 1	MAIS 2	MAIS 3-6	MAIS 7
2006	102,036	30,839	18,478	19,210	2006	2022	3325	9159	1996
2007	132,423	30,069	18,984	18,568	2007	4751	2930	8412	1835
2008	125,774	15,106	12,383	8,873	2008	3416	4409	4868	344
2009	58,890	10,989	13,342	5,043	2009	2469	1118	3682	409
2010	54,688	13,515	6,916	4,174	2010	2256	1746	2852	300
2011	38,965	11,128	6,144	6,273	2011	301	722	2462	169
2012	35,849	8,529	5,439	8,235	2012	595	504	1406	118
2013	35,557	12,022	8,529	4,694	2013	350	521	1997	252
2014	71,256	6,622	5,776	483	2014	966	186	331	93
2015	25,684	5,021	3,237	1,626	2015	69	678	970	709

Table 5 provides the annual weighted occupant MAIS results including vehicle age <=10 years old. If newer vehicle models are preferred with the consideration of FMVSS 216a and 226, the similar occupant MAIS tables, including vehicle age <=4, and <=2 years old, respectively, are listed in Table 5b and 5c in Appendix.

Occupants involved in a rollover crash, and who were also ejected, are shown in Table 6 (with much fewer occupants than Table 5), and Table 6 provides MAIS for each year (CDS 2006-15, and vehicle ages <=10 years old). The ejection rates of occupants of rolled vehicles were related to their MAIS levels: the MAIS 3-6 group had the highest ejection

rate of 36% approximately, the ejection rate for MAIS 2 was 11% approximately, while MAIS 1 had the lower rate of 2.5% (from Tables 5, 6).

Furthermore, if rollover crashes occurred, following Figures 13-14 show the annual injured occupant body regions (AIS 2+) using weighted CDS data during 2006-2015. It can be observed that head and shoulder /back injuries are most frequent, together with other injured body regions of face, neck, chest, upper and lower extremity areas.

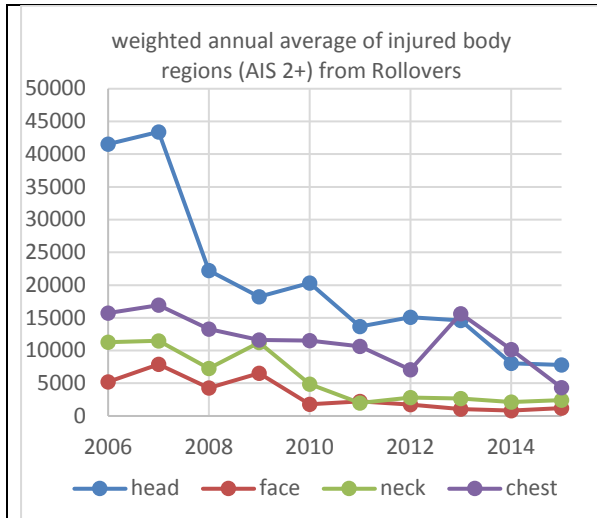


Figure 13: Annual weighted average of injured body regions (AIS 2+) related to rollover crashes (vehicle age <=10 years, CDS 2006-2015)

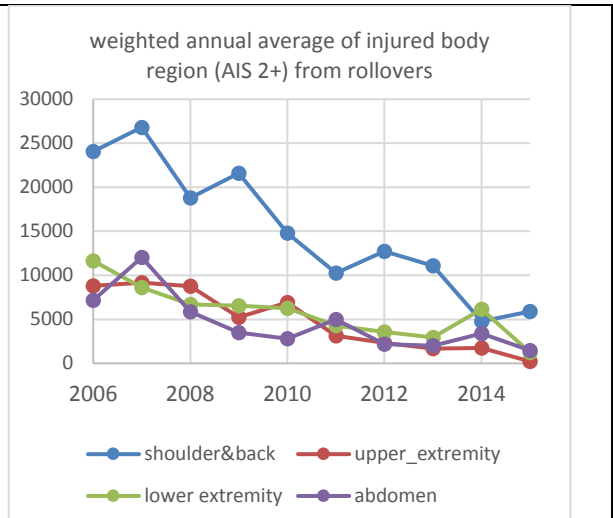


Figure 14: Annual weighted injured body regions (AIS 2+) related to rollover crashes (vehicle age <=10 years, CDS 2006-2015)

5.2 Occupant Injury Modeling with Consideration of Multiple Risks Simultaneously

The goal here is to establish a correlation between the occupant injuries (the outcome) and some contributing risk factors (the independent variables). The risk factors may include various crash types (rollover, side or longitudinal impact), delta-V, belt use and others. Many risk factors contribute to occupant injuries simultaneously, and some factors are more significant than others. Most CDS data are categorical data and are convenient to use for logistic regression. The logit model explores the relative risk of two different crash conditions and the impact from each risk factor on occupant injury severities. Some variables in CDS can be treated as binary data, e.g., injured body regions of AIS being ‘3, 4, 5, 6’ were treated as ‘serious and fatal injury’ case (or ‘1’, dependent variable), while AIS (0, 1, 2, 7) as not-serious case (or ‘0’, dependent variable). Similarly, the common independent factors in the logit model include ‘rollovers, or 1’ vs. ‘not-rollover, or 0’, front seating occupant vs. rear-seating, side impact vs. frontal crash. This study also explored the effect of vehicle age on occupant injuries, and vehicle age is determined by (crash year – model year). The regression modeling intended to consider the impacts on occupant injuries from main risk factors, although not all factors can practically be included in this modeling. The modeling data came from CDS 2006-15, including any crash types, all AIS levels, and vehicle age <=10 years.

Several references provide excellent introduction to logistic regression and categorical data analysis.^{13 14 17} Statistical correlation between the outcome and the independent variables is described as Eq. (2), from this correlation modeling it is possible to compare the occupant injury severity odds ratios (OR) between two very different crash conditions – for example, these include comparing the effects between rollovers versus not-rollovers; higher Delta-V (>35 MPH) versus lower delta-V; ‘not-belted’ occupants versus ‘belted’ occupants; furthermore, to compare side crashed vehicle with frontal crashed one; to compare smaller vehicle size (<3,000 lbs.) with the relatively larger sizes; or to compare older occupant (>65 years old) vs. the younger. This multiple regression model considers the effects of these primary eight risk effects on occupant injuries, simultaneously, as Eq. (2):

$$\ln\left(\frac{p}{1-p}\right) = \beta_0 + \beta_1 VehAge + \beta_2 DeltaV + \beta_3 VehSize + \beta_4 Belt + \beta_5 Rollover + \beta_6 DamageArea + \beta_7 Seating + \beta_8 OccupAge \quad (2)$$

In Eq. (2), ‘ln’ is the natural log sign, ‘p’ is the probability of ‘occupant serious injury (AIS =3,4,5,6)’, and ‘ $\frac{p}{1-p}$ ’ is the odds of ‘occupant serious injury’ versus ‘not serious injury’. This statistical modeling, using SAS procedure of ‘SurveyLogistic’^{16,17} that considers the PSU and sampling weights, provides the serious injury odds ratio (OR) results from eight risk factors, as summarized in Figure 15 and Table 7. Missing data are included and SAS procedures usually handle the missing data reasonably well. The large percentage of unknown or missing AIS could make it challenging to build a correlation model. The receiver operating characteristic (ROC) curve is used to give a measure of the predictive accuracy of a logistic regression model, and ROC curve displays the sensitivity and specificity of the model. The area under the ROC curve, measured by ‘c statistic’, is still relatively low (0.68), and future correlation modeling of using more complete AIS information and with more than eight independent risk factors in Eq. (2) may be desired.

Data Interpretation of Table 7 or Figure 15:

Results indicate that higher occupant serious injury risks are significantly associated with rollover crashes, OR=1.74 (95% confidence interval 1.31 to 2.31, with a significant p-value of 0.0001), e.g., the occupants of rollover vehicles would be 74% more likely seriously injured (AIS 3+) when compared with the occupants of not-rolled vehicles. Similarly, higher injury risk is associated with higher delta-V (>35 MPH, OR=5.59), ‘not-belted’ (OR=3.26, 95% confidence interval 2.63 to 4.04), side crash (OR=1.54), and older occupant age (OR=2.69). On the other hand, older vehicles (>4 years), seating row, and smaller vehicle size (under 3,000 lbs.) did not have significant impact on occupant injuries (with p-values more than 0.05). Figure 15 clearly indicates that three highest risk factors come from higher Delta-V >35 MPH (driving speed or crash severity), ‘not using belt’, and old occupants, and rollover crash is also a significant risk factor.

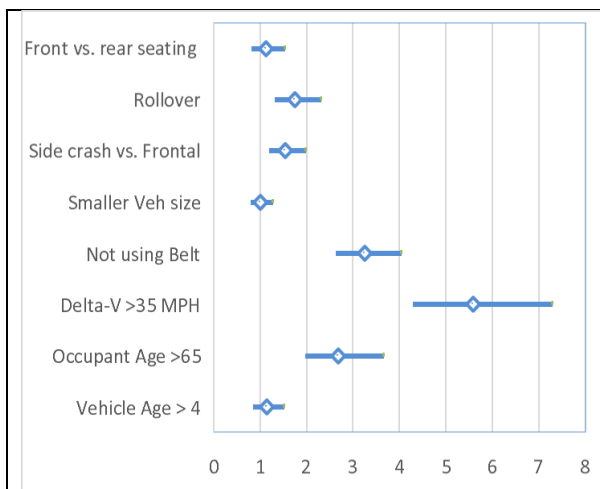


Figure 15: Odds Ratios (Means and 95% Confidence Intervals) of Occupant Serious Injury (AIS 3+), including several risks simultaneously (CDS 2006-15 vehicle age <=10)

Table 7: Odds Ratios (means and 95% Confidence Intervals) of Occupant Serious Injuries (CDS 2006-2015 including vehicle age <=10)

Effect	Point Estimate	95% Wald Confidence Limits		p-Value
Vehicle Age > 4	1.136	0.849	1.522	0.3910
Occupant Age >65	2.686	1.969	3.664	<.0001
Delta-V >35 MPH	5.591	4.282	7.299	<.0001
Not using Belt	3.257	2.625	4.041	<.0001
Smaller veh size	1.004	0.788	1.279	0.9748
Side impact vs. Frontal crash	1.543	1.197	1.990	0.0008
Rollover	1.740	1.308	2.314	0.0001
Front vs. rear seating	1.123	0.815	1.546	0.4778

6. CONCLUSIONS AND DISCUSSIONS

FARS and CDS data systems were used to explore the occupant injuries related to vehicle rollover crashes and occupant ejections, while GES vehicle data could also be used as a reference to CDS data. This data analysis used a simple approach of ‘step-by-step’ approach – e.g., from annual occupant fatalities in FARS data to the vehicles involved in rollovers in both GES and CDS data; from the rollover-related occupant injuries with overall MAIS to the detailed injured body regions (AIS) and injury contact sources (roof or side doors). Finally, this study viewed occupant injuries from a bigger picture by considering multiple risk factors simultaneously. Some key findings from this study are –

- The FARS data indicated annual rollover-caused fatalities decreased from around 10,500 in 2004-2006 to approximate 7,000 in 2014-2017, approximately one thirds of all occupant fatalities of light passenger vehicles are from rollover crashes, but the percentage of rollover-related occupant fatalities among all occupant fatalities

dropped sharply during 2011-2017. The number of both rollover and ejection-caused fatalities decreased from approximately 6,000 in 2004-2006 to 3,600 in 2014-2017. The occupant fatalities associated with various known ejection paths (e.g., side windows, roof, etc.) were approximately 15% of rollover-related occupant fatalities.

- CDS 2013-2015 weighted survey data showed approximately 161,000 light vehicles (cars and light trucks/vans, GVWR \leq 10,000 lbs.) were involved in rollovers (similarly, GES data were also used to estimate the rolled vehicles), and approximately 190,000 occupants of light passenger vehicles were injured (MAIS 1+) annually related to rollovers.
- Rollover crashes tend to be more likely associated with light trucks/vans than passenger cars, and this may be possibly due to higher centers of gravity in light trucks, however, if rollovers did occur, the passenger car occupants were more likely to be seriously injured (MAIS =3,4,5,6) than the light truck/van occupants.
- The CDS data indicated that rollover injuries (especially AIS 2+) were strongly associated with the injury sources of the vehicle roof, side doors, instrumental panes, and seat back/support; and rollover crashes also resulted in primarily the injured body regions of head, shoulder/back, neck, and chest.
- When a rollover crash occurred, contact between occupant and roof primarily caused head injury, as well as neck and shoulder/back injuries.
- The ejection rates of occupants of rolled vehicles were significantly related to their MAIS levels from CDS 2006-15: the MAIS 3-6 group had the highest ejection rate of 36% approximately, the ejection rate for MAIS 2 was 11%, while MAIS 1 group had the lower rate of 2.5%.
- A multiple logit regression was used, with considerations of all crash types and multiple risk factors simultaneously, to predict the occupant injury relative risks of several risk factors, e.g., comparing rollover versus not-rollover, belted occupants versus not-belted, higher delta-V versus lower. It was found that higher occupant injury risks are significantly associated with rollover crash (OR=1.74), delta-V $>$ 35 MPH (OR=5.59), not-belted (OR=3.26), side impacts (OR=1.54), and older occupant age $>$ 65 (OR=2.69). On the other hand, older vehicles ($>$ 4 years), seating position, and relatively smaller vehicle size did not have significant impact on occupant injuries with p-values $>$ 0.05.
- This study paid close attention to data structures and data sorting, data appending vertically and data merging horizontally, logic design of flow-chart, and vehicle crash type identifications using key research variables.
- With consideration of FMVSS 216a and 226 that focused on the newer vehicles after 2011, this study explored the effect of vehicle age and focuses on the recent crash data (CDS 2013-15), the rollover-related occupant injuries, including vehicle age \leq 2, \leq 4, and \leq 10 years old, respectively, are listed, but CDS database is still limited by the sample size, especially if only model years after 2011 are included.
- CDS data analysis is also limited by the high percentages of missing or unknown values of some key variables, such as delta-V, rollover/ejection status, and AIS.
- Overall, this study may enrich the understanding of rollover crashes, ejections and occupant injuries from using recent crash data. Future data analysis, using both NASS Crash Investigation Sampling System (CISS) and Crash Reporting Sampling System (CRSS) data starting since 2016 that are collected from more PSU, may provide more insights of rollover crashes, ejections, and occupant injuries.

7. REFERENCES

1. Summers, S., Willke, D. T., Sullivan, L. K., Duffy, (2007). NHTSA's crashworthiness rollover research program. (Paper No. 05-0279). Proceedings of the 19th International Technical Conference on the Enhanced Safety of Vehicles (ESV), Washington, D.C., June 6-9, 2005.
2. Strashny, A. (2007), "An Analysis of Motor Vehicle Rollover Crashes and Injury Outcomes", DOT HS 810 741, Washington DC.
3. Ridella, S.A. and Eigen, A.M. (2008), "Biomechanical Investigation of Injury Mechanisms in Rollover Crashes from the CIREN Database", *Proceedings of the International IRCOBI Conference on the Biomechanics of Injury*, Bern, Switzerland, pp. 33-47, 2008.
4. Ridella, S.A., Eigen, A.M., Kerrigan, J.R. and Crandall, J. (2009), "An Analysis of Injury Type and Distribution of Belted, Non-Ejected Occupants Involved in Rollover Crashes". *Annals of Advances in Automotive Medicine*, Vol. 53, 2009.
5. Austin, R. (2010), "Roof Strength Testing and real-World roof intrusion in rollovers", DOT HS 811 365.

6. NCSA /NHTSA (1998). *National Automotive Sampling System Crashworthiness Data System Descriptive Summary, 1996-98 Update*, National Highway Traffic Safety Administration, Washington DC.
7. Shelton, T. (1991). "National Accident Sampling System, General Estimates System Technical Note, 1988 to 1990", Report No. DOT HS 807 796. Washington, DC: National Highway Traffic Safety Administration.
8. Zhang, F., & Chen, C-L. (2013). *NASS-CDS: Sample Design and Weights*, (Report No. DOT HS 811 807), Washington, DC.
9. Ridella, S., Kuppa, S., Martin, P., McCullough, C., Rudd, R. W., Scarboro, M. (2007). NHTSA's Vision for Human Injury Research. (Paper Number 07-0043). 20th Enhanced Safety of Vehicles, 2007, Lyon, France.
10. Wu, J., Subramanian, R. & Craig, M. (2013), "The effect of earlier collision notification on Traffic fatality using Survival Analysis", *J. of Traffic Injury Prevention*, 8/2013.
11. Lee, E., Wu, J., Kang, T. and Craig, M. (2017), "Estimate of mortality reduction with implementation of advanced automatic collision notification", *J. of Traffic Injury Prevention*, Vol. 18, 2017.
12. Sharma, D., Stern, S., Brophy, J., & Choi, E-H. (2007), An Overview of NHTSA's Crash Reconstruction Software WinSMASH. (Paper No. 07-0211). 20th Enhanced Safety of Vehicles Conference, France, 2007.
13. Korn, E., & Graubard, B. (1999). *Analysis of Health Surveys*. New York: John Wiley & Sons.
14. Hosmer, D. and Lemeshow (1999), *Applied Logistic Regression*, John & Wiely.
15. Hosmer, D. and Lemeshow (2000), *Applied Survival Analysis*, John & Wiely.
16. SAS Institute (2005), *Categorical Data Analysis using Logistic Regression*, SAS Publishing.
17. SAS Institute (2005), *Design and Analysis of Probability Surveys*, SAS Publishing.
18. Conroy, C., Hoyt, D, Eastman, A.B, etc. (2006), "Rollover crashes: Predicting serious injury based on occupant, vehicle, and crash characteristics", *Accident Analysis and Prevention*, 38 (2006).
19. Kuppa, S., Wang, J. and Haffner, M, "Lower extremity injuries and associated injury criteria", Paper No 457, Proceedings of ESV 2001, NHTSA, US DOT.
20. NHTSA (2018), "Fatality Analysis Reporting System (FARS) Analytical User's Manual", National Center for Statistics and Analysis (NCSA), NHTSA, Washington DC.
21. NHTSA (2014), "National Automotive Sampling System–Crashworthiness Data System (CDS) - Analytical User's Manual, NHTSA, Washington DC.

8. ACKNOWLEDGEMENT

The 1st author appreciates the inspiring inputs from his colleagues, including Dr. Chou-Lin Chen, Dr. Cejun Liu, and Mr. Scott Yon.

9. APPENDIX

Table 5b: Weighted annual averages of occupant MAIS from rollovers crashes (CDS 2006-15, vehicle age <=4)					Table 5c: Weighted annual averages of occupant MAIS from rollovers crashes (CDS 2006-15, vehicle age <=2)				
YEAR	MAIS 1	MAIS 2	MAIS 3-6	MAIS 7	YEAR	MAIS 1	MAIS 2	MAIS 3-6	MAIS 7
2006	35,197	5,180	6,932	6,209	2006	18,151	2,493	3,245	4,641
2007	41,239	12,146	6,574	3,043	2007	23,664	5,894	3,067	955
2008	72,017	7,004	6,217	4,264	2008	14,541	2,510	3,642	2,846
2009	18,981	3,102	3,514	591	2009	7,828	1,611	1,336	314
2010	27,901	3,819	2,349	1,661	2010	16,144	2,850	1,409	1,229
2011	16,133	4,064	1,893	546	2011	8,168	2,148	1,082	395
2012	17,195	3,250	1,998	1,049	2012	11,692	1,004	1,132	726
2013	9,075	4,287	4,569	2,627	2013	3,319	2,947	1,483	1,423
2014	17,540	3,108	1,390	352	2014	12,855	1,395	832	352
2015	15,997	2,998	899	1,007	2015	6,505	1,003	554	666

Real World Accident Analysis of Car-to-Car Intersection Near-Side Impacts: Focus on Pelvis Injury

Chinmoy, Pal

Shigeru, Hirayama

Shinichi, Hayashi

Nissan Motor Company Ltd,

Japan

Manoharan, Jeyabharath

Vimalathithan, Kulothungan

Renault Nissan Technology Business Centre India,

India

Paper Number 19-0090

ABSTRACT

Near-side impacts are one of the severe crash modes of all the impacts. Even though 90% of vehicles have achieved "Good" in IIHS rating, there is hardly any sign of decreasing trend in side impact fatalities for last few years. IIHS is planning to introduce a new test protocol because even the cars with "Good Rating" in IIHS tests can still have AIS3+ injuries. In side impacts, a higher number of severe injuries were found in thorax, head and then followed by pelvic region. Though many researchers addressed the mechanism of thorax and head injuries, there are a few in-detail accident analysis of pelvis injuries. Pelvis injury often leads to significant medical expense and impacts the long-term quality of life. This study is focused to find out (i) the relation between pelvis injury with structural deformation (ii) the frequency and the type of pelvis injuries (iii) the type of target of population to considered (size: small/large, gender: male/female) with the help of accident data and simulation results. C2C intersection accidents were selected from NASS-CDS (CY2004-15, n=913 cases) to identify the influential parameters by logistic regression. From the accident analysis it is found that a) pelvic ring fracture is one of the most frequent injuries, b) 10 o'clock impact caused the highest number of injuries, c) pelvis injury frequency is more in female than male, and d) risk of pelvis injury increases when the maximum intrusion of B-pillar and surrounding door structure exceeds a certain level. Logistic regression indicates that angle of impact, location of impact and initial velocity of the struck car are also important parameters. To gain more benefit in real-world accidents by introducing future side impact protocols, a rational approach is necessary to focus more on evaluating the most frequent pelvic ring fracture by introducing more bio-fidelic dummy (say World-SID) in future protocol tests.

INTRODUCTION

Near-side (lateral impact location on driver side) impacts are one of the most severe crash modes with high frequency in real traffic accidents, commonly resulting in serious injuries (Randa, 2003[4], Matthew, 2015[5], Helena, 2011[2]). In SINCAP tests, at the time of impact, the barrier is moving at 62kph and “crabbed” 27 degrees toward the rear of the test vehicle to keep the front of the barrier parallel to the side of the test vehicle. The resulting change in velocity can vary within a range of 22 to 32kph, depending on the mass of the struck vehicle. Insurance Institute for Highway Safety (IIHS) side-impact crash tests consist of a stationary test vehicle struck on the driver’s side by a moving trolley fitted with a deformable honeycomb barrier for perpendicular impact. The leading end of the barrier is shaped to simulate the typical front end of a pickup or Sports Utility Vehicle (SUV). The 1,500kg moving deformable barrier strikes the vehicle on the driver’s side at a velocity of 50kph. Vehicles with high-hood front-end profile caused more head injuries in passenger vehicles in real world accidents and it could not be assessed with the FMVSS 214 barrier. As a result, the IIHS started its side test program in 2003 with a barrier designed to represent the front end of a typical SUV and pickup. Later, in the FMVSS No. 214, the oblique pole test was introduced. To simulate the real world accidents, the vehicle to be tested is propelled sideways into a rigid pole at an angle of 75 degrees with a speed of 32kph. Three different C2C related side impact protocols were given in Figure 1. For detail information of different NCAP test conditions and regulations of different countries refer to the Safety Companion [24] compiled by CARHS.

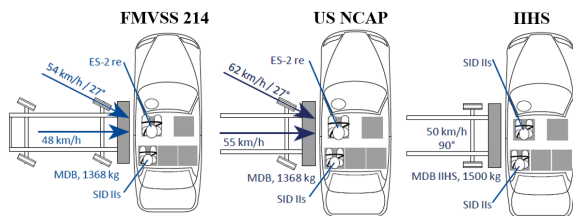


Figure 1. C2C related side impact protocols

Statistics showed that car-to-car(C2C) near side impacts account for more than 60-70% of side impact crashes resulting in serious-to-fatal injuries (Pal 2017[12]). Due to limited survival space on the struck side, near-side occupants, adjacent to the

side of the vehicle subjected to major impact, frequently sustain severe injuries than far-side occupants. Occupant injury can be significantly affected by a different set of crash characteristics and the effects of a crash configuration such as impact direction, impact angle, and change in delta-V need to be studied in detail with real world accident data. Xinghua Lai et al., (2012[9]) investigated the effects of specific impact direction and impact regions on serious-to-fatal injuries of driver occupants involved in near-side collisions using data gathered from National Automotive Sampling System Crashworthiness Data System NASS-CDS (CY1995–2005, [1]) and found that the risk of serious injury was higher for side center (P) and side front distribution (Y) than the side front (F) or rear end (B) locations.

Even though 90% of vehicles have achieved "Good" in IIHS rating, there is hardly any sign of decreasing trend in side impact fatalities for last few years. IIHS is planning to introduce new tests because even the cars with “Good Rating” in IIHS tests can still have AIS3+ injuries. In side impacts, a higher number of severe injuries were found in thorax, head and then followed by pelvic region. Though many researchers addressed the mechanism of thorax and head injuries, [6,7,8], there are a few in-detail accident analysis of pelvis injuries. Pelvis injury often leads to significant medical expense and impacts the long-term quality of life. In order to improve occupant safety in C2C side impact intersection crashes, the objectives of this paper are to find out (i) the relation between pelvis injury with structural deformation (ii) the frequency and type of pelvis injuries and (iii) the type of target of population to be considered (size: small/large, gender: male/female, BMI) with help of accident data, and simulation.

DATA & METHODS

This study used accident data from the National Automotive Sampling System Crashworthiness Data System (NASS-CDS) for the calendar year 2004 to 2015. Table 1 shows the assumptions used to prepare the accident data set for this study. The accident samples are limited to C2C intersection side impact planar collisions (i.e., excluded crashes with the primary general area of damage as top or bottom and rollovers). Values with unknowns have been omitted. In total, 913 vehicles were extracted to perform the accident analysis and logistic regression analysis [13]. Details of those analyses are described in later sections. Table 2 shows the final data set extracted from NASS-CDS CY 2004-15 using the criteria mentioned in Table1. In total, 913 occupants with 4195 injuries involved in near side impacts were

selected with six collision deformation codes (F, P, Y, Z, D, B) and with three main impact angles (8-10 o'clock, driver side) as shown in Figure 2.

Table 1.
List of criteria for input dataset

General Area Damage1=Left
The direction of Force DOF=8-10 o'clock
Impact Location=F, P, Y, B, D, Z
Body Type PV (1-9,17)
Model Year>=2000
Driver Role=1, (Seat Position=11)
Age16+
V2V OBJCTD<=30
Towed Away Vehicles
No Ejection
No Rollover
No Fire Occurrence
Excluded AIS7 injury

Table 2.
List of dataset

	Raw data		Weighted	
	Total no	With pelvis-injury	Total no	With pelvis-injury
Drivers	913	203 (22.2%)	639280	131436 (20.5%)
Injuries	4195	291 (7.0%)	3359148	191858 (5.7%)

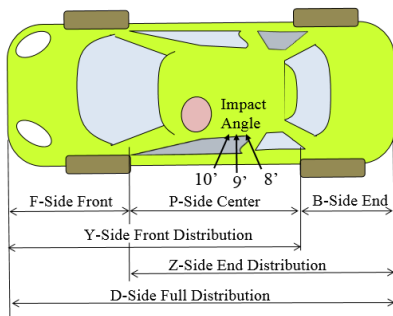


Figure 2. NASS-CDS collision deformation code (8, 9, 10 o'clock impact angles)

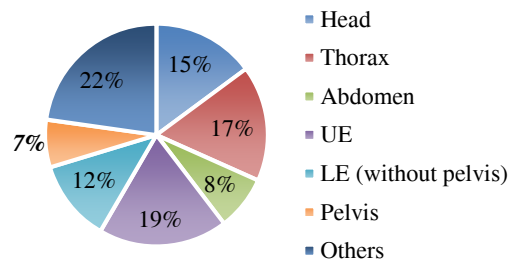
There were 203 cases on driver side impact involving pelvis injuries which account for 22.2% of overall side impact injury cases (Table 2).

RESULTS

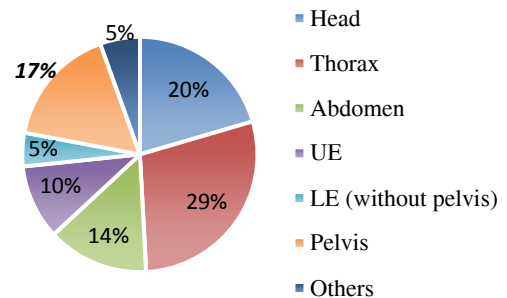
The pelvis injury pattern of occupants involved in C2C near side collisions is discussed in this section. The order of explanation is: a) first, an overview of pelvis region and distribution of injuries, the effect of b) impact angle, c) gender, and d) intrusion magnitude w.r.t pelvis injury. Logistic regression is performed to check the probability of pelvis AIS3+ and AIS2+ injuries occurrence using different factors such as lateral delta-V, gender, the angle of impact, BMI etc. Results were calculated using XLSTAT software[10, 11]. A separate sensitivity analysis was also performed, to see the effect of lateral delta-V and angle of impact and finally, the pelvis injury results were verified using human body simulations. In this study, all the logistic regression models developed using weighted data.

Overview of side impact injuries

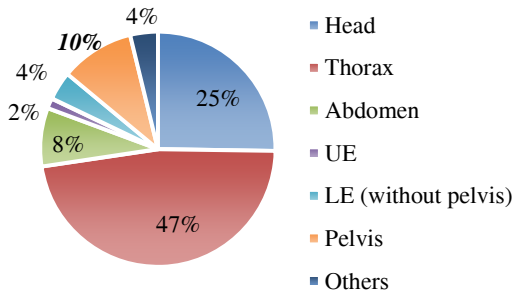
Figure 3 shows the number of injuries in different body regions for three AIS level of severity in nearside impacts. Pelvis AIS1+, AIS2+, and AIS3+ injuries account for 7%, 17%, and 10%, respectively of overall near side impact injuries. The percentage of head and thorax injuries are increasing as the AIS level increases.



a) AIS1+ injuries



b) AIS2+ injuries



c) AIS3+ injuries

Figure 3(a, b, c). Number of AIS injuries in different body regions of near side impacts

Overview of pelvic region and related injuries

Figure A1 shows the important parts associated with the pelvis and they are lumbar spine (cord, disc), sciatic nerve, pelvis ring, acetabulum, symphysis pubis, hip joint, and sacroiliac. Table A1 shows the count of AIS1+, AIS2+ and AIS3+ injuries of each individual sub-parts. AIS2+ and AIS3+ injuries constitute 16.5% (233) and 10.2% (72) of overall side impact injuries. It is interesting to find that, when one plots (refer Figure 4) the percentage of pelvis related AIS injuries as mentioned in Figure A1 and Table A1, AIS2+ was highest. 75% of those AIS2+ injuries were pelvis ring fracture (refer Figure 5). Hence, together with AIS3+, AIS2+ pelvis injuries need some attention in the future. Note that the percentage is calculated with respect to different AIS levels among the injuries of different body regions when pelvis injury occurred.

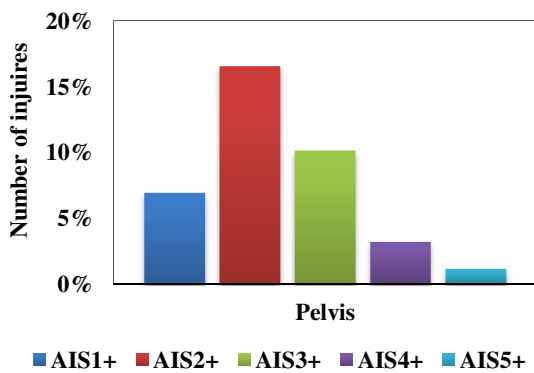


Figure 4. Percentages of pelvis injury across different AIS levels within the injuries of various body regions, when pelvis injury occurred.

Figure 5 shows the distribution of different injuries in each part of the pelvis region. It is found that the pelvic ring fracture (60%) is the most frequent compared to all the injuries and then followed by

lumbar spine (cord+disc, 31%) injuries. Symphysis pubis fracture is also one of the common injuries within the pelvis region.

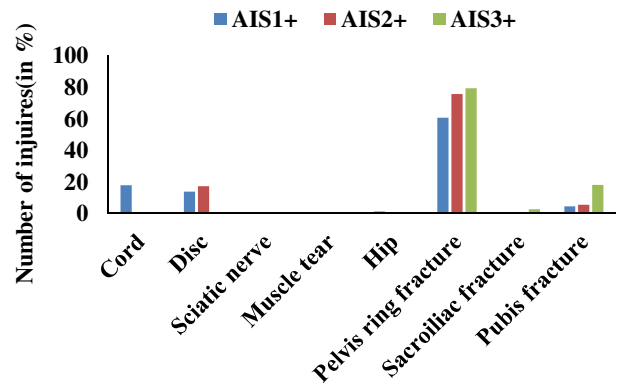


Figure 5. Distribution of pelvis injuries

Effect of angle of impact

Figure 6 shows the effect of angle of impact on the pelvis injuries for different AIS injury levels. It is observed that the oblique 10 o'clock impact angle caused the maximum no. of injuries when compared with those of 9 o'clock and 8 o'clock impacts.

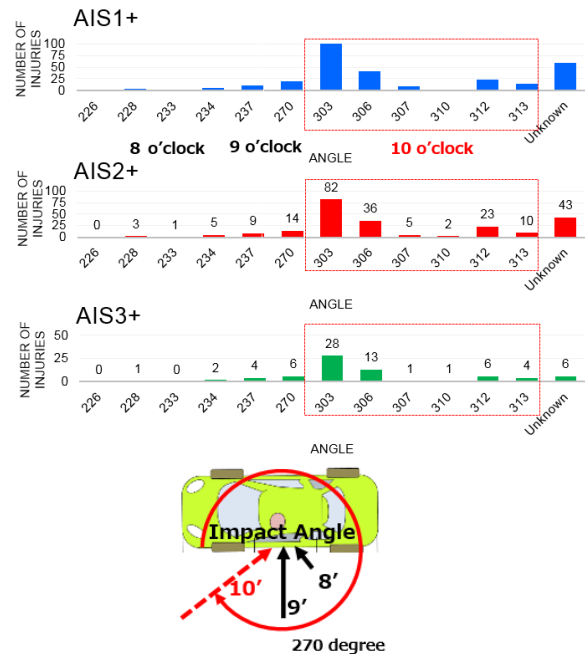


Figure 6. Variation of pelvis injury w.r.t angle of impact. (255~285 deg. corresponds to 9 o'clock)

This shows that most of the real world side injuries are due to oblique impact but not caused by perpendicular impact. The angle of impact of each case is verified by the ratio of delta-V (longitudinal and lateral components) as mentioned in the accident

report. The present real accident data clearly indicates that in future test protocol, proper consideration has to be given about the angle of impact during the loading phase of the pelvis in dummies to capture the real world phenomena.

Effect of gender

Figure 7 shows the effect of gender on the pelvis injury. It is observed that female were having more number of injures than male. This shows that female were most likely to have higher pelvis injuries than male. Some of the possible reasons may be that (i) the females sit further forward towards the steering wheel than males who are usually taller in height than females (refer Figure A6) and (ii) the shape and strength of pelvis are different. It is to be noted that the pelvis injury is influenced by trochanteric soft tissue thickness and BMD of female occupants [15].

Logistic models: lateral delta-V, gender, and angle of impact

Logistic regression is performed to check the probability of pelvis AIS3 and AIS2+ injury occurrence using different factors such as lateral delta-V, gender, and angle of impact.

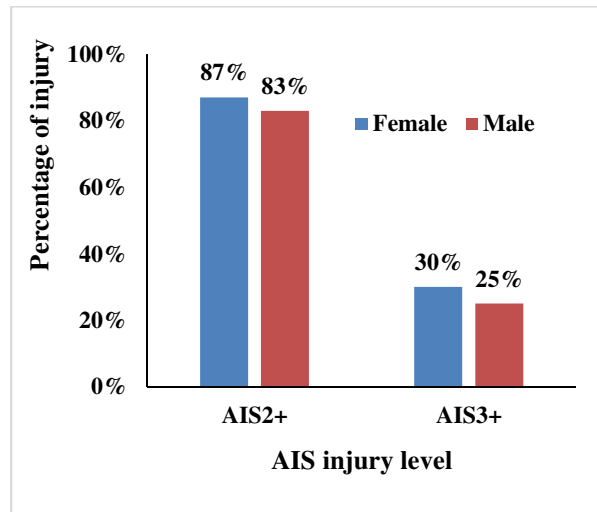


Figure 7. Variation of injuries w.r.t gender

Results of logistic regression were mentioned in Table 3 and Table 5 with AIS3+ and AIS2+ pelvis injury as dependent variables. All the probability values are calculated by varying the lateral delta-V for two 9 o'clock and 10 o'clock impact angles. As shown in Figures 8 and 10, it is clearly evident that the probability curve for 10 o'clock impact is above the 9 o'clock impact curve for both AIS3+ and AIS2+

injuries. The probability of AIS3+ injury is higher for 10 o'clock impact than 9 o'clock impact. Table 4 and 6 show the typical examples of the change in probability values for 10 and 9 o'clock impacts with respect to lateral delta-V changes. At 25kph (equiv. to 50kph barrier impact) and 30kph (equiv. to 60kph barrier impact) lateral delta-V, the probability values changes from 5.5% to 17.38% (3.16 times) and 8.87% to 26.04% (2.93 times) for inclined 10 o'clock and perpendicular 9 o'clock impacts, respectively.

Table 3.

Logistic Model when predicting pelvis AIS3+

n=221, Pelvis AIS3+(0:158,1:63)	Value	Pr. > Chi ²	Odds ratio
Intercept	-11.911	< 0.0001	
Ln(Lateral delta-V)	2.826	< 0.0001	16.88
Gender Male: 0	0.000		
Gender Female: 1	-0.030	0.945	0.970
Angle 9 o'clock: 0	0.000		
Angle 10 o'clock: 1	1.286	0.007	3.617

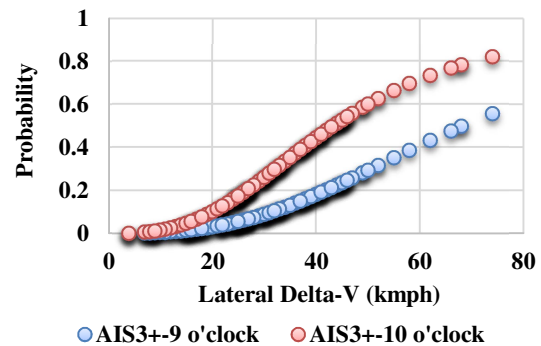


Figure 8 Comparison of probability of AIS3+ for 10 and 9 o'clock impacts with respect to lateral delta-V.

Table 4.

Example of the probabilities of AIS3+ of 10 and 9 o'clock impacts with respect to change in lateral delta-V from 25kph to 30kph

Lateral delta-V (kph)	9 o'clock impacts	10 o'clock impacts	Ratio of 10→9 o'clock impacts
25	5.50%	17.38%	3.16
30	8.87%	26.04%	2.93
Probability ratio of 30→25kph change in delta-V	1.61	1.50	Effect of angle is more than 5kph delta-V increase

Table 5.
Logistic Model when predicting pelvis AIS2+

n=221, Pelvis AIS2+(0:41,1:180)	Value	Pr. > Chi ²	Odds ratio
Intercept	-19.137	< 0.0001	
Ln(Lateral delta-V)	6.481	< 0.0001	652.5
Gender Male: 0	0.000		
Female: 1	-2.912	< 0.0001	0.054
Angle 9 o'clock: 0	0.000		
10 o'clock: 1	2.466	< 0.0001	11.777

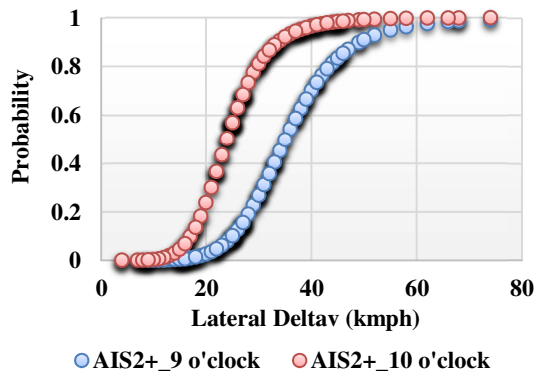


Figure 9. Comparison of probability of AIS2+ for 10 and 9 o'clock impacts with respect to lateral delta-V.

Table 6.
Example of the probabilities of AIS3+ of 10 and 9 o'clock impacts with respect to change in lateral delta-V from 25kph to 30kph

Lateral delta-V (kph)	9 o'clock impacts	10 o'clock impacts	Ratio of 10→9 o'clock impacts
25	10.08%	56.91%	5.64
30	26.76%	81.15%	3.03
Probability ratio of 30→25kph change in delta-V	2.65	1.43	Effect of angle is more than 5kph delta-V increase

Similar results were observed when predicted with AIS2+ injury level (refer to Table 5, 6 and Figure 9).

Effect of impact location (CDC code)

Figure 10(a,b,c) shows the number of pelvis injuries with respect to the location of impact. Y region had the highest number (for AIS1+: 40%, AIS2+: 43%, AIS3+: 39%) of injuries compared to other locations and then followed by P and Z locations. Combined Y and P locations cover more than 2/3rd of all injuries from AIS1-3.

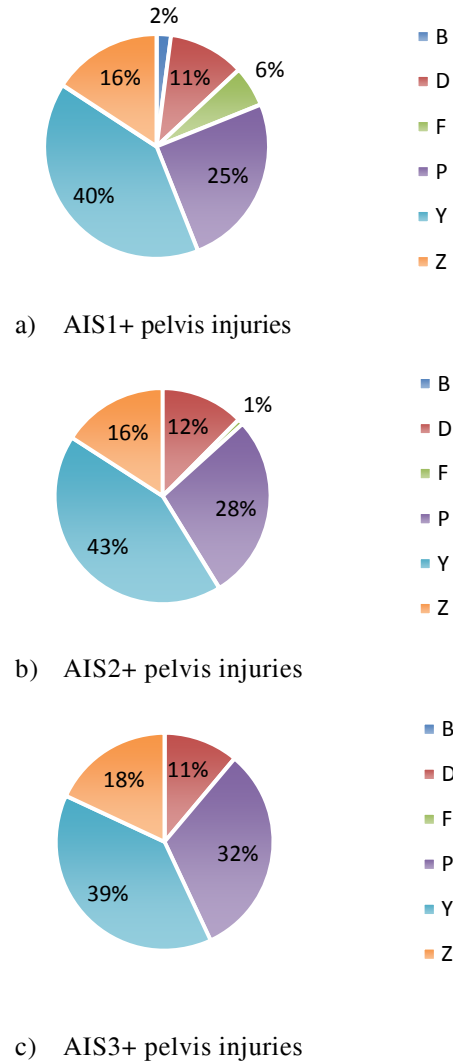


Figure 10 (a, b, c). Number of AIS injuries with respect to the location of impact (based on CDC code)

Effect of impact location (from crash pictures)

In order to estimate more accurately the effect of impact location, BMI and intrusion magnitude, the number of cases were increased from 203 (driver alone) to 265 by adding pelvis injury of right side passengers cases also(Figure 11). By detail inspection of damage pictures of each case in the

NASS-CDS database, one could identify the location of impact from B pillar accurately. This will help one to estimate the changes of injury pattern with respect to the impact location of maximum external deformation.

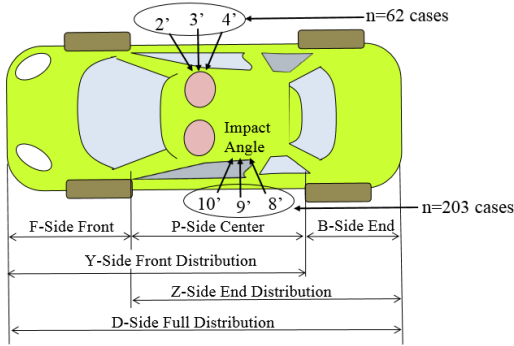


Figure 11. Driver plus passenger cases selection criteria

In order to observe the overall picture of impact location on pelvis injuries, the distribution of AIS2+ (Figure 12) and AIS3+ (Figure 13) injuries (based on binary count Yes=1 and No=0) was plotted with respect to the location of maximum external deformation. It is observed that AIS2+ and AIS3+ injuries are more when impact location is close to B pillar. It is also observed that 80% of serious AIS3+ injuries are coming between -50cm to +50cm, which means more pelvis serious injuries in this region.

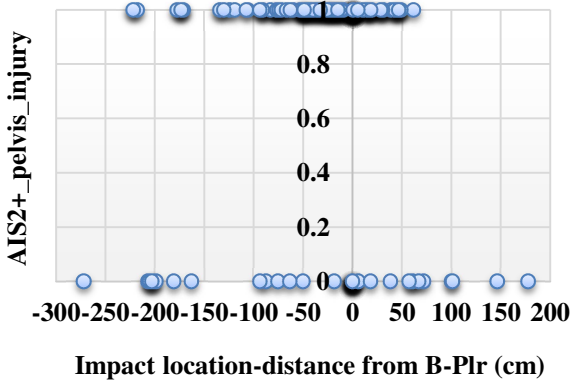


Figure 12. Distribution of AIS2+ injury (binary cases: serious: 1, minor: 0) with respect to impact location-distance from B pillar (cm).

Figure 14 shows the distribution of AIS2+ and AIS3+ injuries with the location of impact as a continuous

variable. It is observed that as the maximum deformation of impact location moves away from B pillar to either left or right of the vehicle, the percentage of injuries were decreasing. The peak values were observed near to B pillar (around driver sitting position). There was a high chance (AIS2+: 96%, AIS3+:60%) of injury when the impact location was very close to the driving position near B-pillar.

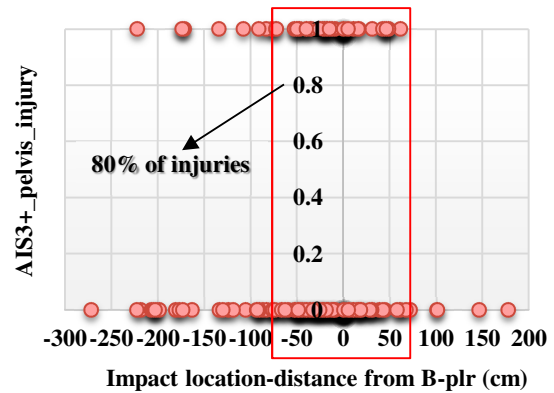


Figure 13. Distribution of AIS3+ injury (binary cases: serious: 1, minor: 0) with respect to impact location-distance from B pillar (cm).

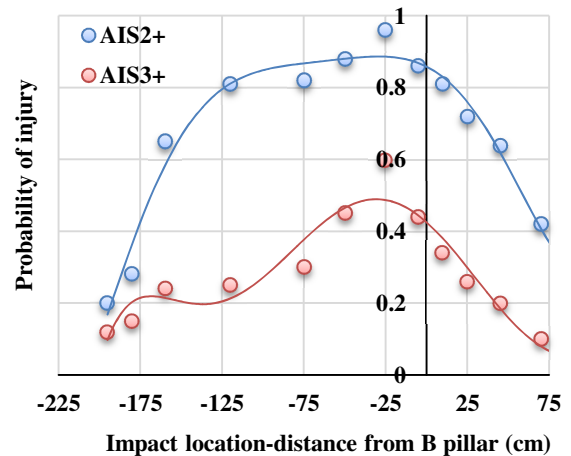


Figure 14. Comparison of probabilities of AIS2+ and AIS3+ injury with respect to impact location-distance from B-pillar (cm) of maximum deformation.

Real world accident data

Figure 15 shows the variation of pelvis injury with respect to various compartment (door inner) intrusion magnitudes 0-8cm, 8-15cm, 15-30cm, and > 30cm.

The X-axis shows different injury levels and Y-axis shows the number of cases considered. All the injury levels are labeled in different categories of intrusion magnitude. It is observed that the risk of pelvis injury increases if the magnitude of intrusion increases beyond a certain level to cause more serious AIS3+ injuries as indicated by two circled portions (①, ②).

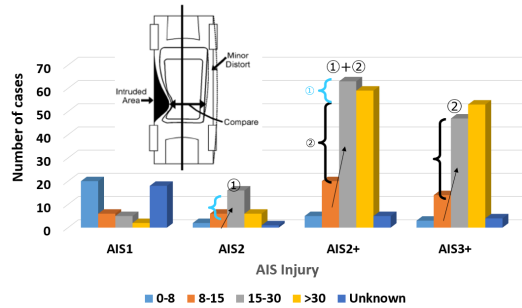


Figure 15. Variation of number of cases (AIS levels) w.r.t compartment intrusion magnitude

Figure 16 shows the probabilities of AIS2+ and AIS3+ injury with respect to intrusion magnitude. As the intrusion magnitude was increasing the probability of both the injuries were increasing. Hence, the magnitude of intrusion is a useful parameter in identifying the injury classification. Figure 17 shows the average intrusion magnitude (AIS2+ and AIS3+) with respect to impact location. It is observed that even though the intrusion magnitude was low near the B-pillar, AIS2+ and AIS3+ injuries are likely to occur. As the impact location moves further away from B-pillar, either forward or rear side of the vehicle, the average of maximum intrusion magnitude was increasing in order to cause the same AIS level of injuries.

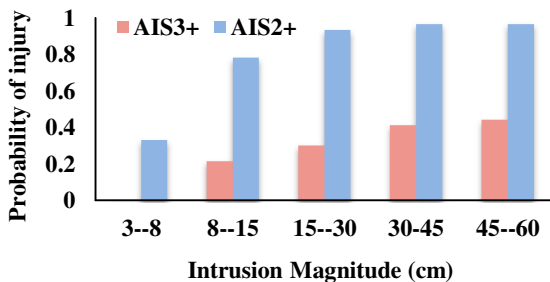


Figure 16. Comparison of probabilities of AIS2+ and AIS3+ injury with respect to intrusion magnitude (cm).

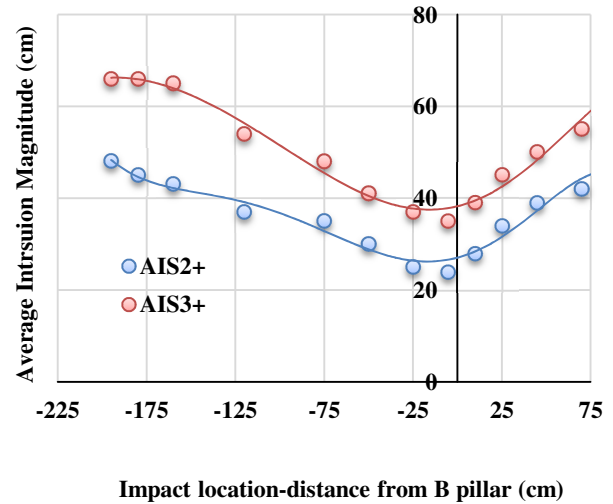


Figure 17 Comparison of average intrusion magnitude for AIS2+ and AIS3+ injury with respect to impact location-distance from B pillar (cm) at maximum external deformation.

Effect of BMI

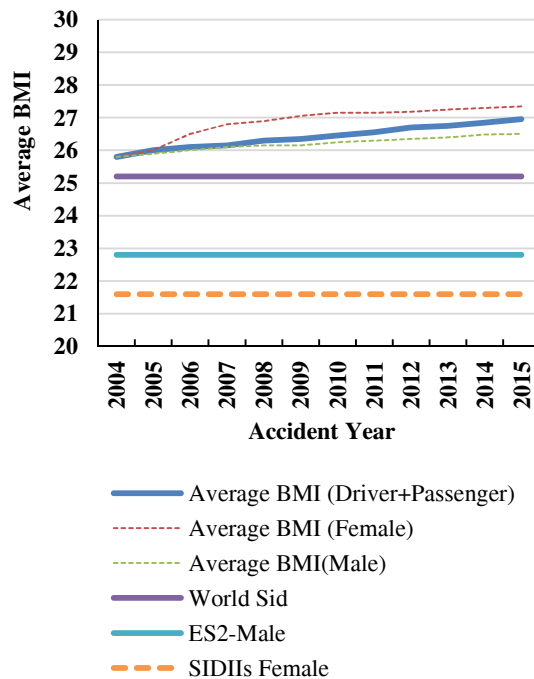


Figure 18 Comparison of Average BMI variation with respect to year of the accident

In order to estimate the effect of BMI on pelvis injuries in a side impact, average BMI was calculated

using 11 years of accident data. Figure 18 shows the variation of average BMI of US driving population with respect to the accident year. BMI values of World SID, ES2 Male and SID-IIs female also plotted in the same graph. It clearly captures the increasing trend of average BMI values (average is around 26). In general, the average BMI values of females were greater than that of the male. Hence, BMI can be an influential factor for identifying the injury classification. Figure 19 shows the percentage of injures for below and above the average value of BMI=26.

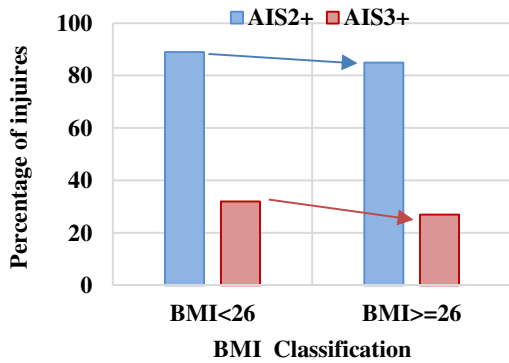


Figure 19 Comparison of AIS2+ and AIS3+ injuries for BMI classification (Average 26)

It is found that the percentage of injuries for <26 was more than >26 which indicates that as the BMI is increasing the percentage of injuries were decreasing. This is may be due to the fact that the relatively shorter and more obese occupants were getting fewer injures than less obese occupants. As the amount of accumulated fat in pelvis and abdomen region is increasing, there may be less chance of injury in the pelvis region.

Logistic Models (BMI and intrusion magnitude)

In order to find out the effect of BMI and intrusion magnitude, logistic regression models (Table 7 and 8) were developed for both AIS2+ and AIS3+ pelvis injury prediction using the variables such as belt usage (not used:0, used:1) and age (Age<65: 0, Age>=65: 1). In these logistic regression models, total delta-V was splitted into two components as longitudinal and lateral delta-V as continuous variables.

Table 7.
Logistic Model when predicting pelvis AIS3+ injuries when all the variables were considered

n=209 AIS3+: 64, AIS3-: 145 ROC: 0.65	Value	Pr > Chi²	Odds ratio
Intercept	-4.19	0.00	
Longitudinal delta-V	-0.06	0.04	0.95
Lateral delta-V	0.02	0.03	1.02
Belt not used: 0	0.00		
Belt used: 1	-1.55	0.00	0.21
BMI<26: 0	0.00		
BMI>=26: 1	-0.85	0.05	0.43
Age<65: 0	0.00		
Age>=65: 1	0.91	0.05	2.48
Intrusion<15cm: 0	0.00		
Intrusion>=15cm: 1	3.17	0.01	23.7

Table 8.
Logistic Model when predicting pelvis AIS2+ injuries when all the variables were considered

n=209 AIS2+: 184, AIS2-: 25 ROC: 0.83	Value	Pr> Chi²	Odds ratio
Intercept	0.29	0.61	
Longitudinal delta-V	-0.10	0.00	0.90
Lateral delta-V	0.02	0.02	1.02
Belt not used: 0	0.00		
Belt used: 1	-1.58	0.00	0.21
BMI<26: 0	0.00		
BMI>=26: 1	-0.43	0.21	0.65
Age<65: 0	0.00		
Age>=65: 1	-0.74	0.05	0.48
Intrusion<15cm: 0	0.00		
Intrusion>=15cm: 1	1.21	0.01	3.35

As the average BMI is around 26, BMI was categorized into a binary variable (BMI<26: 0, BMI>=26: 1) and the percentage of AIS3+ injury was more than 20% around 15cm of compartment intrusion, the intrusion level was splitted in to a binary variable (Intrusion<15: 0, Intrusion>=15: 1). It is observed from the Table 7 that when predicting the AIS3+ pelvis injury, longitudinal component delta-V,

lateral component of delta-V, belt-usage, BMI, age and intrusion variables were significant ($p < 0.05$). However, when predicting AIS2+ injuries (Table 8) all the variables were significant except BMI ($p = 0.21$). In both AIS3+ and AIS2+ predictions, BMI coefficient was negative (-0.85, -0.43) which indicates that as the BMI is increasing, the injury level may be less for occupants of higher obesity. Total delta-V was splitted into two to verify the effect of each individual component. It is observed from both the logistic prediction models that the lateral component is more significant than the longitudinal one. However, they also indicate that in side impact accident cases, the longitudinal component is also an influential parameter. As ROC value (0.65) is not high for AIS3+ logistic regression (Table 7), it needs further investigation. Hence, a non-linear SOM clustering analysis is carried out to verify the results of the above linear logistic cluster analysis and it is discussed briefly in the discussion section. SOM stands for Self Organization Map. It is a neural network based classification technique which can be used efficiently in accident analysis to find out the inherent relationship of complex phenomena (Pal 2017, [17]).

Human body model simulation

To understand the influence of BMI on pelvis injury, human body model (HBM) based impactor simulation was carried out. Based on prior studies (Petit P, 2018, [18] & Matthieu Lebarbé, 2016 [19]) a simple rigid rectangular impactor of size: 400mm x 200mm, mass: 23.4kg & speed: 11.2m/s is used to impact the HBM near pelvis region as shown in Figure 20.

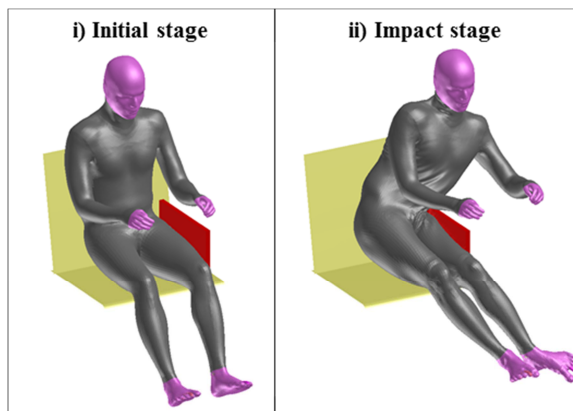


Figure 20 Simple sled impactor test near pelvis region with latest GHMBC Human Body Model.

People with high BMI, have more fat/ flesh content in the hip region as explained in the introduction section. To understand its influence on pelvis injury, an additional layer of flesh is added in the hip region of human body model as shown in Figure 21 to represent occupants of slightly higher BMI=30 based on the information of the reference paper [15].

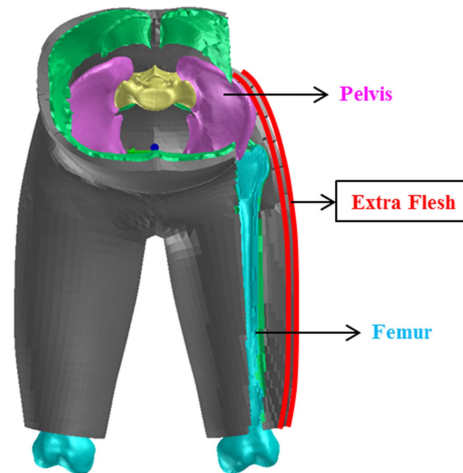


Figure 21 Extra layer of flesh added to hip region of HBM to simulate increased BMI occupant.

Higher BMI human body model with extra outer layer of flesh was impacted against the impactor and the pelvis injury values are compared with the base GHMBC human model. Pelvis bone injury was measured using volume ratio of region which crossed the plastic limit threshold (T^*) and the region which do not cross threshold limit. (Note: Threshold T^* = one-tenth of GHMBC reference value for fracture). Additional flesh content near the hip region act as a cushion layer to reduce pelvis injury as shown in Figure 22 and Figure A7. Higher BMI is one of the causes of less pelvis ring fracture injury.

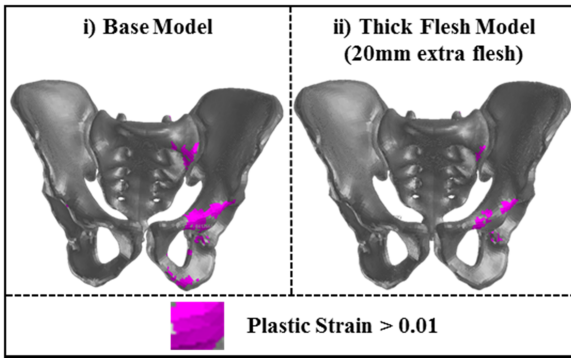


Figure 22 Comparison of pelvis bone injury patterns for base and high BMI thick flesh HBMs

DISCUSSION

The results, as discussed above, suggest that in order to properly evaluate the crash worthiness and occupant performances of different types and sizes of vehicles, it is worth thinking about more rational approach with respect to types and location of structural deformation on the vehicle to identify the actual benefits of existing and future protocols. Collecting more detail intrusion data at relevant different locations near the occupant will be very helpful. Modern camera based image analysis can be one of the possible ways to measure that. In addition to that, EDR data before the crash will add more useful (dimension and depth) of information as future vehicles will be fitted with various sensors.

As the bio-fidelity of the pelvis of SID-2s is low, World-SID is one of the better choices [16]. It is necessary to focus more on evaluating the most frequent pelvic ring fracture by introducing more bio-fidelic dummies equipped with advanced sensors in future protocol tests (refer to Figure A2 and A3). It is also true from the change in BMI trend of US driving population as shown in Figure 18.

To verify the relation between BMI and AIS injury, Self-Organizing-Maps(SOM) based non-linear analysis results were plotted using the pelvis injury input data(refer Figure A4 and A5) related to Tables 7,8. SOM reduces the n-dimensional feature information into 2-dimensional space. The objects (each individual accident case) which are of similar characteristics are placed side by side. The accident cases which are dissimilar are placed further away. A few regions were highlighted using thick black lines to illustrate the effect of BMI on AIS3+ and AIS2+ injury levels in Figures A4 and A5. There are as many numbers of feature based SOM maps as the number of independent

input variables of the above mentioned logistic regressions of Tables 7, 8 together with corresponding AIS2+ and AIS3+ injury levels as a dependent variable.

As shown in Figure A4, there were few AIS3+ injuries for BMI>30 within the area surrounded by a thick black line. It indicates that the level of pelvis injury (corresponding to the blue area) will be reduced for obese occupants of older (>65yrs) and younger (<65yrs) occupants. However, there are some small patches of red regions with AIS3+ injury within this thick black line where either the amount of compartment intrusion or the age of the occupants is extremely high. On the other hand, outside the thick black line where AIS3+ SOM map indicates the occurrence of AIS3+ injury (red color), BMI is not that high. These visual clustered results of SOM analysis match well with those of linear logistic regression analysis of Table7.

As shown in Figure A5, the SOM map of AIS2+ injury is clearly clustered in red(AIS2+: 1, yes) and blue(AIS2+: 0, no) regions separated by a thick black closed boundary line marked by 'a'. The blue part contains a wider range of variations of BMI values and compartment intrusion levels of different accident cases with mixed similarity and dissimilarity patterns. It suggests that BMI (a measure of obesity) is not a definite influential factor for the occurrence of AIS2+ pelvis injury. These visual results of SOM analysis match well with those of logistic regression of Table8. However, one should also note that in the rectangular region as indicated by 'b' having AIS+2 injury, there are relatively slim occupants with less BMI (<19), higher compartment intrusion and sitting position very close to B-pillar. This is opposite to the trend of higher BMI obese occupants group as mentioned above. In linear logistic regression analysis, it is difficult to identify correctly such non-linear change in the trend of AIS2+injuries with respect to the change of BMI.

LIMITATIONS

A limited number of cases were studied in this research work. However, considering all possible accident scenarios, more detailed verifications are needed by using various combinations of physical C2C experiments and simulations using different dummies and types of vehicles in order to make any generalized statement as stated above. It is also necessary to do a similar accident analysis for

other countries having good accident database for further verification.

CONCLUSION

This paper discussed the sensitivity of the pelvis injury patterns of C2C side impact accidents at the intersection for PV vehicles using NASS-CDS CY 2004-2015 data. From the accident analysis it was revealed that a) pelvic ring fracture is one of the most frequent injuries, b) 10 o'clock impact caused the highest number of injuries, c) pelvis injury frequency is higher in female than male, d) risk of pelvis injury increases when the maximum intrusion of B-pillar and surrounding door structure exceeds a certain level.

It is also verified using HBM simulation that higher BMI>30 obese occupants will probably have less chance of AIS+3 injury when compared with those of normal occupants with BMI<26 in similar severity of C2C intersection impact. Non-linear SOM cluster analysis supports the effect of BMI on pelvis injury.

REFERENCES

- [1] National Highway Traffic Safety Administration (NHTSA), National Automotive Sampling System (NASS) Crashworthiness Data System Analytical User's Manual 2014, National Centre for Statistics and Analysis, U.S. Dept. of Transportation, Washington, DC.
- [2] Helena, S., et al, 2011. "Effect of Side Impact Protection in Reducing Injuries" 22th ESV, Paper Number 11-0319 (2011).
- [3] Tomiji, S., et al, 2011. "Study on Car-To-Car Side Impact" 22th ESV, Paper Number 289 (2011).
- [4] Randa, R.S., et al, 2003. "NHTSA Side Impact Research: Motivation for Upgraded Test Procedures" ESV, Paper Number 492 (2003).
- [5] Matthew, L. 2015. "Occurrence of Serious Injury in Real-World Side Impacts of Vehicles with Good Side-Impact Protection Ratings" IIHS, Ruckersville, Virginia. Traffic Injury Prevention 16.S125-S132, (2015).
- [6] Narayan, Y., et al, 2008. "Chest Deflections and Injuries in Oblique Lateral Impacts" Traffic Injury Prevention (2008) 9:162-167, 2008.
- [7] Pintar, F.A., et al, 2009. "Test program to define oblique chest loading in side impact" Paper presented at Experimental Safety of Vehicles; June 6–11, 2009; Washington, DC.
- [8] Shaw, J.M., et al, 2006. "Oblique and lateral impact response of the PMHS thorax" Stapp Car Crash J. (2006), 50:147–167.
- [9] Xinghua, L. 2012. "Impact direction effect on serious-to-fatal injuries among drivers in near-side collisions according to impact location: focus on thoracic injuries" Accident Analysis Prevention 48, page 442-450, (2012).
- [10] David G. Kleinbaum Mitchel Klein, 2010. "Logistic Regression, A Self Learning Text" Third Edition. ISBN: 978-1-4419-1741-6 (2010).
- [11] XLSTAT User's Guide, version, 2015.1.1(2015).
- [12] Safety Companion 2016, CARHS publications
- [13] Chinmoy Pal, et al. 2017. "Improvement of injury severity prediction (ISP) of AACN during on-site triage using vehicle deformation pattern for Car to Car side impact", short communication, AAAM 2017.
- [14] Chinmoy Pal, et al. 2015. "Development of High Efficiency Load Path Structure to Enhance Side Impact Safety Performance", ESV2015 Paper Number 15-0363.
- [15] Sven A. Holcombe, Stewart C. Wang. "Subcutaneous Fat Distribution in the Human Torso", IRCOBI Conference 2014 IRC-14-43.
- [16] Taewung Kim, et al, 2016. "Biofidelity evaluation of WorldSID and ES-2re under side impact conditions with and without airbag", Accident Analysis and Prevention 90 (2016) 140–151
- [17] Chinmoy Pal, et al, 2017, "An insight of World Health Organization (WHO) accident database by cluster analysis with self-organizing map (SOM)", Traffic Injury Prevention, Vol. 19, 2018. <https://doi.org/10.1080/15389588.2017.1370089>
- [18] Petit, P., et al., "Update of the WorldSID 50th Male Pelvic Injury Criterion and Risk

Curve,” SAE Technical Paper 2018-01-0539, 2018, doi:10.4271/2018-01-0539.

[19] Matthieu Lebarbé et al., “Investigation of Pelvic Injuries on Eighteen Post Mortem Human Subjects Submitted to Oblique Lateral Impacts”, Stapp Car Crash Journal, Vol. 60 (November 2016), pp. 89-134

NOMENCLATURE:

AF05: 5th percentile American female
AIS: Abbreviated Injury Scale (1998 version)

AM50: 50th percentile American male
C2C: Car to Car
BMD: Bone mineral density, the mass of mineral per volume of bone
BMI: Body Mass Index, the measure of body fat based on height and weight
IIHS: International Institute of Highway Safety
NCAP: New Car Assessment Program
NASS-CDS: National Automotive Sampling System Crashworthiness Data System
PV: Passenger Vehicle
SOM: Self Organization Map
SUV: Sports Utility Vehicle

APPENDIX A.

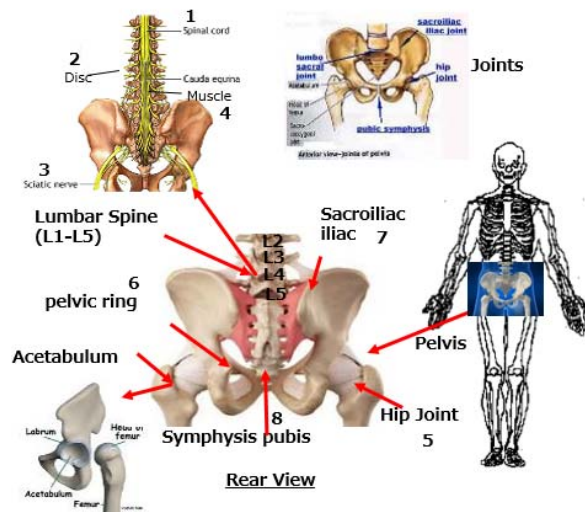


Figure A1. Schematic view of the pelvis region

Table A1.
Distribution of injuries in each part of the pelvic body structure

		AIS1+	AIS2+	AIS3+
<i>All body region (AIS98 code)</i>	<i>Injury code</i>	4195	1408	709
<i>Lumbar spine</i>				
1.Cord	640601	52	0	0
2.Disc	650699	40	40	0
<i>Lower extremity</i>				
3.Sciatic nerve	830476	2	2	0
4.Muscle tear	840604	2	0	0

5.Hip (Acetabulum; femur head)	850699	4	0	0
6.pelvic ring fracture	852602	176	176	57
7.Pelvis Sacroiliac fracture	852800	2	2	2
8.Symphysis pubis fracture	853000	13	13	13
Lumbar spine + Lower extremity related pelvis injury		291 (7.1%)	233 (16.5%)	72 (10.2%)

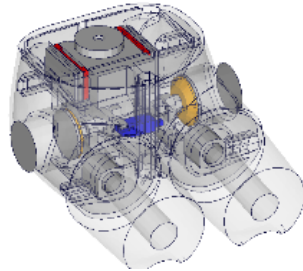


Figure A2. Schematic view of SID-II's pelvis

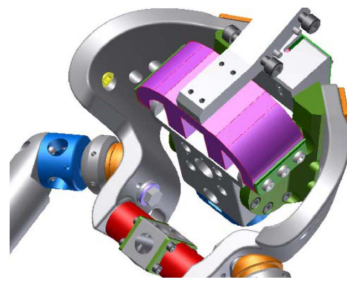


Figure A3. Schematic view of World-SID pelvis

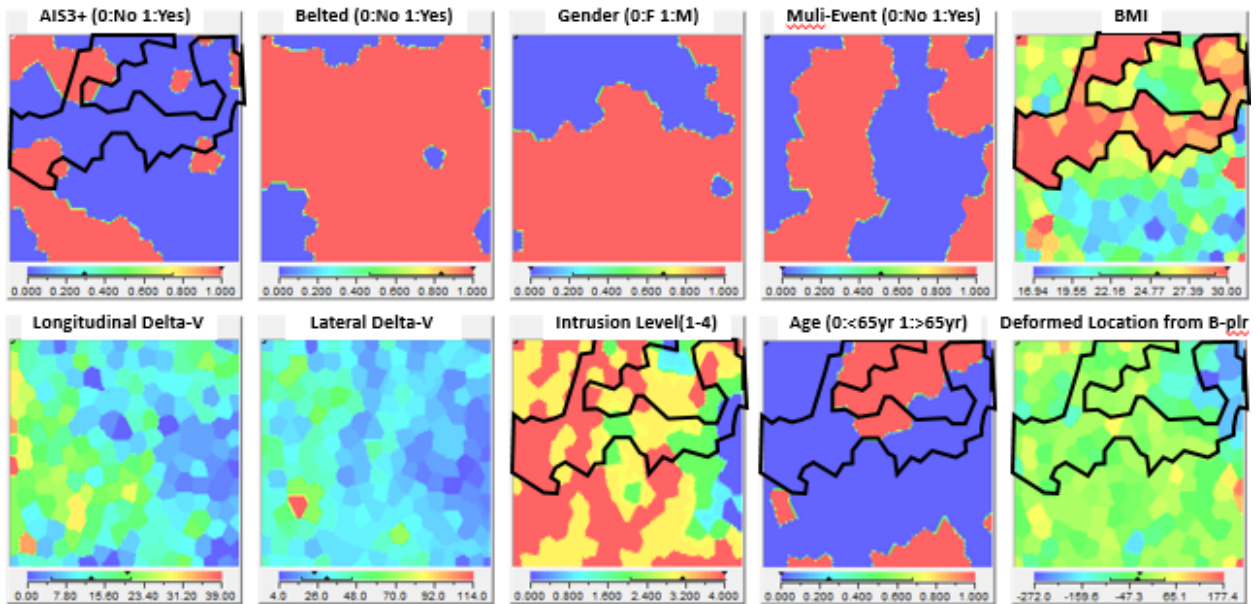


Figure A4. Self-Organizing-Maps (SOMs) of AIS3+ pelvis injury (10 attributes with 10 maps) to visualize the nonlinear relationship of the variables of the linear logistic regression analysis of Table 7. At the bottom of each SOM map, the red and blue scale bars indicate the corresponding highest and lowest values of corresponding variables.

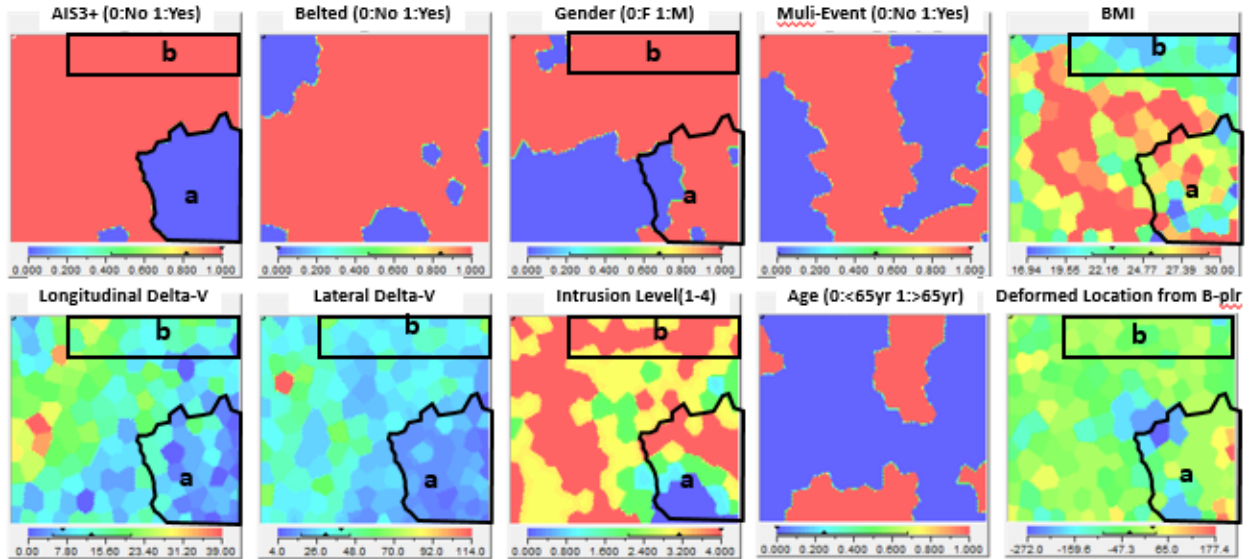


Figure A5. Self-Organizing-Maps (SOMs) of AIS2+ pelvis injury database (10 attributes with 10 maps) to visualize the nonlinear relationship of the variables of the linear logistic regression analysis of Table 8. At the bottom of each SOM map, the red and blue scale bars indicate the corresponding highest and lowest values of corresponding variables.

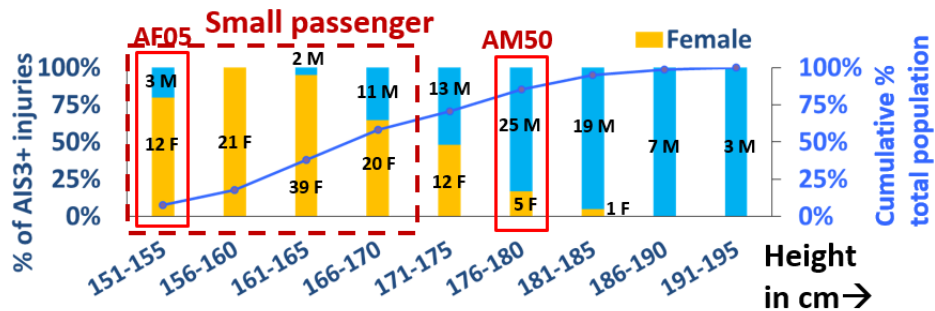


Figure A6. Distribution of occupant height in cm

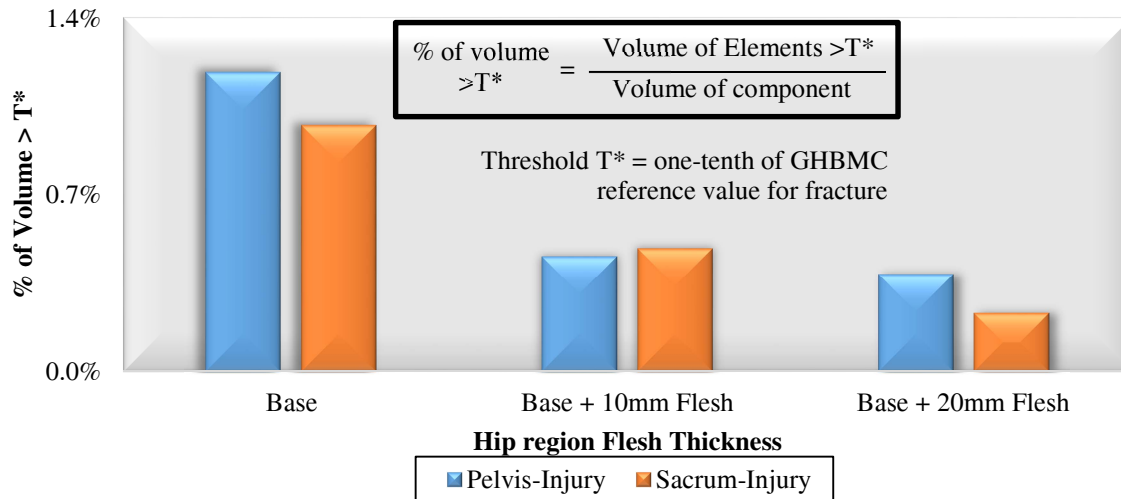


Figure A7. Influence of hip region flesh thickness on pelvis injury

REPEATABILITY OF THE CAROUSEL DYNAMIC STABILITY AND ROLLOVER TEST DEVICE

Garrett Mattos

Keith Friedman

Safety Research Institute

USA

Kennerly Digges

Carl Nash

Automotive Safety Research Institute

USA

Acen Jordan

Jordan & Co

USA

Paper Number 19-0330

ABSTRACT

A novel test device (Carousel) for measuring the dynamic rollover stability of vehicles and initiating a full-scale dynamic rollover test has been installed and evaluated for repeatability and reliability. This work describes the test device function and presents results from preliminary repeatability testing. Both the test device and the test article were evaluated to objectively identify the repeatability between tests using correlation analysis. The results demonstrate that the fixture is capable of producing highly repeatable responses.

INTRODUCTION

Rollovers of passenger cars, vans, and light trucks not equipped with electronic stability systems in the U.S. are typically single-vehicle events (82.5%) initiated by a yaw followed by tripping (>80%) such as a furrowing, and gouging [1]. Vehicle rollover resistance ratings in the U.S. are determined by the National Highway Traffic Safety Administration (NHTSA) New Car Assessment Program (NCAP) using two methods; a static measurement of vehicle dimensions and a dynamic handling test. The static measurement method uses a vehicle's track width (T) and center of gravity (CG) height (H) to calculate a *static stability factor* (SSF) (Eq. 1). The vehicle's CG height is generally measured dynamically on a vehicle inertia measuring machine. A lower SSF indicates a higher risk of rollover [2], however more stable vehicles (higher SSF) have been shown to have higher injury risk during rollovers likely due to the increased speeds required to initiate a rollover [3]. The relationship between SSF and rollover risk has been shown to extend to smaller vehicles such as quad bikes [4] and larger vehicles such as heavy trucks [5].

$$SSF = \frac{T}{2H} \quad \text{Eq. 1}$$

While the SSF does not account for the effects of tire design, suspension characteristics, wheelbase, effects of braking, or electronic stability control these parameters are considered during dynamic tests [2]. Depending on the scenario dynamic tests generally fall into two categories: closed-loop and open-loop maneuvers. Closed-loop maneuvers, such as the ISO 3888 double lane change, require all vehicles to follow a given path and are generally described as evaluations of vehicle maneuverability, not rollover resistance. Open-loop testing, such as the J-turn or fishhook maneuver, provides the same steering input for all vehicles and more frequently produces tip-up. While automated steering controllers are used to improve steering input repeatability, the complexity of the dynamic tests provide challenges in repeatability and reproducibility due to variations in environmental factors (e.g. temperature, humidity), road surface friction and finish, effects of safety outriggers, electronic stability control (ESC), and suspension age. Dynamic maneuver testing is much more expensive, time consuming, and potentially dangerous to drivers than static testing.

Centrifuge-style test methods were considered as an improvement to SSF in a NHTSA notice of proposed rulemaking that was generated in response to the Transportation Recall, Enhancement, Accountability and

Documentation (TREAD) Act of November 2000 [6]. Tests using this method are similar to the tilt-table and side-pull ratio tests and have been promoted for replicating rollover events initiated by both tripped or turn-over mechanisms [7]. The major drawbacks to a rollover rating system that solely used a centrifuge method include the potential for rewarding undesirable suspension characteristics (e.g. oversteer, roll stiffness distribution), lack of sufficient “dynamic” loading, and the fact that ESC would provide no benefit. Coupling a centrifuge test with a dynamic maneuver test would solve this issue. It is worthwhile to note that many manufacturers suggested that ESC be switched off for dynamic testing so that it couldn’t be used to mask poor rollover resistance. The benefits of a centrifuge test include simple test setup, small test area, quick turnaround times, reliable tripping mechanism, insensitivity to pavement friction, and low cost of operation. The centrifuge test results would be expected to have a high correlation with SSF while improving the rating due to more realistic evaluation of the test article response by including vehicle load transfer and tire and suspension deflections. Concept tests conducted by the NHTSA at NASA’s High Capacity Centrifuge facility demonstrated consistent liftoff values that were in agreement with expected lateral acceleration for rollover initiation.

The objective of this research was to evaluate and quantify the repeatability of a centrifuge-style test fixture (Carousel) with regard to both test fixture and test article response. While the device concept was born out of an interest related to vehicle rollover stability testing it can be applied to many other aspects of physical testing. The Carousel is simply a circular sled that could potentially be used in the same manner as traditional linear sleds following some modifications and/or additions such as a decelerator or test buck stand. The simplicity and compact nature of the device coupled with its high level of repeatability support its use in a wide range of applications.

METHODS

Two Series of tests without test article release were conducted; a Series of four (4) low-speed tests with no tip-up and a Series of four (4) high-speed tests with tip-up.

The test device, shown in Figure 1, consists of a stationary pivot at the center of a 5.4 m radius (approximate test article center) concrete circular track. A steel-framed wood-topped platform rotates about the stationary pivot and rolls on six (6) pairs of 20 cm wheels. The platform designed to accommodate a test article up to 2500 kg with track width and wheelbase not to exceed 1.7 m and 4.4 m, respectively. The device is powered pneumatically with on-board air stored in twin 0.227 m³ (60 gallon) pressurized tanks at a maximum pressure of 1240 kPa. The pressurized air is used to force two (2) pistons down parallel cylinders. The angular acceleration is controlled by the amount of air pressure. Each piston is attached to a steel wire rope that is wound around a central sheave which is rigidly attached to the stationary pivot. As the pistons are forced down the cylinders a torque is developed between the sheave and the platform which accelerates the platform around the track as the wire ropes unwind from the central sheave. The ratio of the central sheave circumference to wire rope length provides approximately 340 deg of angular acceleration. After the platform reaches a displacement of 340 degrees it coasts to a stop unless otherwise decelerated.



Figure 1 Test fixture with test article at start position

The test article was a 2000 Ford Ranger two-door super cab pickup with the dimensions and inertial properties summarized in Table 1. The test article is positioned on the platform with the transmission in ‘park’ and the parking brake engaged. Square aluminum tubes are positioned in front of and behind each tire and clamped to the platform to prevent fore-aft motion during the test. The outside faces of the outside tires are positioned in contact with trip bars. The trip bars consist of aluminum plates that pivot as they are loaded by the tires and the vehicle rotates over them as shown in Figure 2. Inside tire lift-off height is controlled with the used of chains affixed to the platform.

Table 1 Test article dimensions

Parameter	Value
Test weight / Distribution	1610 kg / 59 % front
Roll moment of inertia	638 kg m ²
Yaw moment of inertia	2661 kg m ²
Pitch moment of inertia	2628 kg m ²
Wheelbase	3.2 m
Track Width front/rear	1.5 m / 1.45 m
CG height	0.625 m
SSF	1.18
Tires	BF Goodrich All-Terrain 31x10.50R15 100s

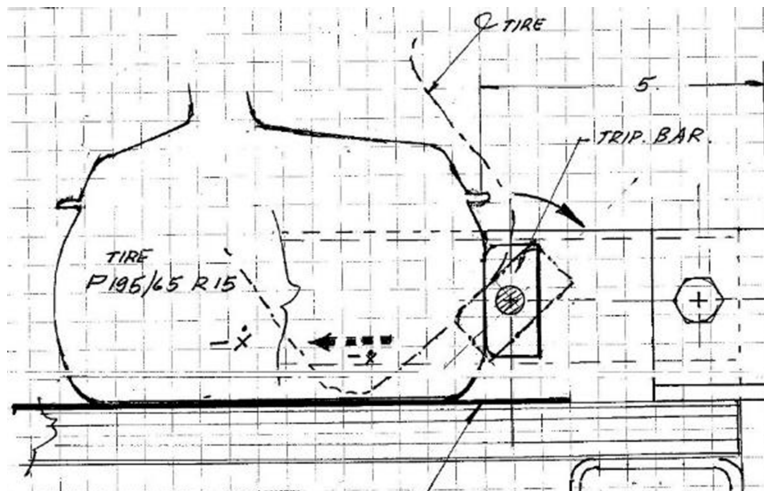


Figure 2 Cross-section view of tire and trip bar

A dual-output rotary potentiometer (Novotechnik RSC2832) was used to measure platform angular displacement. String potentiometers (Space Age Control 301432) were placed between the platform and the inside frame rail at the front and rear of the test article to measure the displacement of the test article during three of the Series 2 tests (Figure 3). The string potentiometer data in the fourth Series 2 test was erroneous and is not included below. Onboard real-time cameras were used to record each tire response and off-board cameras recorded the event from multiple angles.



Figure 3 Front (left) and rear (right) string potentiometer placement

The first Series of four (4) tests was selected to replicate a non-tip-up event. A test pressure of 689 kPa (100 psi) was expected to produce a test article lateral acceleration of approximately 0.6 g. The goal of the second test Series was to provide enough lateral acceleration to initiate a rollover. The second test Series comprised four (4) tests and used a tank pressure of 1034 kPa (150 psi). In all tests the inside tires of the test article was restrained to allow for a maximum lift of approximately 75 mm. A summary of the test conditions is provided in Table 2.

Table 2 Test summary

Test Series	Test parameters	Goal values
1	Tank pressure	689 kPa (100 psi)
	Test article lateral acceleration	0.6 g
	Peak platform velocity	60 deg/s
	Number of tests	4
2	Tank pressure	1034 kPa (150 psi)
	Test article lateral acceleration	1.1 g
	Peak platform velocity	80 deg/s
	Number of tests	4

The tests were conducted over a two-day period from 10 am to 6 pm each day. The weather was stable with temperatures ranging from 25 to 37° C (77 to 99° F) and humidity ranging from 84 to 35 % between the morning and afternoon. Multiple warmup and practice runs were performed prior to conducting the test Series to ensure that the moving parts of the test fixture and test article had loosened up. After the initial setup and practice runs were complete the test runs in each test Series was completed consecutively within 90 minutes from start to finish.

Correlation analysis (CORA) was utilized to objectively compare the platform angular displacement and the test article displacement in each test to the average values for a given test Series. CORAplus version 4.04 with

recommended global settings was used to calculate the scores using the cross correlation method. Curves were filtered according to J211 recommended protocol.

RESULTS

At test initiation the accelerating platform produced a slight rearward pitching motion of the test article which can be seen in the initial negative displacement of the rear string pot data. As the platform angular velocity increased the vehicle began to roll outboard. None of the tires lifted off of the platform in the Series 1 tests. The goal test conditions were achieved in all tests.

The platform angular displacement time history matched very well between tests in a given series as shown in Figures 4 and 5. The average maximum angular velocity for each test series was 60.1 deg/s and 79.25 deg/s. On average, the platform reached 340 deg of displacement (end of angular acceleration) in 9.7 seconds and 7.6 seconds in test series 1 and 2, respectively.

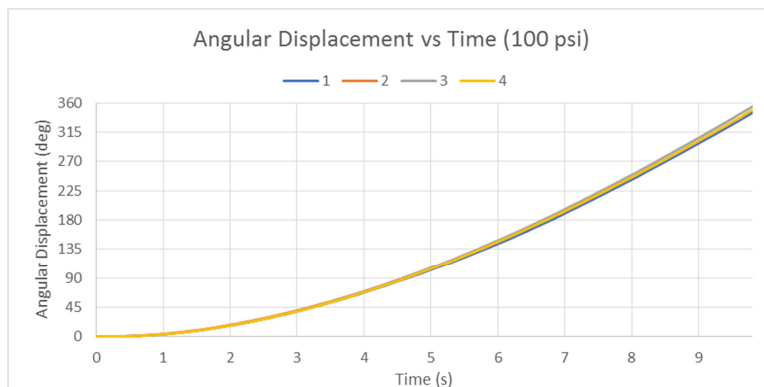


Figure 4 Platform angular displacement time-history (Test Series 1)

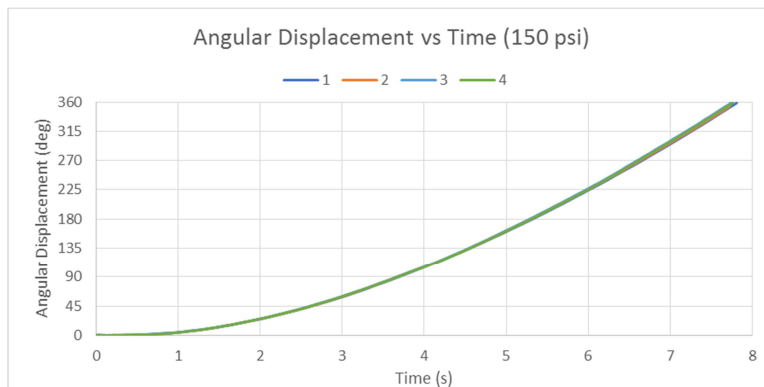


Figure 5 Platform angular displacement time-history (Test Series 2)

Test article displacement was consistent between tests as shown in Figures 6 and 7. String potentiometer data from the fourth Series 2 test was erroneous is not included here. The average maximum displacement at the front and rear string potentiometer locations was approximately 31 mm and 47 mm, respectively. The values correspond to the maximum displacement allowed by the tie-down chains. In the Series 2 tests the front and rear tires lifted off at approximately 4.5 and 7.7 seconds, respectively. The video footage indicates that a difference in chain response in Test 2 is likely the reason for the relatively large difference in displacement for that test.

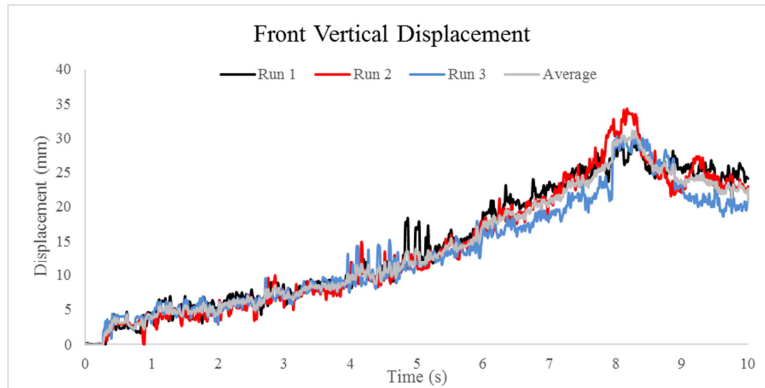


Figure 6 Test article displacement time-history (front; Test Series 2)

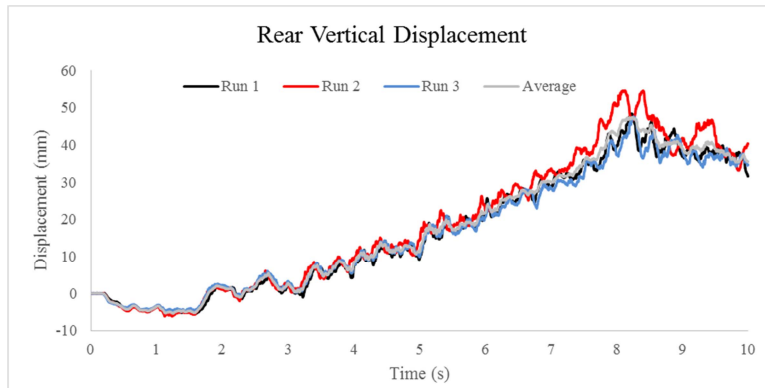


Figure 7 Test article displacement time-history (rear; Test Series 2)

The results of the CORA analysis are summarized in Table 3. Values above 8.6 are considered to indicate excellent repeatability.

Table 3 CORA results summary

Test Series	Measurement	Test	Cross correlation rating – per test				Total Series rating
			Cross correlation	Size	Phase shift	Total	
1	Platform displacement	1	1.0	0.966	1.0	0.992	0.995
		2	1.0	0.984	1.0	0.996	
		3	1.0	0.974	1.0	0.993	
		4	1.0	0.993	1.0	0.998	
2	Platform displacement	1	1.0	0.997	1.0	0.999	0.998
		2	1.0	0.978	1.0	0.994	
		3	1.0	0.987	1.0	0.997	
		4	1.0	0.999	1.0	1.0	
2	Test article displacement (rear)	1	0.994	0.937	1.0	0.981	0.968
		2	0.990	0.845	1.0	0.956	
		3	0.993	0.884	1.0	0.968	
2	Test article displacement (front)	1	0.987	0.939	1.0	0.978	0.975
		2	0.986	0.946	1.0	0.980	
		3	0.984	0.90	1.0	0.967	

DISCUSSION

The test fixture and test article demonstrated excellent repeatability for the two test series evaluated above. After initial test setup, tests could be performed with two technicians and 45 minute turnaround times. The greatest time-cost between tests included re-pressurizing the system and downloading the data. During test setup it was observed that initial ‘warm-up’ runs would be required to exercise both the fixture and the test article such that all joints and suspensions were loosened up and would perform consistently.

The lowest levels of repeatability were related to test article performance, though the repeatability was still considered excellent. This was expected as the test article introduced many additional characteristics that could affect response such as suspension and tire properties that could vary with changes in temperature or use. One proposed method to limit the effects of tire characteristics is to define a standardized tire or tire surrogate that would be used for all vehicles and provide a consistent interface between the tire and the trip-bar.

Some lateral motion of the test article was expected based on the results of a similar test series conducted by the NHTSA at National Aeronautics and Space Administration’s High Capacity Centrifuge [8], however no custom mechanisms were created to account for this with regard to the string pot measurements. It is anticipated that future rollover stability testing will require the use of custom-designed load cell mounts that move laterally with each tire. The lateral motion of the vehicle during initial warm-up testing and subsequent calibration testing presents a challenge in identifying the initial position of the vehicle for a test. Differences in the initial lateral position of the vehicle, specifically regarding pre-loading against the trip-bar, could potentially alter the performance. Lateral positioning of the vehicle during initial setup proved challenging and pre-loading the outside tires against the trip-bar was not possible. A pre-load could be applied by conducting one or more low-speed tests, however variations in the suspension spring back were observed after the platform came to rest.

While this paper has focused on using the Carousel to evaluate the dynamic rollover resistance of a passenger vehicle it could easily be extended to evaluating all-terrain vehicles (ATVs) and side-by-side vehicles. The device has the potential to evaluate restraint performance under varying yaw and roll rates in a repeatable, safety, and non-destructive manner. The platform can be modified with addition of a deformable barrier face to apply impact loads to stationary test articles. Various high- and low-rate deceleration mechanisms have been proposed that would allow the Carousel to perform as a traditional non-destructive deceleration sled.

CONCLUSIONS

A centrifuge-style test device (Carousel) was described. The performance of the Carousel and the response of a test article were evaluated to quantify their repeatability under low and high-speed test conditions. The Carousel and the test article both demonstrated excellent repeatability according to cross-correlation analysis using the CORA methods. The results demonstrate that the device is a suitable candidate for performing repeatable dynamic stability tests.

REFERENCES

- [1] Bose, D., et al., Planar impacts in rollover crashes: significance, distribution and injury epidemiology. *Ann Adv Automot Med*, 2011. **55**: p. 243-52.
- [2] Boyd, P.L. NHTSA's NCAP rollover resistance rating system. in *The 19th International Technical Conference on the Enhanced Safety of Vehicles*. 2005. Washington DC: NHTSA.
- [3] Brumbelow, M.L. and E.R. Teoh, Roof strength and injury risk in rollover crashes of passenger cars. *Traffic Inj. Prev.*, 2009. **10**(6): p. 584-592.
- [4] Grzebieta, R., et al., Final Project Summary Report: Quad Bike Performance Project Test Results, Conclusions, and Recommendations. 2015, UNSW: Transport and Road Safety Research.

- [5] Mengert, P., et al., Statistical Estimation of Rollover Risk. 1989, Research and Special Programs Administration: NHTSA, US DOT, Washington D.C.
- [6] NHTSA, 49 CFR Part 575: Consumer Information Regulations; Federal Motor Vehicle Safety Standards; Rollover Resistance, in Notice of proposed rulemaking. 2001.
- [7] Patel, B. and P. Atkinson, Towards A Definition of A Test Methodology for Rollover Resistance and Rollover Performance. 2004.
- [8] Chambers, W.V., SUV Rollover Test, in 23rd IEST-NASA/ASTM/AIAA/CSA Space Simulation Conference. 2004, NASA; AIAA; ASTM; CSA: Annapolis, MD; USA.

STATUS OF NHTSA'S EJECTION MITIGATION RESEARCH

Aloke Prasad

National Highway Traffic Safety Administration
United States of America

Corinn Pruitt

Transportation Research Center Inc.
United States of America

Paper Number 19-0036

ABSTRACT

The objective of this paper is to present an update on the research conducted by the National Highway Traffic Safety Administration (NHTSA) to assess the performance of roof glazing in production vehicles and certain countermeasure designs in preventing occupant ejections.

Federal Motor Vehicle Safety Standard (FMVSS) No. 226 "Ejection mitigation" set requirements for ejection mitigation systems to reduce the likelihood of complete and partial ejections of vehicle occupants through side windows during rollovers or side impact events.

In the preamble of the final rule establishing the standard (Jan 2011), the agency stated "NHTSA is interested in learning more about roof ejections and would like to explore this area further..." It also stated that while sun/moon roof ejection could be potentially cost effective to mitigate, the agency was not in a position to extend coverage to roof glazing in the final rule because the agency wanted to research a viable performance test procedure.

The assessment of ejection protection offered by sunroofs was made using a guided impactor (18 kg) directed toward roof glazing (pre-broken) from inside the vehicle, based on the procedures developed in the FMVSS No. 226 regulation², with test speeds of 14, 16, and 20 kilometers per hour.

Tests were conducted on production and countermeasure sunroof designs for the 2016 Ford F-150, production sunroofs for 2012 Toyota Prius, and production sunroofs provided by the Aisin Technical Center of America.

For sunroofs with both a fixed and a moving panel (F-150, Aisin), the movable panels presented more challenges to contain the headform than fixed panels. For the moving panels, the sunroof attachment structure separated at the inserts (into the rails). Fixed panels had higher excursions at unsupported transverse edges or edges without any metal encapsulation frames. The F-150 fixed rear panel had front and rear transverse unsupported edges, while the Aisin had longitudinal edges without metal frames. Laminated glazing panes with thicker polyvinyl butyral (PVB) inner layer in and polyethylene terephthalate (PET) film with tempered panes used as countermeasures for the F-150 sunroof reduced glazing stretch (and ram excursions). However, this transferred more forces to the edges and presented a greater challenge for movable panel containment at rail attachments.

The fixed polycarbonate panel used in the Prius had low ram excursions but high ram decelerations.

Meeting some excursion limit will require designs that have strong attachments to the vehicle roof or rails. Deformation of the glazing and encapsulation frame should be limited when impacted at the center of the panel. Any tear/rip of the plastic layer would add to the excursion of the ram.

The number of vehicle designs tested was limited by the availability of laminated glazing used in production or countermeasure designs.

This paper details performance of selected production and countermeasure sunroof designs in limiting headform excursions. Some of the fixed sunroof designs had excursions of less than 100 millimeters. The movable sunroof designs tested will require additional countermeasures to perform at this level.

INTRODUCTION

The National Highway Traffic Safety Administration (NHTSA) is continuing its exploration of roof ejection mitigation which commenced following NHTSA's issuance of FMVSS No. 226. FMVSS No. 226 sets requirements for ejection mitigation systems to reduce the likelihood of complete and partial ejections of vehicle occupants through side windows during rollovers or side impact events.

The final rule (Jan 2011) preamble said, "NHTSA is interested in learning more about roof ejections and would like to explore this area further..."¹ It also stated that while sun/moon roof ejection could be potentially cost effective to mitigate, the agency was not in a position to extend coverage to roof glazing in the final rule because the agency wanted to research a viable performance test procedure.

This paper addresses testing on production and prototype countermeasure sunroof designs to evaluate performance in preventing occupant ejections. In addition, a modified test setup with updated headform orientation and test speeds was evaluated. Additional production sunroof and countermeasure tests were completed with the new test setup.

TEST PROCEDURE AND EQUIPMENT

This study involved impacting three different production sunroofs and potential countermeasures aimed at improving occupant protection. Sunroofs and countermeasures were selected to represent a variety of constructions currently available in the market. The test method (equipment, initial selection of speeds) was adapted from the procedure used for FMVSS No. 226 and involved impacting the sunroofs with a featureless headform at different velocities.² The performance of each sunroof was evaluated by analyzing ram excursion, edge excursion using photogrammetry, observations of failures, and high-speed video.

Vehicle and Buck Descriptions

2016 Ford F-150 Construction The 2016 Ford F-150 (gross vehicle weight rating of 2767 kg to 3198 kg) was selected as it had large panels and was one of the widest sunroofs available at the time (Figure 1). It had a tilt slide sunroof with the front moveable panel sliding underneath the rear fixed panel. The sunroof module was bolted to the roof at twenty locations indicated by red arrows in Figure 2. The sunroof module consisted of a fixed panel and a movable panel (Figure 3). Both panels were assembled to the sunroof module using screws along the left and right sides, leaving the transverse sides unsupported (Figure 4). The production panels were made of laminated glass (2.1 – 0.76 – 2.1 mm; annealed glass – PVB – annealed glass) and were used as a baseline condition for the vehicle. Two countermeasure sunroof designs were tested. The first countermeasure increased the thickness of the PVB interlayer (2.1 – 1.52 – 2.1 mm; annealed glass – PVB – annealed glass). The second countermeasure investigated the performance of a polyethylene terephthalate (PET) protective film (Protec[®] II) applied to tempered glass (Protec[®] II film on inner surface; 5.0 mm tempered glass). The two countermeasure glass panels were attached to the sunroof assembly in the same manner as the production panels.

¹ 76 FR 3262, January 19, 2011

² 49 C.F.R. § 571.226, S5. Test Procedures

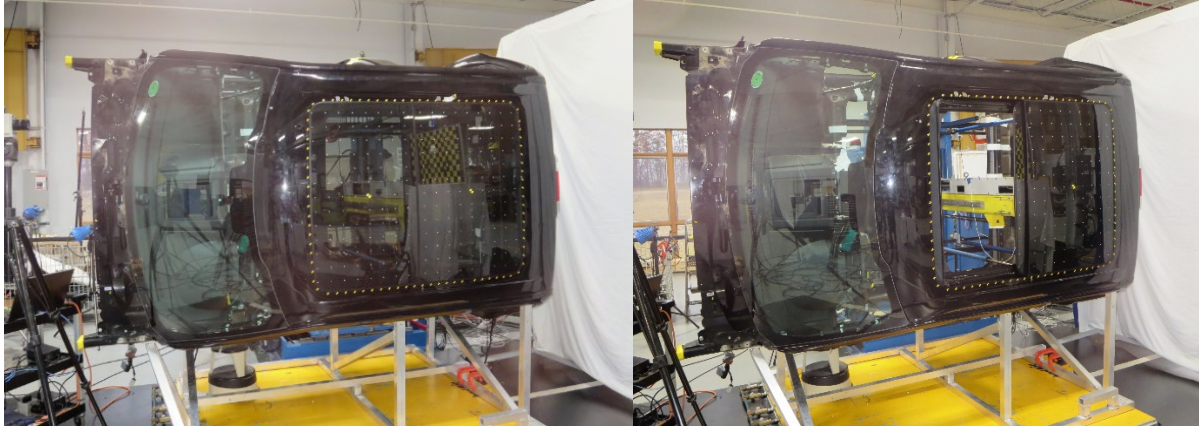


Figure 1. View of F-150 sunroof panel in both closed (left) and open (right) positions from outside. The F-150 had one of the largest sunroofs available at the time.



Figure 2. Red arrows indicate where sunroof module was bolted to the roof of the vehicle.



Figure 3. F-150 sunroof panels – left: front moveable panel, right: rear fixed panel.

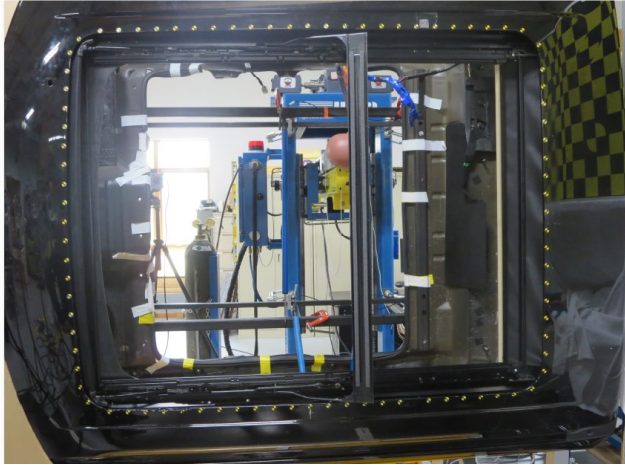


Figure 4. Front and rear panels assembled to module using screws along longitudinal edges.

2012 Toyota Prius V The 2012 Toyota Prius V had a large polycarbonate sunroof composed of one fixed panel with two daylight openings (Figure 5). The overall size of the panel was approximately one meter wide by one meter long. The test area of the daylight openings was approximately 0.29 meter². The panel was glued with polyurethane to the roof of the vehicle (Figure 6).



Figure 5. Toyota Prius V large polycarbonate sunroof with two daylight openings.



Figure 6. Sunroof panel glued to roof of vehicle with polyurethane.

Aisin Sunroofs Aisin Technical Center of America (Aisin) provided panoramic moveable sunroofs to be used for testing. The glazing composition of these sunroofs were 2.0-millimeter annealed glass (outside) – 0.76-millimeter PVB – 1.8-millimeter glass (inside). They were outer slider type sunroofs where the moveable front panel slides outside of the fixed rear panel (Figure 7). The sunroof module was attached to a custom-made test fixture at the same locations that it would be attached to the vehicle roof (Figure 8). The panels were attached to the sunroof module along the left and right longitudinal sides using a combination of plastic brackets and glue, while the transverse sides were unsupported (Figure 9).



Figure 7. Aisin outer slider sunroof – front slides outside of rear panel.



Figure 8. Sunroof module attached to custom-made frame at same locations as vehicle roof.

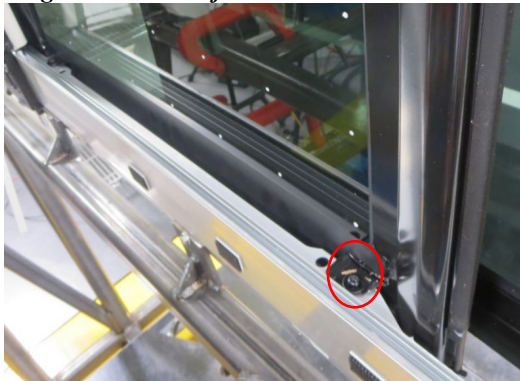


Figure 9. Panels attached to module using plastic brackets and glue along longitudinal edges.

Test Set-Up Description

The F-150 and Prius had the floor and other non-integral components removed, then were turned 90 degrees and mounted sideways to a rigid frame to allow the impactor to be aimed at the roof structure. The Aisin sunroof module was attached to a frame of the same geometry and attachment locations as the vehicle roof. To simulate damage experienced in a rollover crash, glass was pre-broken on both sides in a 75-millimeter offset pattern following the FMVSS No. 226 procedure,³ except for the Protec® II film which was only punched on one (glass) side. The method used a 75-millimeter offset pattern, with a 75-millimeter by 75-millimeter pattern on the outside surface and the same pattern offset by 37.5 millimeters on the inside surface. Glass was broken using a spring loaded centerpunch. Prior to testing, the daylight opening was established, and an offset line 25 millimeters inside of the daylight opening was marked on the glass.

The ejection impactor used in this project meets FMVSS No. 226 specifications. It was a guided impactor that used a featureless headform (176.8 x 226.1 mm) attached to a shaft (Figure 10). The impactor had a mass of 18 kilograms. Impact velocities used in this project were 14, 16, and 20 kilometers per hour. Both 16 and 20 kilometers per hour are standard speeds used in FMVSS No. 226.



Figure 10. Ejection guided impactor with 18 kg featureless headform.

Measurements were recorded with a variety of transducers, which are summarized in Table 1.

Table 1.
Summary of Transducers Used.

Measurement	Transducer Details
Ram Velocity	LVDT (differentiated)
Ram Excursion	LVDT
Dynamic edge excursion	High speed video with targets (analyzed with photogrammetry)

Photographs were taken to document the test setup and post-test observations. High-speed video was used to capture the impact during each test.

Initial Baseline and Countermeasure Tests for the Ford F-150

The 2016 Ford F-150 production sunroof and countermeasures were initially evaluated using the test setup from previous rounds of testing (center and corner impact locations) with additional locations added. Additional locations were selected based on engineering judgement to greater evaluate loading on the glass and loading on panel attachments. These locations were believed more likely to have poor performance. To select these locations, it was assumed that the left and right sides of the panels were identical but the front and rear sides were not. Test locations used are shown in Figure 11. The headform was aligned so that its longitudinal axis was parallel to the vehicle's longitudinal axis. Test speeds were 16 and 20 kilometers per hour. The sunroof panels were replaced after each impact. The entire sunroof module was replaced after each panel was tested once.

³ FMVSS No. 226, S5.4.1, Window glazing pre-breaking procedure

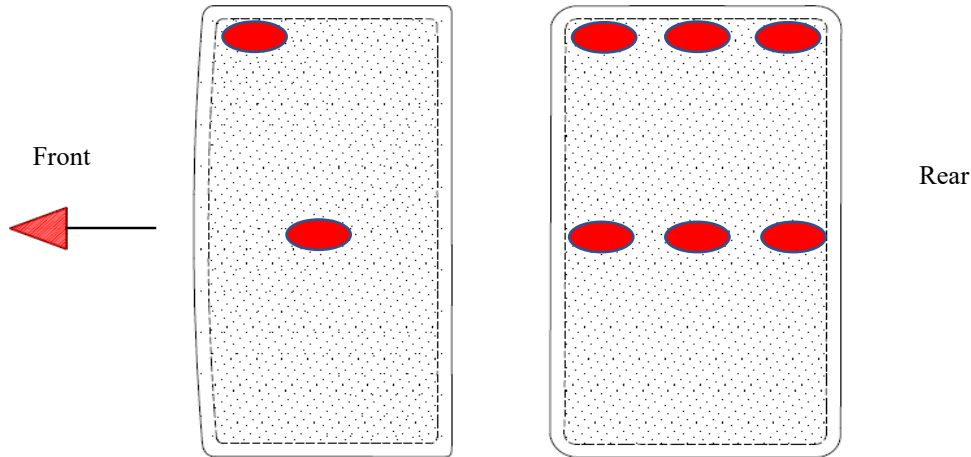


Figure 11. Initial test locations and headform orientation (F-150).

Countermeasures tested were the thicker PVB interlayer and the Protec® II glazing. Countermeasures were only tested at the center and front corner locations. Production glass was tested at the additional locations shown above. The test was setup following the procedure outlined in the section above for each of the tests. The only exception was test 74 where the Protec® II glazing was punched on both sides.

Initial Countermeasure Results

Countermeasures were compared to production glass and results are shown in the figures below. The top and bottom values represent ram excursion at 16 and 20 kilometers per hour respectively, at each location. Any asterisk (*) represents a rail mount failure (separation of the moving panel frame from the rail) at that speed and location. Excursion values exceeding 100 millimeters are shown in red color.⁴ For the countermeasure tests, the percent change from the baseline production glass is also shown in parenthesis for instances without detachment at the rails. Full results (ram and edge excursions) can be found in Appendix A (Table A.1).

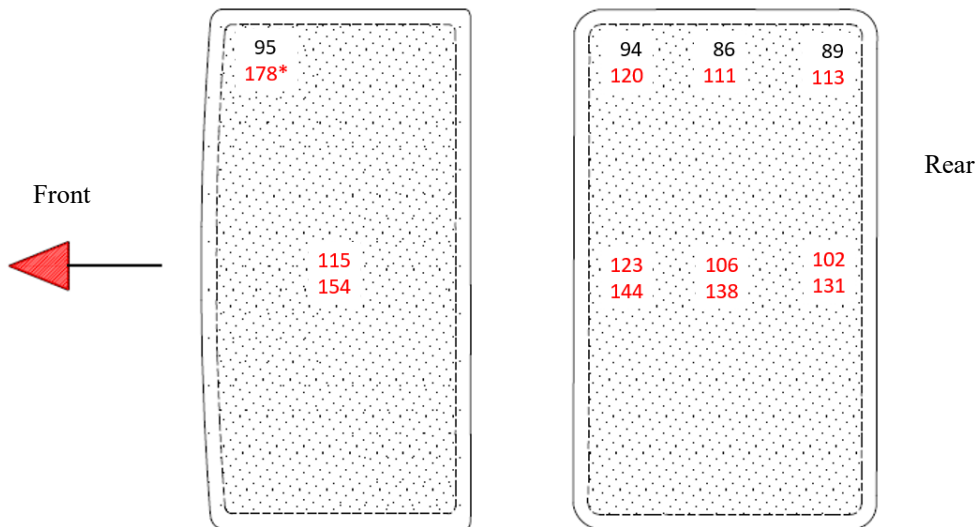


Figure 12. Production Glass (baseline) Results.

⁴ FMVSS No. 226, S4.2.1 limits the headform displacement to 100 millimeters after impact with the glazing pane surface.

For production glass, on the front movable panel, hits at the center had PVB stretch and transverse frame bending. At the corner of the front panel there was rail failure using the higher impact speed and therefore a large ram excursion. On the rear fixed panel, there was no edge failure for any location. At 16 kilometers per hour, ram excursions were below or just over 100 millimeters, except for at the forward transverse edge which is thinner and weaker and therefore had a higher excursion.

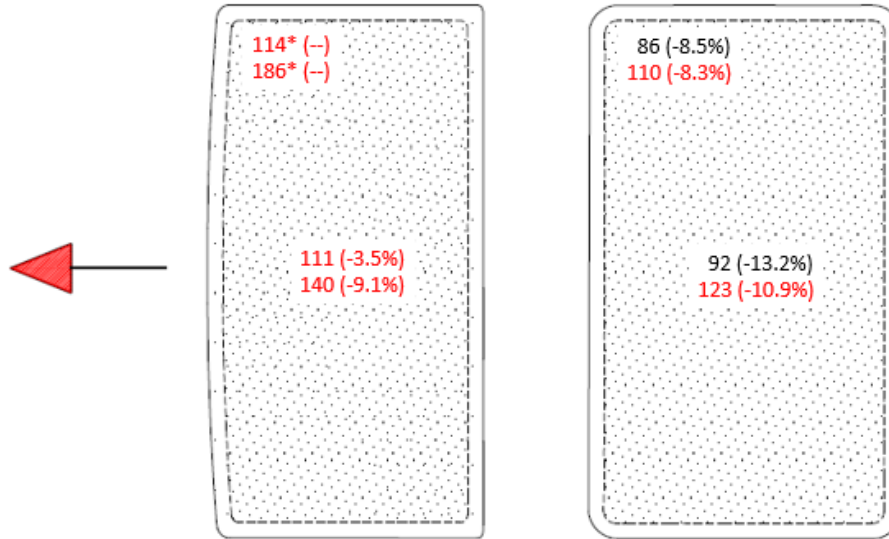


Figure 13. Thicker PVB Results.

For the thicker PVB panels, on the front movable panel, hits at the center showed less stretch but more transverse frame bending than the baseline panels. At the corners, catastrophic edge failure (complete detachment of the panel frame from the rail) was seen. On the rear panel, the thicker PVB reduced excursions by approximately 10 percent.

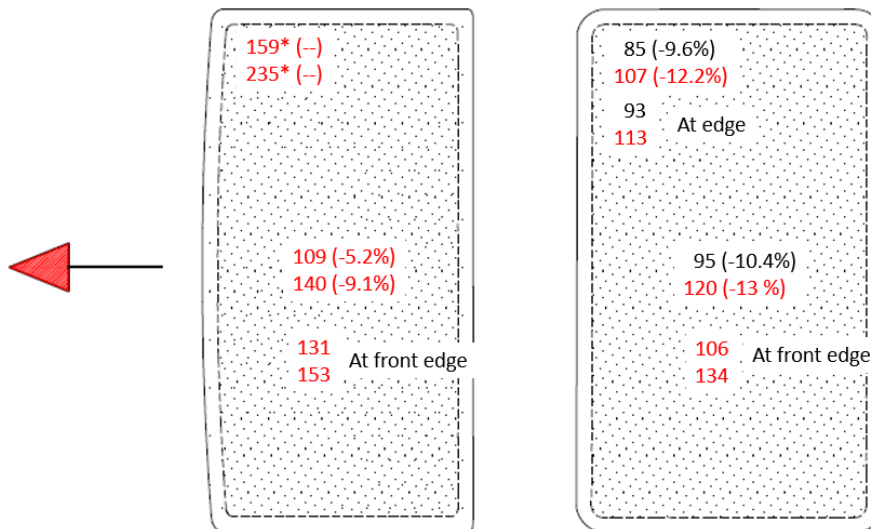


Figure 14. Protec® II Results.

For the Protec® II panels, hits on the front movable panel, at the center, had less film stretch but much more transverse frame bending than the baseline panels. At the corner, there was catastrophic edge failure at both speeds. On the fixed rear panel, there was approximately a 12 percent reduction in excursions. Like the thicker PVB, the reduced film stretching of the Protec® II led to increased loads on the edges.

Movable panels presented more challenges for containing the headform than fixed panels, for both the production panels and countermeasure panels. The thicker PVB and Protec® II panels did not tear and had reduced stretch, however this lead to more forces being transferred to the edges. Overall, baseline production panels showed feasibility at 16 kilometers per hour. Countermeasures showed they can improve the feasibility of meeting a 100-millimeter excursion limit; however, results can change for different panel designs.

Modified Test Conditions

Based on results from initial F-150 testing, impact locations and speeds were modified for future evaluations. The new test setup was based on the wording of FMVSS No. 226, as adapted for ejections through roof portals. Test locations included the corners, center, midpoint of transverse edges, and two-thirds of the longitudinal edge as shown in the figure below. Head orientation was changed so that the longitudinal axis of the headform was perpendicular to the longitudinal axis of the vehicle (Figure 15).

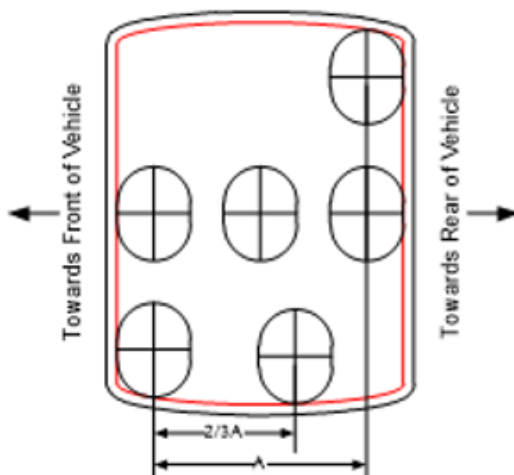


Figure 15. New Test Setup.

A test speed of 14 kilometers per hour was added. Each location was first hit at 16 kilometers per hour. If the ram excursion was greater than 100 millimeters, that location was then impacted at 14 kilometers. If the ram excursion was less than 100 millimeters at 16 kilometers per hour, then it was impacted at 20 kilometers per hour.

The test was setup following the procedure described in the section titled “Test Set-Up Description.”

Photographs were taken to document the test setup and post-test observations. High-speed video was used to capture the impact during each test. This video was also used for photogrammetry analysis to determine edge excursion.

EJECTION TEST RESULTS

Ford F-150 Results

The top, middle, and bottom values in Figure 16 represent the ram excursions (in millimeters) at speeds of 14, 16, and 20 kilometers per hour, respectively. An asterisk (*) indicates a rail mount failure. Green represents ram excursion values less than 100 millimeters and red represents excursion values greater than 100 millimeters. Six tests with thicker PVB (3 front panel and 3 rear panel) and one test with Protec® II were done. Tests with thicker PVB are shown in yellow and the test with Protec® II is shown in purple. Full results (ram and edge excursions) can be found in Appendix A (Table A.2).

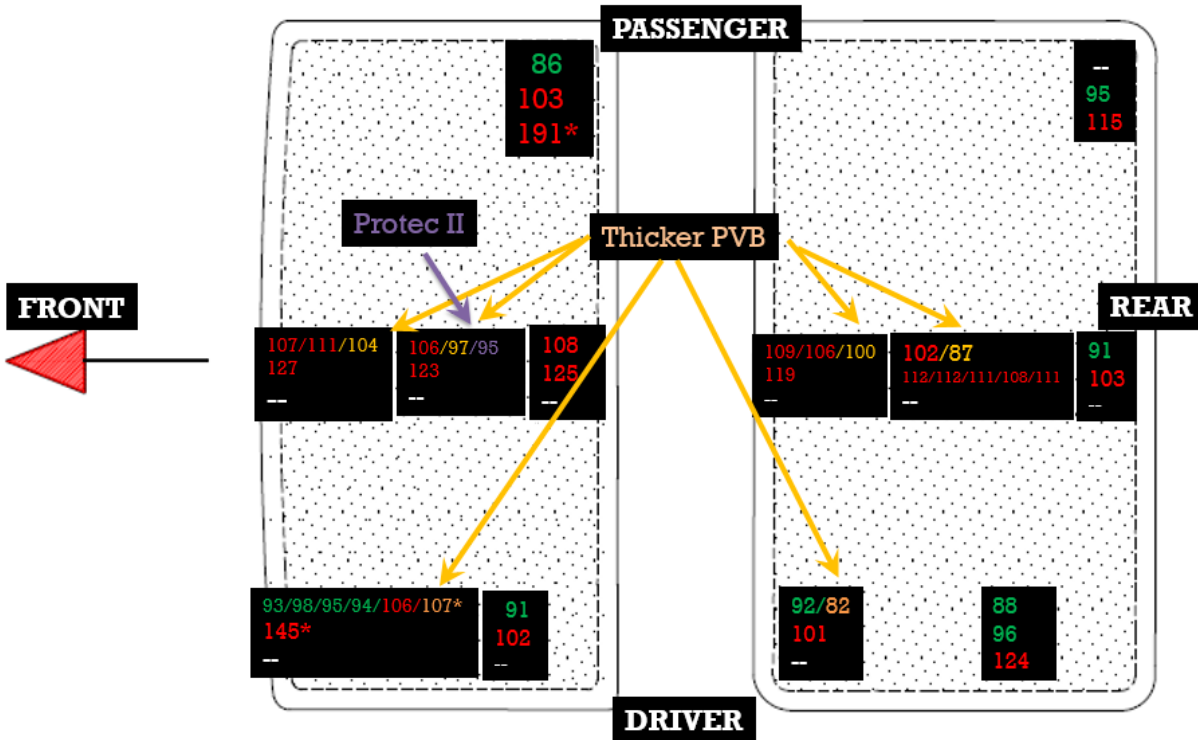


Figure 16. Ford F-150 Results.

As seen in previous testing, the movable panels presented more challenges in containing the headform than fixed panels. Failure at the inserts into the rails occurred on the moving panel. The fixed panel had higher excursions at the unsupported edges (front and rear edges of rear panel).

The plastic layer of the countermeasures (thicker PVB and Protec® II) did not tear in any test. Both countermeasures reduced plastic layer stretch and ram excursions compared to baseline. However, since more forces were transferred to the edges, larger openings were sometimes produced at the edges (i.e. edge excursions, highlighted in yellow in Tables A.1 and A.2).

Toyota Prius V Results

The polycarbonate panel on the Toyota Prius V was replaced after the first nine tests by a professional glass installer using the original glue sourced from Japan. There was no separation at the panel-roof glue interface during the entire test series for the Prius V roof. Ram excursions (in millimeters) can be seen in Figure 17 below. The top, middle, and bottom values represent excursions at speeds of 14, 16, and 20 kilometers per hour, respectively. Three tests were conducted on the rear panel at the two-thirds longitudinal edge locations and at 20 kilometers per hour, to assess the effect of repeated impacts. All three tests produced a ram excursion of 50 millimeters. The test with the * cracked the front windshield of the test vehicle. The windshield was replaced after this test. The test with ** caused the nearby roof structure to deform, however, this was a small static deformation of the structure. The roof structure was pushed back into its pre-impact shape and reinforcement was added. Full results (ram and edge excursions) can be found in Appendix A (Table A.3).

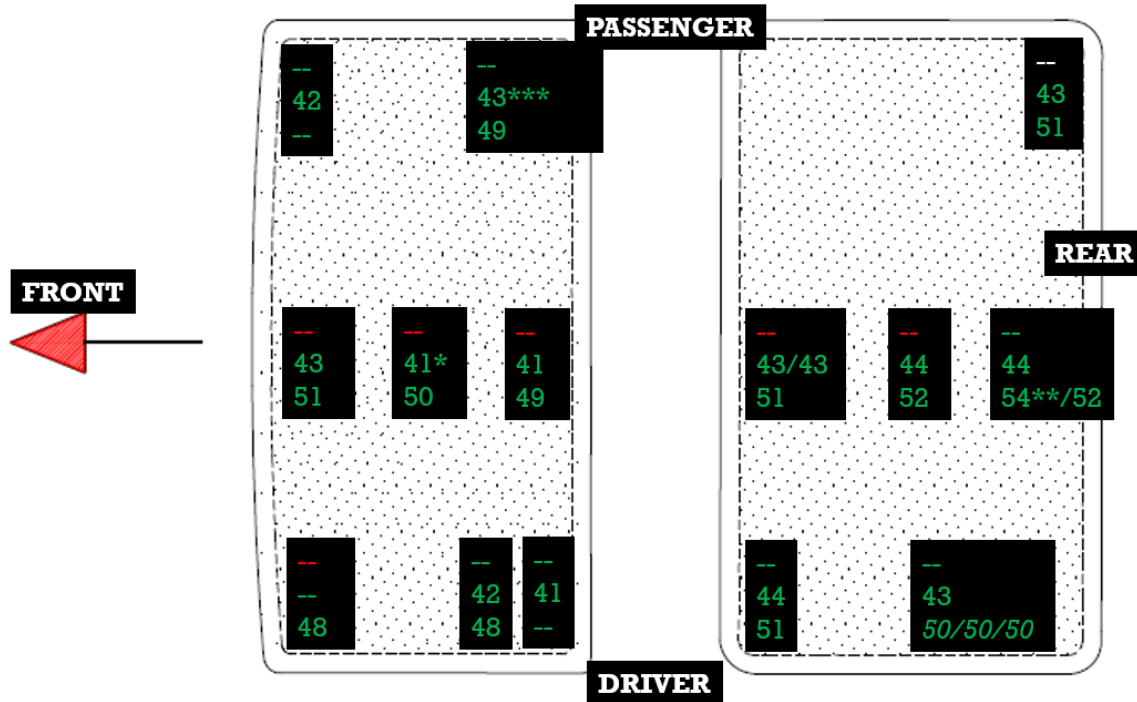


Figure 17. Toyota Prius V Results.

All Prius impacts had less than 100 millimeters excursions, generally around 50 millimeters. No separation at the glue interface was seen. Additionally, no failure of the polycarbonate or glue interface was seen even for multiple impacts at 20 kilometers per hour at the same location. Overall there were low ram displacements, however, due to less flexion of the sunroof panel there were high head deceleration values and therefore high forces on the headform. For example, when comparing an impact in the center of the Ford F-150 fixed panel at 16 kilometers per hour to an impact in the center of the Toyota Prius panel at 16 kilometers per hour, the forces on the headform were 2282 and 8663 Newtons, respectively. This is shown in Figure 18 below, with the F-150 in red and the Prius in blue.

REM FF15065: 2016 Ford F150 / Rear Fixed Panel / Pos. -- Center / 16kph / 136psi / 8th Frame / 11-7-17

REM TP001: 2012 Toyota Prius / Front Panel / Pos - Impact center / 16kph / 136psi / 1-17-18

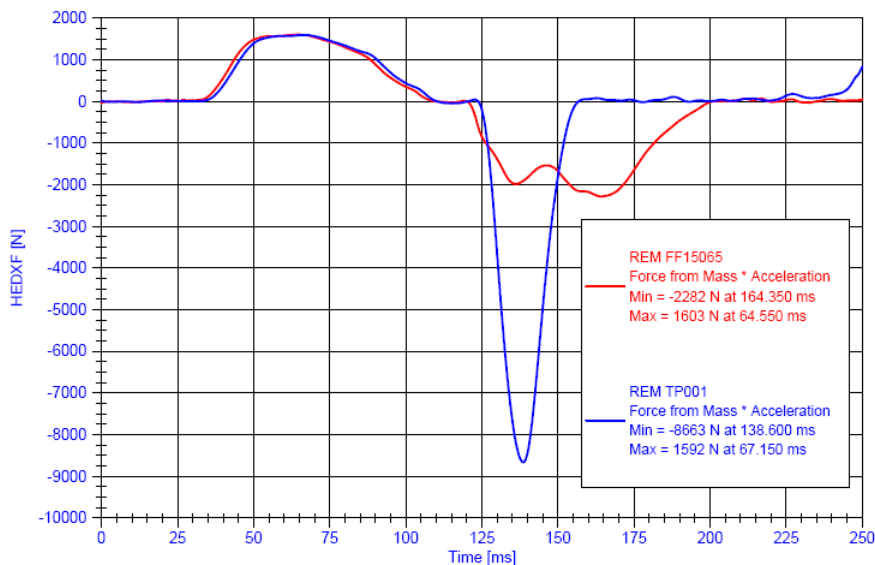


Figure 18. Comparison of forces on headform of F-150 (red) and Prius (blue).

Aisin Sunroof Results

Ram excursions (in millimeters) are shown in Figure 19 below. The top, middle, and bottom values represent excursions at speeds of 14, 16, and 20 kilometers per hour, respectively. An asterisk (*) means a rail insert failure occurred, double asterisks (**) mean an attachment bracket failure, triple asterisks (***) mean attachment glue-to-glass adhesion failure, and a # means a PVB failure, usually a rip in the PVB. Green values indicate excursions less than 100 millimeters and red indicate excursions greater than 100 millimeters. The four yellow values represent tests on the front movable panel where the panel was partially open so that the pin was in the metal rail. The panel was positioned so that for each of these four tests, the front edge of the window trim was 265 millimeters from a target on the front supporting frame. Full results (ram and edge excursions) can be found in Appendix A (Table A.4).

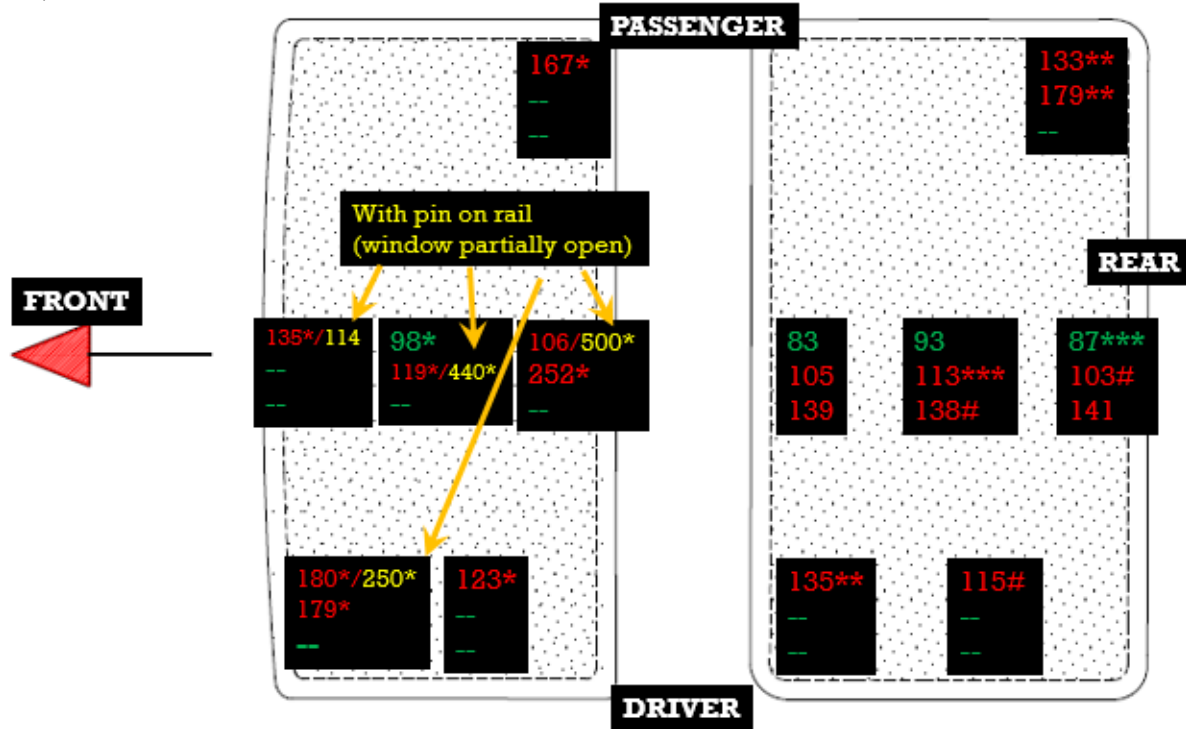




Figure 19. Aisin Sunroof Results.

The Aisin sunroof had many failure modes. Some examples of these failure modes are shown in Table 2 below.

Table 2.
Failure modes of Aisin sunroof.

		
Rear panel - attachment bracket	Rear panel bracket – glue attachment	Rear panel – PVB tear at attachment
		
Glass PVB tear	Front panel corner pin -rail insert	Front panel corner pin and rear attachment

The headform did not push through the PVB layer for any of the tests. In some tests, where the frame inserts didn't fail, the PVB layers had tears in it. On the front movable, panel brittle fracture of the plastic cam, which is used to raise the front edge when sliding the panel to open, occurred in some tests. In tests where the panel was moved to a partially open configuration there were also rail insert failures. The rail inserts had weakness at all locations impacted on the front panel. The rear fixed panel had weakness at the attachment brackets. Failures occurred at the bracket to glass glue adhesion as well as at the bracket attachment bolt. Bending of the encapsulation frame was also observed for many tests.

CONCLUSIONS

This paper details performance of selected production and countermeasure sunroof designs in limiting headform excursions. Additionally, it describes a new test setup that was developed for roof ejection tests adapted from the wording of FMVSS No. 226. Test locations include the corners, center, midpoint of transverse edges, and two-thirds of the longitudinal edge. Head orientation was changed so that the longitudinal axis of the headform was perpendicular to the longitudinal axis of the vehicle. These locations tested attachment, frame, and glazing performance. On movable panels, failure of rail inserts happened when impacted near the rail attachments, and unsupported transverse edges bent when the panel was hit at the center or near the transverse edges. Stronger glazing transferred more load to the attachments.

Some of the fixed sunroof designs had excursions of less than 100 millimeters. The movable sunroof designs tested will require additional countermeasures to perform at this level. The research findings suggest that meeting some excursion limit similar to the 100-millimeter requirement of FMVSS No. 226 will require designs that have limited deformation of the glazing and encapsulation frame when impacted at the center of the panel, strong attachments, with no separation at the attachments. Tears or rips in the plastic layer may lead to additional impactor excursion. Impacts in close proximity to attachments frequently caused failure at the attachments. PVB elasticity also affects the excursions, particularly for center impacts. Any glued plastic sun roofs with low excursions, such as that of the Prius, can cause higher forces on the impactor than those produced from impacts to glass sunroofs. No comparison was made to forces produced from impacts with roofs that do not have a sunroof. The relationship between this loading and potential occupant injury was not assessed.

APPENDIX A: RESULTS TABLES

Table A1: 2016 Ford F-150 - Initial Tests

		Production																	
		Front Movable Panel						Rear Fixed Panel											
		Center		Forward Edge - Corner		Forward Edge - Mid		Center		Forward Edge - Corner		Forward Edge - Mid		Top Edge - Mid		Rear Edge - Mid		Rear Edge - Top Corner	
		Ram	Edge	Ram	Edge	Ram	Edge	Ram	Edge	Ram	Edge	Ram	Edge	Ram	Edge	Ram	Edge	Ram	Edge
16 Km/h		115 mm	86 mm	95 mm	75 mm	---	---	106 mm	80 mm	94 mm	70 mm	123 mm	89 mm	86 mm	56 mm	102 mm	64 mm	89 mm	43 mm
20 Km/h		154 mm	106 mm	178 mm	233 mm	---	---	138 mm	101 mm	120 mm	84 mm	144 mm	132 mm	111 mm	67 mm	131 mm	71 mm	113 mm	56 mm

		Double PVB											
		Front Movable Panel						Rear Fixed Panel					
		Center		Forward Edge - Corner		Forward Edge - Mid		Center		Forward Edge - Corner		Forward Edge - Mid	
		Ram	Edge	Ram	Edge	Ram	Edge	Ram	Edge	Ram	Edge	Ram	Edge
16 Km/h		111 mm (-3.5%)	95 mm	114 mm (--%)	174 mm	---	---	92 mm (-13.2%)	94 mm	86 mm (-8.5%)	54 mm	---	---
20 Km/h		140 mm (-9.1%)	137 mm	186 mm (--%)	241 mm	---	---	123 mm (-10.9%)	113 mm	110 mm (-8.3%)	98 mm	---	---

		Protec II											
		Front Movable Panel						Rear Fixed Panel					
		Center		Forward Edge - Corner		Forward Edge - Mid		Center		Forward Edge - Corner		Center (punch both sides)	
		Ram	Edge	Ram	Edge	Ram	Edge	Ram	Edge	Ram	Edge	Ram	Edge
16 Km/h		109 mm (-5.2%)	131 mm	159 mm (--%)	235 mm	---	---	95 mm (-10.4%)	106 mm	85 mm (-9.6%)	93 mm	96 mm	109 mm
20 Km/h		140 mm (-9.1%)	153 mm	235 mm (--%)	363 mm	---	---	120 mm (-13%)	134 mm	107 mm (-12.2%)	113 mm	---	---

Rail mechanism failure
 Edge excursion greater than ram excursion

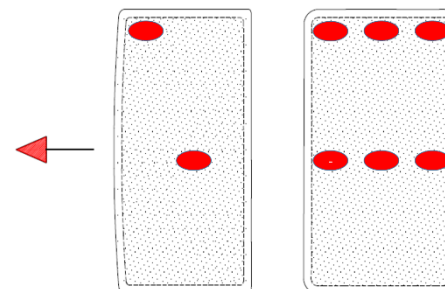


Table A2: 2016 Ford F-150 – New Test Setup

Production												
Front Movable Panel												
Forward Edge - Corner		Forward Edge - Mid		Center		Side Edge - 2/3 A		Rear Edge - Corner		Rear Edge - Mid		
Ram	Edge	Ram	Edge	Ram	Edge	Ram	Edge	Ram	Edge	Ram	Edge	
14 Km/h	93/98/95/94/106	ND/120/114/104/127	111/107	96/99	106	63	91	No video	86	---	108	91
16 Km/h	145	194	127	121	123	81	102	66	103	76	125	106
20 Km/h	---	---	---	---	---	---	---	---	191	208	---	---

Production												
Rear Fixed Panel												
Forward Edge - Corner		Forward Edge - Mid		Center		Side Edge - 2/3 A		Rear Edge - Corner		Rear Edge - Mid		
Ram	Edge	Ram	Edge	Ram	Edge	Ram	Edge	Ram	Edge	Ram	Edge	
14 Km/h	92	67	109/106	87/87	102	69.3	88	42	---	---	91	47
16 Km/h	101	120	119	99	112/112/111/108/111	78/84/84/90/86	96	50	95	37	103	58
20 Km/h	---	---	---	---	---	---	124	56	115	58	---	---

Double PVB												
Front Movable Panel						Rear Fixed Panel						
Forward Edge - Corner		Forward Edge - Mid		Center		Forward Edge - Corner		Forward Edge - Mid		Center		
Ram	Edge	Ram	Edge	Ram	Edge	Ram	Edge	Ram	Edge	Ram	Edge	
14 Km/h	107 mm	147 mm	104 mm	No Data	97 mm	86 mm	82 mm	74	100 mm	95 mm	87 mm	78 mm

Protec II											
Front Movable Panel						Rear Fixed Panel					
Forward Edge - Corner		Forward Edge - Mid		Center		Forward Edge - Corner		Center (punch both sides)		Center	
Ram	Edge	Ram	Edge	Ram	Edge	Ram	Edge	Ram	Edge	Ram	Edge
14 Km/h	---	---	---	---	95 mm	93 mm	---	---	---	---	---

Rail mechanism failure
 Edge excursion greater than ram excursion

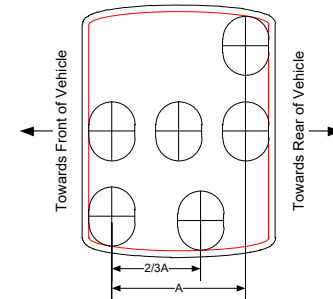


Table A3: 2012 Toyota Prius V

Production											
Front fixed Panel											
Forward Edge - Corner		Forward Edge - Mid		Center		Side Edge - 2/3 A		Rear Edge - Corner		Rear Edge - Mid	
Ram	Edge	Ram	Edge	Ram	Edge	Ram	Edge	Ram	Edge	Ram	Edge
14 Km/h											
16 Km/h	42	34	43	37	41	23	42	16	41/43	15/9	41 22
20 Km/h	48	10	51	21	50	10	48	7	49	10	49 9

Production											
Rear Fixed Panel											
Forward Edge - Corner		Forward Edge - Mid		Center		Side Edge - 2/3 A		Rear Edge - Corner		Rear Edge - Mid	
Ram	Edge	Ram	Edge	Ram	Edge	Ram	Edge	Ram	Edge	Ram	Edge
14 Km/h											
16 Km/h	44	26	43/43	32/7	44	7	43	6	43	8	44 9
20 Km/h	51	7	51	9	52	9	50/50/50	ND	51	10	54/52 69/19

Edge excursion greater than ram excursion
 Tests on original sunroof

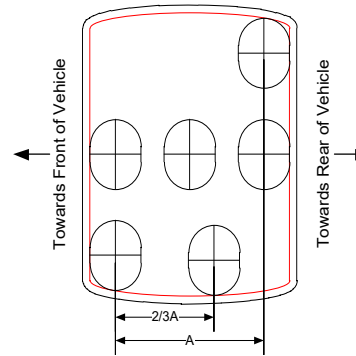


Table A4: Aisin Sunroof

Production												
Front moving Panel												
Forward Edge - Corner		Forward Edge - Mid		Center		Side Edge - 2/3 A		Rear Edge - Corner		Rear Edge - Mid		
Ram	Edge	Ram	Edge	Ram	Edge	Ram	Edge	Ram	Edge	Ram	Edge	
14 Km/h	180/250*	197/500*	135/114*	143/272*	98	84	123	103	167	155	106/500*	96/500*
16 Km/h	179	212			119/440*	189/586*					252	315
20 Km/h												

Production												
Rear Fixed Panel												
Forward Edge - Corner		Forward Edge - Mid		Center		Side Edge - 2/3 A		Rear Edge - Corner		Rear Edge - Mid		
Ram	Edge	Ram	Edge	Ram	Edge	Ram	Edge	Ram	Edge	Ram	Edge	
14 Km/h	135	107	83	39	93	45	115	108	133	93	87	ND
16 Km/h			105	82	113	93			179	197	103	38
20 Km/h			139	105	138	109					141	85

- Rail mechanism failure (Front Panel)
 - Attachment failure (Rear Panel)
 - PVB failure (Rear Panel)
 - Edge excursion greater than ram excursion
- * Pin on aluminum rail

